

AD771547
AFAPL-TR-73-85

DEVELOPMENT OF HIGH SPEED TAPERED ROLLER BEARING

**R. F. Cornish
P. S. Orvos
S. R. Gupta**

The Timken Company

TECHNICAL REPORT AFAPL-TR-73-85

October 1973

**Approved for public release;
distribution unlimited.**

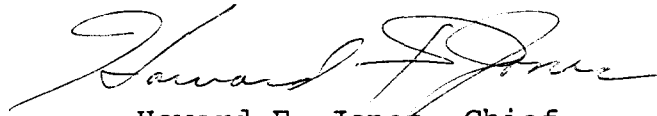
**Air Force Aero Propulsion Laboratory
Air Force Systems Command
Wright-Patterson Air Force Base, Ohio**

FOREWORD

This is an interim report covering the work conducted by the Physical Laboratories of The Timken Company, Canton, Ohio to fulfill the requirements of U.S.A.F. Contract No. F33615-72-C-1890, Project No. 304806. This work was administered under the direction of the Air Force Aero Propulsion Laboratory, with Mr. John Jenkins (AFAPL/SFL) acting as project engineer.

This report covers work conducted from 1 July 1972 to 1 July 1973.

Publication of this report does not constitute Air Force Approval of the reports findings or conclusions. It is published only for the exchange and stimulation of ideas.



Howard F. Jones, Chief
Lubrication Branch
Fuels and Lubrication Division

ABSTRACT

This report presents the analytical work conducted to evaluate the effects of various material, design and lubrication parameters on the performance of a high speed tapered roller bearing. The program objective is to operate the proposed bearing to 3.5 million DN (107.95 mm bore x 32422 RPM) under 5000 pounds thrust load.

The analysis includes the following: bearing geometry and design, effects of fit, kinematics, dynamics, load distribution, stresses, EHD and friction forces, analysis of the cone rib lubrication system.

ACKNOWLEDGEMENT

The authors acknowledge the contribution of P. M. Ku and Dr. H. J. Carper of Southwest Research Institute of San Antonio, Texas. They consulted on the subjects of lubricant properties, EHD and frictional analysis.

TABLE OF CONTENTS

	<u>Page</u>
1. INTRODUCTION	1
1.1 Objective	1
1.2 Current Technology	1
1.3 Analytical Approach	2
2. BEARING GEOMETRY	4
2.1 Geometrical Relationships	4
2.2 Cage	8
3. MATERIAL SELECTION	12
3.1 Cone, Cup and Roller	12
3.2 Cage	15
4. INTERFERENCE FIT AND INERTIA STRESSES	18
4.1 Contact Pressure	18
4.2 Mean Cone OD Increase	19
4.3 Mean Cup ID Decrease	19
4.4 Inertia Stresses in Cone	19
4.5 Loss of Interference Fit Due to Inertia Stresses	20
4.6 Combined Effects of Interference Fit and Inertia Stresses	21
5. KINEMATICS AND DYNAMICS	22
5.1 Epicyclic Speeds	22
5.2 Surface Velocities	23
5.3 Sliding Velocity	24
5.4 Roller Centrifugal Force	24
5.5 Normal Load Components Due to Roller Centrifugal Force	25
5.6 Induced Thrust Due to Roller Centrifugal Force.	31
5.7 Moments of Inertia of Roller	31
5.8 Gyroscopic Couple	31
5.9 Combined Effect of Roller Centrifugal Force and Gyroscopic Couple	33
6. LOAD DISTRIBUTION UNDER EXTERNAL LOAD	37
6.1 Thrust Load.	37
6.2 Combined Radial and Thrust Load	37

TABLE OF CONTENTS

	<u>Page</u>
7. CONTACT STRESSES	40
7.1 Roller-Body/Cone-Race	40
7.2 Roller-Body/Cup-Race	40
7.3 Roller-End/Cone-Rib	41
8. LUBRICANT (MIL-L-7808G) PROPERTIES	45
9. EHD FILM THICKNESS	49
9.1 Sum Velocities	49
9.2 Equivalent Radii	50
9.3 Roller-Body/Race Contacts.	53
9.4 Roller-End/Rib Contact	54
9.5 Thermal Reduction Factor	55
10. CAGE FRICTIONAL FORCES	57
10.1 Roller-Body/Cage-Pocket Friction	57
10.2 Cage-Pilot/Race-Guide Friction	61
11. EHD FRICTION AND PRESSURE FORCES	64
11.1 Roller-Body/Race Friction and Pressure Forces.	66
11.2 Roller-End/Rib Friction.	67
12. CONE RIB LUBRICATION SYSTEM.	69
12.1 System Pumping	69
12.2 Manifold Flow.	80
12.3 Effectiveness of System	84
13. DISCUSSION AND RECOMMENDATIONS	88
APPENDICES	
A. Friction Analysis for High Sliding Combined with Rolling	99
B. Sample Computer Printout	106
REFERENCES.	122

LIST OF FIGURES

<u>No.</u>	<u>Page</u>
1. Typical Tapered Roller Bearing	5
2. Bearing Symbols	6
3. Typical Tapered Roller	7
4. Nomenclature and Geometry of Typical Roller Guided Cage	9
5. Nomenclature and Geometry of Typical Race Guided Cage	11
6. Hot Hardness Characteristics of Various Bearing Steels	14
7. Normal Loads Due to Roller Centrifugal Force	26
8. Enlarged Roller Section	28
9. Mass Moments of Inertia	32
10. Roller-Body/Cup-Race Load Due to Centrifugal Force	34
11. Roller Loads Due to Both Centrifugal Force and Gyroscopic Couple	34
12. Roller-End/Rib Contact	42
13. Equivalent Radii	51
14. Section Views Through Roller Mean Diameter for Roller and Race Guided Cages	58
15. Friction as a Function of Reynolds Number for Unloaded Journal Bearings	59
16. Method of Piloting Race Guided Cage	62
17. EHD Friction and Pressure Forces	65
18. Cone Large Rib Lubrication System	70 & 71
19. Segment of Rotating Shaft Duct	73
20. Nikuradse's Data from Artificially Roughened Pipe Flows	77

LIST OF FIGURES (Continued)

<u>No.</u>		<u>Page</u>
21.	Control Volume for Analysis of Manifold	81
22.	Manifold Section Adjacent Shaft Duct	82
23.	Coordinate System to Calculate Effectiveness of Lubrication System	86
24.	Proposed Test Bearing with Roller Guided Cage	89
25.	Proposed Test Bearing with Race Guided Cage	90
26.	Film Thickness Versus % Apex Roller Spherical End Radius	93
27.	Forces Effecting Roller Moment Loading	95
28.	Percent Lubricant Coverage Versus Rib Speed	97
29.	Friction Coefficient Behavior for $G_2 = 41 \times 10^{-3}$	101
30.	Friction Coefficient Behavior for $G_2 = 107 \times 10^{-3}$	102
31.	Behavior of Ceiling Friction Coefficient with G_2	103

LIST OF TABLES

<u>No.</u>		<u>Page</u>
I.	Chemical Composition of Various High Temperature Bearing Steels	13
II.	Scuffing Resistance Tests of SAE 4620 Case-Carburized Versus Timken CBS-1000M Case-Carburized Steel	16
III.	J_R, J_T, ϵ vs. $\frac{R \tan \alpha}{T - T_i}$ for Line Contact	39
IV.	Density, Viscosity and Pressure-Viscosity Coefficient for MIL-L-7808G as a Function of Temperature.	47
V.	Specific Heat and Thermal Conductivity for MIL-L-7808G as a Function of Temperature	48
VI.	Empirical Formulas for Friction Coefficient	60
VII.	Empirical Formulas for Friction Factor	78
VIII.	Effects of Bearing Geometry on Operating Parameters	92
IX.	Summation of Moments About Roller Center	96

NOMENCLATURE

a	Semi-major axis of roller-end/rib contact ellipse, in.
A	Defined in Section 5.5.
A_c	Area of cone duct, in. ² .
A_m	Area of manifold trap, in. ² .
A_o	Area of manifold, in. ² .
A_s	Area of shaft duct, in. ² .
b	Semi-minor axis of roller-end/rib contact ellipse, in.
B	Defined in Section 5.5.
c_p	Specific heat of lubricant, BTU/lb.°F.
cos(T)	Geometry factor, defined in Section 7.3.
C_1	Normal load, roller-body/cone-race due to C_F only, lb.
C_2	Normal load, roller-body/cup-race due to C_F only, lb.
C_3	Normal load, roller-end/rib due to C_F only, lb.
C_F	Centrifugal force per roller, lb.
C_g	Clearance between cage-pilot/race-guide, in.
C_p	Clearance between roller-body/cage-pocket, in.
d	Mean roller diameter, in.
d_o	Shaft I.D., in.
d_1	Roller large end diameter, in.
d_2	Roller small end diameter, in.
d_3	Diameter at roller-end/rib contact center measured perpendicular to bearing centerline, in.
D	Defined in Section 5.5.
D_o	Bearing housing O.D., in.
D_1	Cone bore, in.
D_2	Mean Cone O.D., in.

NOMENCLATURE

D_3	Cone base diameter, in.
D_4	Cup O.D., in.
D_5	Mean cup I.D., in.
D_{11}, D_{12}, D_{13}	Defined in Section 5.5.
D_g	Diameter of cage pilot (large end) in.
D_s	Diameter of cage pilot (small end), in.
D_{cd}	Diameter of cone duct, in.
DN	Cone bore x shaft speed, mm.-rev./min.
E	Modulus of elasticity for bearing, shaft and housing material, 30×10^6 psi.
E'	Reduced modulus of elasticity, psi.
E_s	% cone rib circumference supplied with oil.
E(X)	Complete elliptic integral of the second kind.
e_f	Surface finish, in.
f	Flow friction factor.
f_1, f_3	Numerical functions for thermal reduction.
f_c	Cage friction factor.
f'	Intermediate flow friction factor.
F_g	Friction force, cage-pilot/race-guide, lb.
F_p	Friction force, roller-body/cage-pocket, lb.
F_1, F_2, F_3	Friction force, lb.
g	Acceleration due to gravity, 386 in./sec. ²
G	Rheological constant for lubricant, $\alpha_o E$
G*	Dimensionless EHD parameter

NOMENCLATURE

G_h	Defined in Section 7.3.
G_1, G_2, G_3	Dimensionless friction parameters, defined in Section 11.2.
h	Height of roller-end/rib contact center, measured perpendicular to cone-race, in.
h_1	EHD film thickness, roller-body/cone-race, micro-in.
h_2	EHD film thickness, roller-end/rib, micro-in.
h_3	EHD film thickness, roller-end/rib, micro-in.
h_{cg}	Height of roller c.g. measured perpendicular to the plane of roller large end, in.
H	Headloss, in. ² /sec. ²
H_1, H_2	Heights of right circular cones. (Fig. 9), in.
H^*_{min}	Dimensionless minimum EHD film thickness in general.
I_x	Mass moment of inertia of roller about roller centerline perpendicular to the plane of roller large end, lb.-in. ² .
I_y	Mass moment of inertia of roller about an axis through the center of gravity of roller and perpendicular to roller centerline, lb.-in. ² .
$I_{x_1}, I_{y_1}, I_{x_2}$	Mass moments of inertia (Fig. 9) lb.-in. ²
$I_{y_2}, I_{x_3}, I_{y_3}$	
J_R	Sjovall's radial integral.
J_T	Sjovall's thrust integral.
k	Thermal conductivity of lubricant, BTU/hr.ft.°F.
K	K-factor of bearing.
$K(X)$	Complete elliptical integral of the first kind.

NOMENCLATURE

l	Effective roller length, in.
l_p	Axial length of contact, roller-body/cage-pocket, in.
L_1	Roller slant length, in.
L_2	Roller apex length, in.
L_g	Axial length of cage pilot guide, in.
L_{cd}	Length cone duct, in.
L_{arc}	Arc length of roller-body pocket surface conjunction, in.
M_c	Drag or drive couple applied to cage due to race-pilot, in.-lb.
M_j	Gyroscopic couple per roller, in.-lb.
n_{cd}	Number of cone ducts.
N_{sd}	Number of shaft ducts.
N_c	RPM of cage.
N_r	RPM of roller about its own center.
p	Hertz contact stress, psi.
p_1, p_2, p_3	Pressure at points designated by subscripts, psi.
p_i	Static contact pressure due to interference fit, cone/shaft, psi.
p_o	Static contact pressure due to interference fit, cup/housing, psi.
p_e	Effective contact pressure, cone/shaft, psi.
P	Lubricant pressure, psi
P_1	Normal load, roller-body/cone-race, due to external bearing load and considering C_F , lb.
P_2	Normal load, roller-body/cup-race, due to external bearing load and considering C_F , lb.
P_3	Normal load, roller-end/rib, due to external bearing load and considering C_F , lb.

NOMENCLATURE

P_{atm}	Atmospheric pressure, psi.
P_{max}	Normal load roller-body/cone-race for max. loaded
q_1	Load per unit length, roller-body/cup-race adjacent small end of roller considering C_F and M_g only, lb./in.
q_2	Load per unit length, roller-body/cup-race adjacent large end of roller considering C_F and M_g only. lb./in.
Q^*	Dimensionless EHD pressure force.
Q_1, Q_2	EHD pressure force, lb.
r	Roller large end spherical radius, in.
r_x	Radial distance measured from bearing centerline, in.
r'	Radius of curvature of rib, in.
r_{cg}	Radial distance of center of roller c.g. measured perpendicular to bearing centerline, in.
r_o, r_1, r_2, r_3, r_4	Radial distances, in.
R	External bearing radial load, lb.
Re	Reynold's number, cone rib lubrication system.
Re_p	Reynold's number, roller-body/cage-pocket.
re_g	Reynold's number, cage pilot.
R_1, R_2, R_3	Equivalent radii roller-body/cone-race, roller-body/cup-race, roller-end/rib.
s	Slip ratio
S	Cone RPM
t	Time, sec.
t_e	Elapsed time, sec.
T	External bearing thrust load, lb.
T_i	Induced bearing thrust load due to roller centrifugal force, lb.
T_o	Oil inlet temperature, °F.

NOMENCLATURE

T_1, T_2, T_3	Conjunction temperatures, °F.
U^*	Dimensionless EHD parameter.
U_1, U_2, U_3	Sum velocities roller-body/cone-race, roller-body/cup-race, roller-end/rib, in./sec.
U_{sum}	Sum velocity in general, in./sec.
v	Lubricant velocities, in./sec.
V_1	Tangential velocity of roller-body mid-point with respect to roller centerline, in./sec.
V_2	Tangential velocity of the point on the roller at roller-end rib contact center with respect to roller centerline, in./sec.
V_3	Tangential velocity at mean cone O.D. with respect to bearing centerline, in./sec.
V_4	Tangential velocity of cage-pilot relative to race-guide, in./sec.
V_5	Sliding velocity at roller-end/rib contact center, in./sec.
V_{rib}	Rib velocity i.e. tangential velocity at the point on the rib at roller-end/rib contact center, in./sec.
w	Weight of roller, lb.
W^*	Dimensionless EHD parameter
x	Section 7.3.
X_e, Y_e	Coordinates of point where lubricant intersects roller-end/rib contact, in.
Y_1, Y_2	Relative height, in.
z	Number of rollers.
α	Half included cup angle, deg.
α_o	Pressure-viscosity coefficient at atmospheric pressure, in. ² /lb.
α^*	Thermal reduction parameter. (Section 9.5).

NOMENCLATURE

β	Half included cone angle, deg.
β_o	Temperature-viscosity coefficient, $(^{\circ}\text{F})^{-1}$ (used in Section 11.2).
β_o'	Temperature-viscosity coefficient, $^{\circ}\text{R}$ (used in Section 9.5).
γ	Half included centerline angle, deg.
γ_{rib}	Large rib angle, deg.
δ_1	Increase in mean cone O.D. due to static cone/shaft interference fit, in.
δ_2	Decrease in mean cup I.D. due to cup/housing interference fit, in.
δ_i	Initial diametral interference fit, cone/shaft, in.
δ_o	Diametral interference fit, cup/housing. in.
δ_{loss}	Loss of diametral interference fit due to rotation, cone/shaft, in.
Δ_p	Pressure difference, psi
ΔR	Infinitesimal length, in.
Δ_x	Distance of resultant normal load, roller-body/cup-race, due to roller centrifugal force (C_F) and gyroscopic couple (M_g) only and measured from roller-body mid-point along cup-race, in.
ϵ	Load zone parameters
θ	Rib-race angle, deg.
θ_H	Cone duct angle relative to backface, deg.
μ	Poisson's ratio, 0.3.
μ_o	Lubricant viscosity at atmospheric pressure, lb.sec./in. ² (Reyn).
$\mu_{o/100}$	Lubricant viscosity at 100°F, lb.-sec./in. ²
$\mu_{o/210}$	Lubricant viscosity at 210°F, lb.-sec./in. ²

NOMENCLATURE

μ_h	Hertzian parameter, roller-end/rib contact ellipse.
ν	Half included roller angle, deg.
ξ	Section 7.3.
ν_h	Hertzian parameter, roller-end/rib contact ellipse.
ν_o	Lubricant kinematic viscosity at atmospheric pressure, centistokes.
ρ	Density of steel, assumed same for bearing, shaft and housing, .283 lb./in. ³ .
ρ_o	Density of lubricant at atmospheric pressure, gm/cc.
ρ_o'	Density of lubricant at atmospheric pressure, lb.in. ³
σ	Contact stress, psi
σ_1	Contact stress at center of roller-body/cone-race contact, ksi.
σ_2	Contact stress at center of roller-body/cup-race contact, ksi.
σ_3	Contact stress at center of roller-end/rib contact, ksi.
σ_4	Maximum radial stress in cone due to rotation, psi.
τ	Tangential stress in cone due to rotation, psi
τ_i	Maximum tangential stress in cone due to rotation, psi.
τ_l	Tangential stress at cone bore due to rotation and effective diametral fit (δ_{eff}), psi.
τ_o	Lubricant shear rate, psi.
ϕ	Angle, defined in Section 2.1, deg.
ϕ_t	Thermal reduction factor.
ϕ_s	Ellipticity factor.
ψ	Load zone, deg.
ψ_o	Angle, defined in Figure 7, deg.
ψ_n	Angular position of any roller measured from maximum loaded roller, deg.

NOMENCLATURE

- ω Angular speed of shaft, radians/sec.
- ω_c Angular speed of cage, radians/sec.
- ω_r Angular speed of roller about its own center, radians/sec.

1. INTRODUCTION

1.1 Objective

The objective of this program is to develop a high speed tapered roller bearing capable of operating at a speed of 3.5 million DN under 5000 pounds thrust load. For the 4.25" (107.95 mm) bore bearing to be tested, this is a shaft speed of 32,422 RPM. It is the first program to determine the feasibility of using a tapered roller bearing in a turbine engine environment of high speed and temperature combined with moderate thrust and negligible radial loading.

1.2 Current Technology

Development of high speed tapered roller bearings commenced approximately four years ago (1969) at The Timken Company in conjunction with Boeing-Vertol. The program goals were to develop spiral bevel gear support bearings for use in helicopter transmissions. The bearings ranged in bore sizes from 3.5" (88.9 mm) to 5.11" (125.8 mm). These were tested successfully to 1.4 and 1.8 million DN, respectively.

The problems encountered during development testing were not of the usual nature of high speed ball and cylindrical roller bearings. Review of the open literature indicated that the minimization or control of roller/cage slip

(deviation from epicyclic motion) was the prime objective in ball and cylindrical roller bearing development whereas, the tapered roller bearings did not exhibit any detectable slip. The prime problem encountered was maintaining a supply of lubricant to the cone thrust rib. Various devices were used in an effort to supply the oil to the rib. Some of these are documented in Ref. 1. The most successful technique was to provide a second source of lubricant supply at the cone large rib. This system design will be incorporated in the test program.

1.3 Analytical Approach

This report represents the analytical studies conducted prior to hardware tests. Existing and new technology have been combined to form a comprehensive study of bearing parameters under high speed operation. Note: Throughout the remaining text of this report the term "bearings" will refer to tapered roller bearings.

In Section 2, bearing nomenclature and geometry are defined. Two cage designs, roller and race guided, are presented. Whether the standard stamped roller guided cage has sufficient strength to withstand inertia stresses will be determined in initial testing.

Section 3 covers material requirements and selection for the test bearings. Effects of interference fit and inertia stresses are described analytically in Section 4.

Sections 5 through 11 represent the formulation of speed, load, stress, deformation, EHD and frictional effects.

The analysis of the cone large rib lubrication system (second source of lubricant) from a design and effectiveness standpoint is given in Section 12.

Discussion and results of analytical studies conducted on the candidate test bearing for this current program are presented in Section 13.

2. BEARING GEOMETRY

2.1 Geometrical Relationships

Based on basic principles of plane geometry we can derive the following useful formulae:

$$\text{Roller apex length} = L_2 = \frac{d_1}{2 \sin v} \quad (\text{Fig. 1}) \quad (2.01)$$

$$\text{Cone base diameter} = D_3 = 2L_2 \sin \beta \quad (\text{Fig. 2}) \quad (2.02)$$

$$\text{Roller slant length} = L_1 = \frac{d_1 - d_2}{2 \sin v} \quad (\text{Fig. 3}) \quad (2.03)$$

$$\text{Mean cone OD} = D_2 = \frac{d \sin \beta}{\sin v} \quad (\text{Fig. 2}) \quad (2.04)$$

$$\text{Mean cup ID} = D_5 = \frac{d \sin \alpha}{\sin v} \quad (\text{Fig. 2}) \quad (2.05)$$

$$\begin{aligned} &\text{Height of roller-end/rib contact center, measured} \\ &\text{perpendicular to cone-race} = h = r(\sin \phi + \cos \theta) \end{aligned} \quad (2.06)$$

$$\text{where, } \phi = \left[\sin^{-1} \left(\frac{d_1}{2r} \right) - v \right] \quad (2.07)$$

and θ = rib-race angle

Diameter of roller-end rib contact center measured perpendicular to bearing centerline

$$d_3 = D_3 + 2h \left(\frac{\sin(\theta - \beta)}{\sin \theta} \right)$$

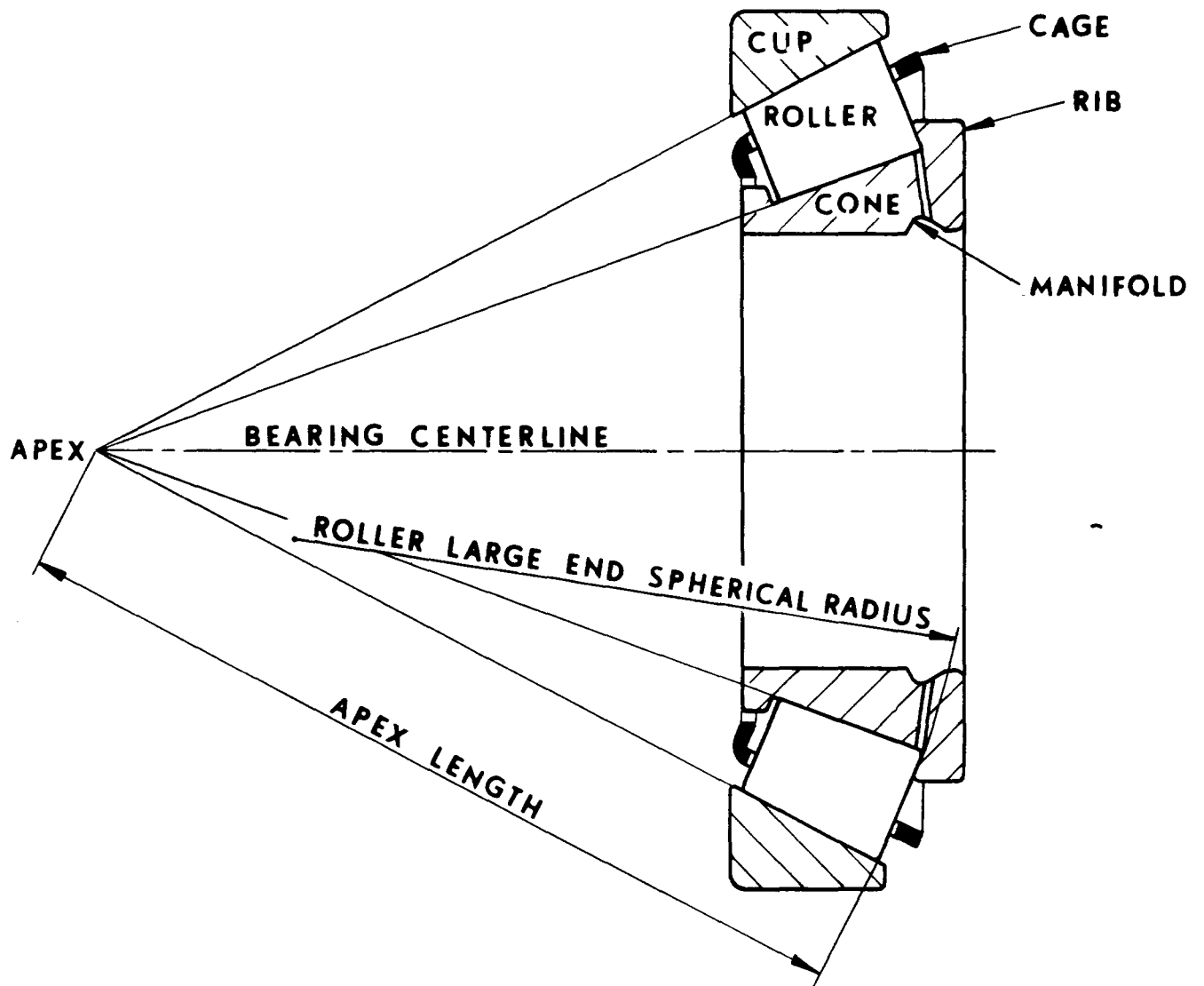


Figure 1 - Typical Tapered Roller Bearing

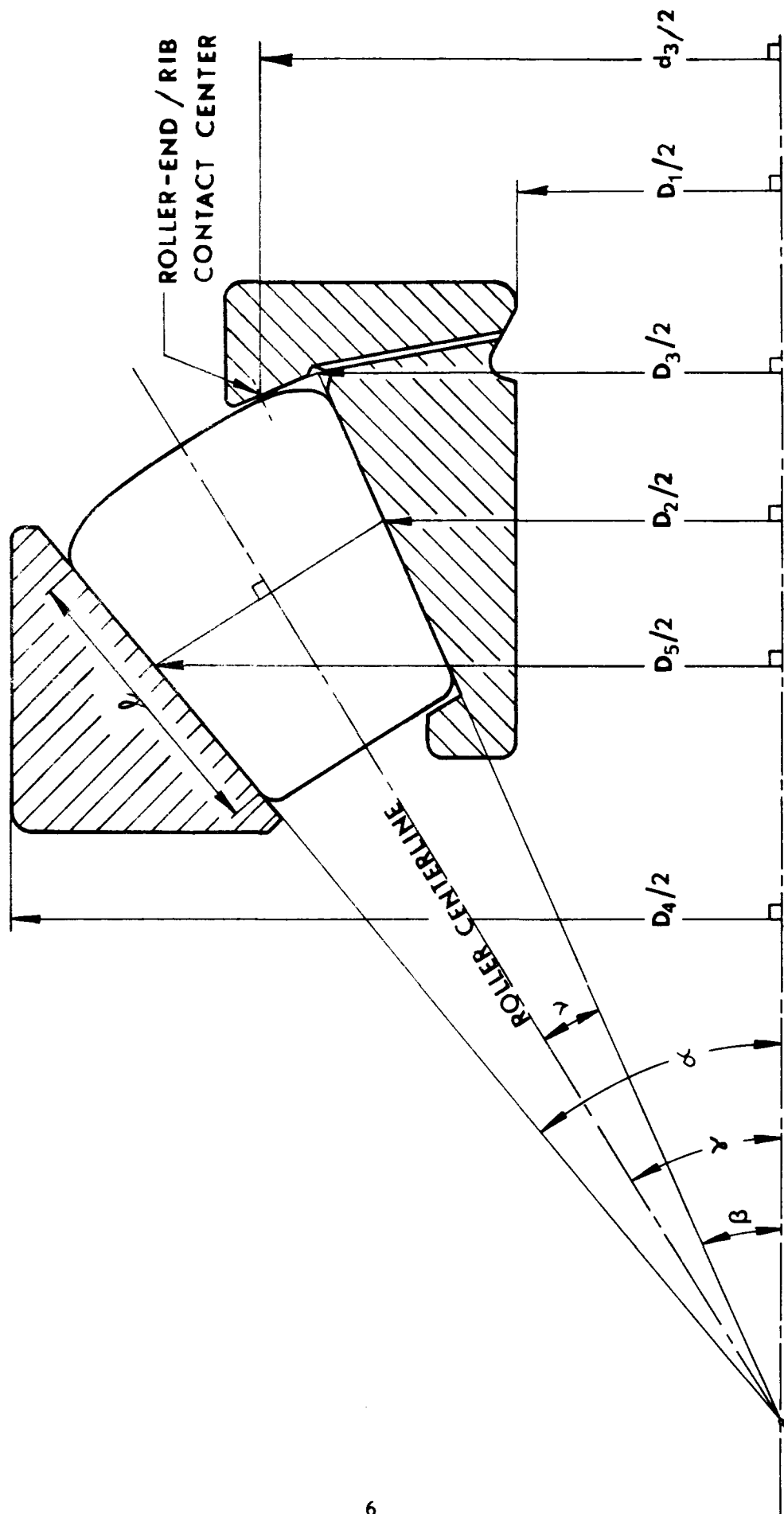


Figure 2 - Bearing Symbols

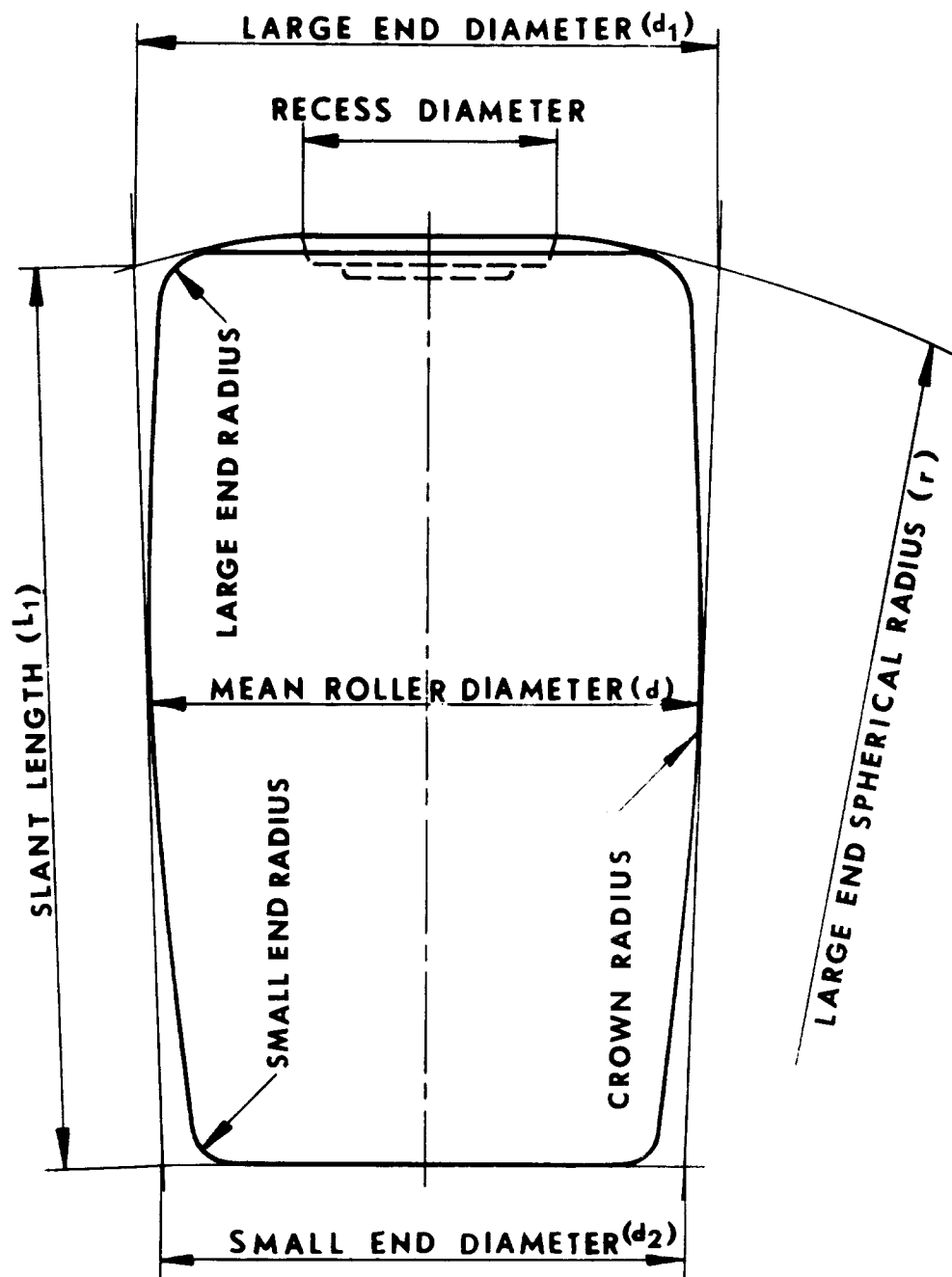


Figure 3 - Typical Tapered Roller

Height of roller c.g. measured perpendicular to the
plane of roller large end = h_{cg}

$$h_{cg} = \frac{L_1 \cos v}{4} \left[\frac{d_1^2 + 2d_1d_2 + 3d_2^2}{d_1^2 + d_1d_2 + d_2^2} \right] \quad (2.09)$$

Radial distance of roller c.g. measured perpendicular
to bearing center = $r_{cg} = (L_2 \cos v - h_{cg}) \sin \gamma$ (2.10)

2.2 Cage

Two types of cage design are considered for this bearing. These are the standard stamped design that guide on the roller bodies and the race guided type, which is piloted to either/or both races and the shaft and/or housing. The sole function of both of these cage designs is to maintain roller spacing. Throughout the remaining text these will be referred to as roller or race guided.

Figure 4 shows the roller guided cage. Unless cage breakage occurs, this will be the design used exclusively in the test program. Estimates of the tensile hoop stress at 3.5 million DN indicate the cage will be operating at 20,000 psi, which is near the tensile yield stress for the material. For calculations of fluid drag, the contact arc is considered to be projection of the wing length of the roller body.

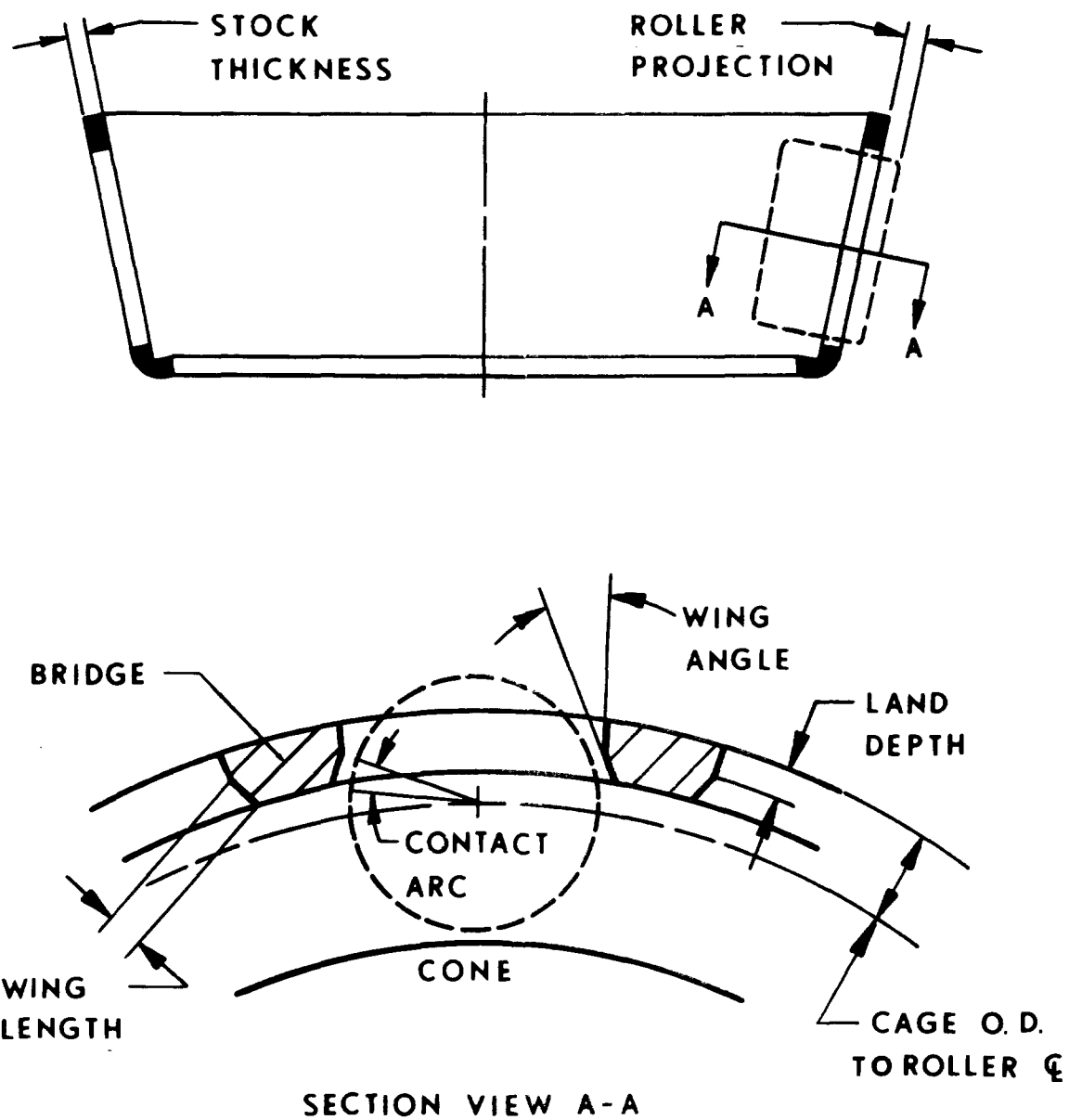


Figure 4 - Nomenclature and Geometry
of Typical Roller Guided
Cage

Figure 5 is a drawing of the race guided cage. The design shown is piloted on the cone large rib O.D. and a spacer abutting the cup backface. This "Z" configuration allows oil jets to be directed at the small end of the roller and eliminates excessive lubricant churning at the large end. Under operating conditions the clearance between the pilots and guide surfaces range from .002" to .008". Fluid drag forces are calculated considering the contact arc to be a projection of the stock thickness on the roller body.

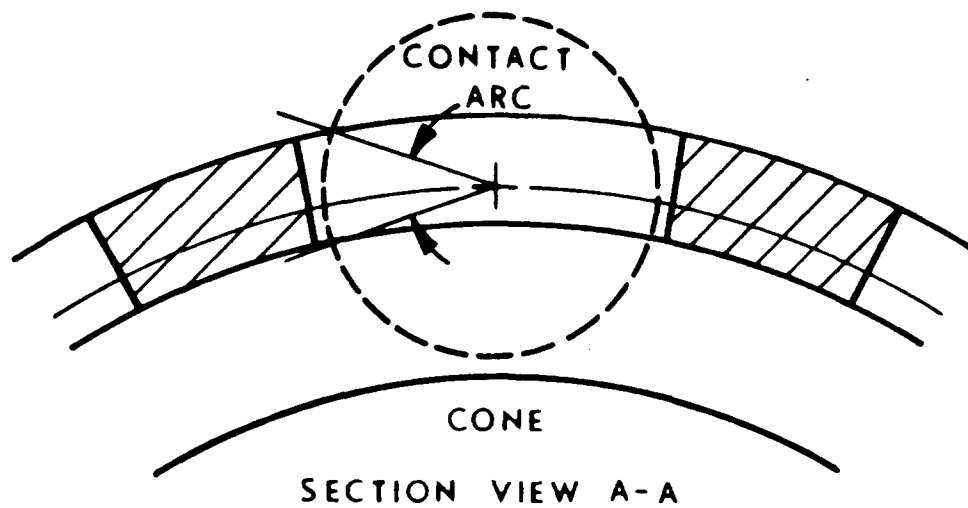
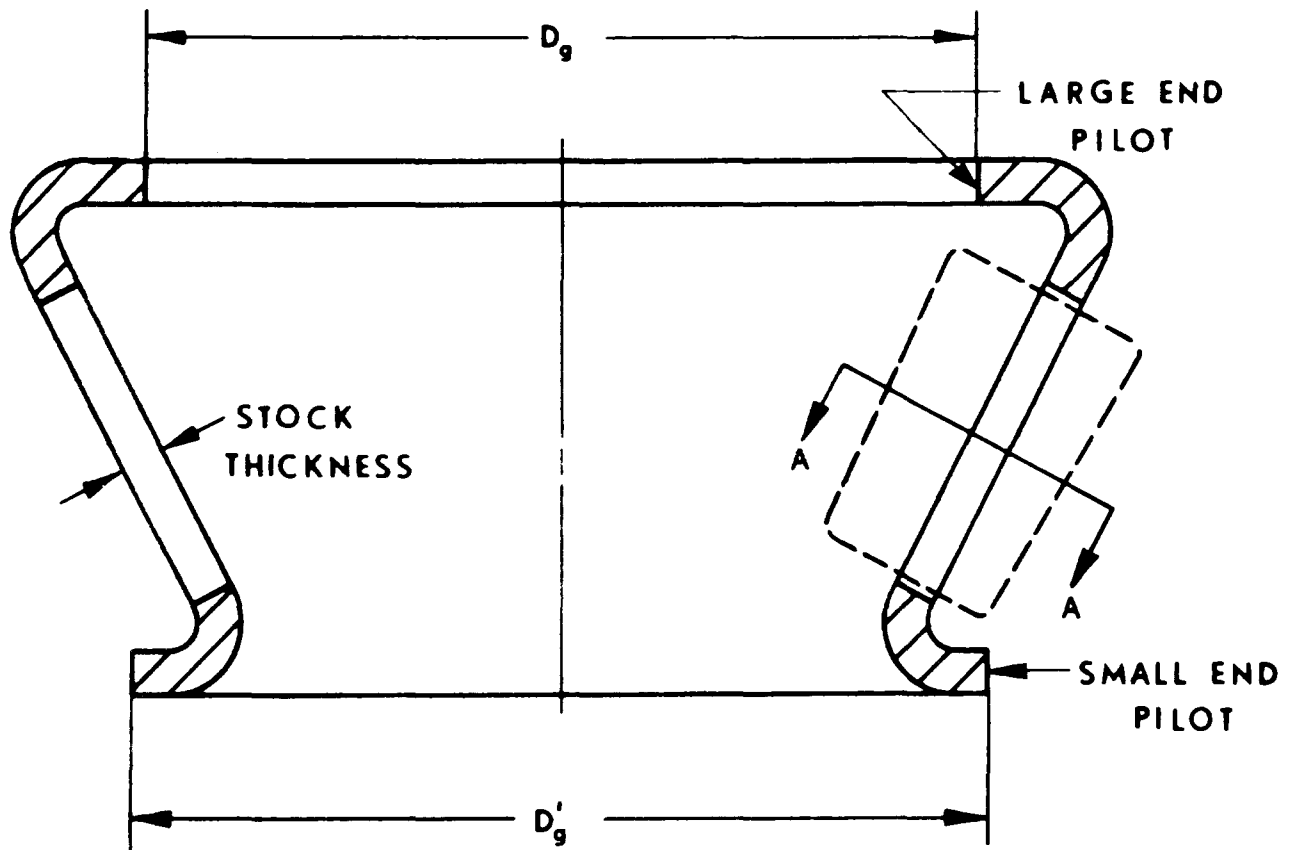


Figure 5 - Nomenclature and Geometry
of Typical Race Guided Cage

3. MATERIAL SELECTION

3.1 Cone, Cup and Roller

The material used in a high-speed tapered roller bearing must satisfy three requirements. Under operating conditions, it must permit the bearing to maintain its structural integrity through resistance to cracking, provide adequate temper resistance and hot hardness, and exhibit resistance to fatigue damage. From a metallurgical standpoint, consumable electrode vacuum melted (CEVM) Timken CBS-1000M carburizing grade of steel meets the above requiremenets.

The bearings will operate with a lubricant supply temperature of 300° F (constant), and lubricant outlet temperature will be in excess of 400° F. Considering these conditions it is reasonable to assume a continuous localized temperature at the rolling or sliding conjunctions in excess of 500° F. The Chemical Analyses and Hot Hardness Characteristics of CBS-600, CBS-1000 and M-50 are shown in Table I and Figure 6, respectively. M-50 is included becuae it has been the most common temper resistant steel used in high speed ball and straight roller bearings. Timken CBS-600 is recommended for continuous service to 500° F with intermittent service to 600° F.

Refer back to any of the figures showing bearing sections and it is readily apparent that the cone creates unique problems

TABLE I

CHEMICAL COMPOSITIONS OF VARIOUS HIGH TEMPERATURE BEARING STEELS

Steel Type	C	Mn	P	S	Si	Cr	Ni	Mo	Cu	Al	V
CBS-600*	.16/.22	.50/.70	.025 Max.	.025 Max.	.90/1.25	1.25/1.65	---	.90/1.10	--	--	----
CBS-1000*	.18/.23	.40/.60	.025 Max.	.025 Max.	.40/.60	.90/1.20	---	4.75/5.25	--	--	.75/1.00
M-50**	.77/.85	.35 Max.	.025 Max.	.025 Max.	.25 Max.	3.75/4.25	.10 Max.	4.00/4.50	--	--	.90/1.10

* Case-Carburized Timken Specification

** Through-Hardened

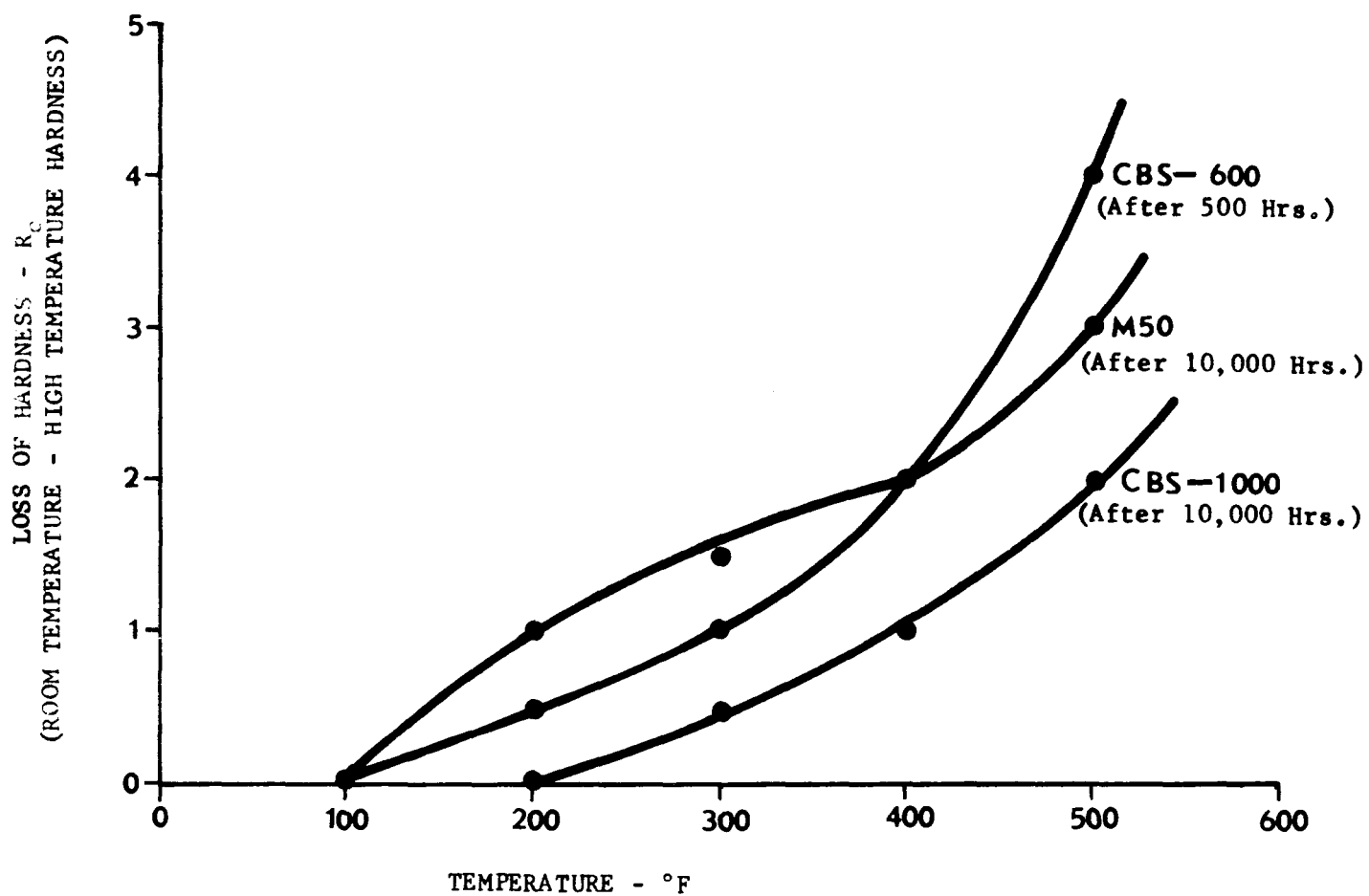


Figure 6 - Hot Hardness Characteristics of Various Bearing Steels

for materials. The standard profile with the large rib and undercut presents a narrow section that is susceptible to cracking and fracture, when produced from through hardened material. The manifold and lubrication ducts add even more stress risers. Other considerations of residual stress distribution and unstable crack extension indicate that a low carbon, case-carburized steel offers the best properties for this application.

The third point is in regard to fatigue resistance. It has been repeatedly demonstrated that CEVM steel will improve bearing life when applied for the express purpose of eliminating nonmetallic inclusion origin fatigue damage. The improvement factor varies a great deal in individual tests but a generally accepted average factor ranges from two to five times improvement over conventional vacuum degassed air melted steel.

A fourth item, not previously mentioned, is that CBS-1000M apparently exhibits greater resistance to scuffing than conventional bearing steels. Admittedly, these test results are limited, however, at higher speeds and boundary lubrication conditions this would be an added advantage. Table II summarizes these test results.

3.2 Cage

Calculations show that tensile hoop stresses due to rotation could reach 20,000 psi at 3.5 million DN with the conventional roller guided stamped steel cages. Provided the effects of

TABLE II

Scuffing Resistance Tests of SAE 4620 Case-Carburized Versus
Timken CBS-1000M Case-Carburized Steel.

T E S T A P P A R A T U S

Timken Extreme Pressure Tester as described in ASTM Standard
D2782. Test cups (1.938" O.D.) in all tests were SAE 4620
case-carburized steel. The test blocks consisted of three (3)
SAE 4620 case-carburized specimens and four (4) CBS-1000M
case-carburized specimens.

P R O C E D U R E

The procedure consisted of applying 1 pound/minute dead weight
to the load lever for ten minutes with the cup rotating at 1165
RPM. Ten pounds lever weight is equivalent to a normal force
of 116.6 pounds or 36,000 psi compressive stress between the
cup and test block. Throughout the load-up cycle and a
subsequent 10 minute run-in period, the sliding conjunction was
lubricated with a stream of MIL-L-23699 oil at 100°F. At this
time, the supply of oil was shut off and any excess was blown
away with shop air. Running time prior to scuffing a scoring
was recorded.

R E S U L T S

<u>Quantity of</u> <u>Test Blocks</u>	<u>Material</u>	<u>Running Time</u> <u>Prior to</u> <u>Scoring</u>
3	4620 Case-Carburized	< 10 sec.
1	CBS-1000M Case-Carburized	2.75 min.
2	CBS-1000M Case-Carburized	4.38 min.
1	CBS-1000M Case-Carburized	7.97 min.

unbalance can be minimized and the pocket corners are carefully formed, an SAE 1010 steel should suffice for this application. If cage breakage occurs, added strength can be obtained from heat treatment and/or surface preparation.

For the machined, race guided cage, a higher carbon steel with greater strength would be used.

4. INTERFERENCE FIT AND INERTIA STRESSES

In the following sections 4.1 through 4.6 the varying sections of cone and cup have been approximated to sleeves of uniform section thickness. The mean cone O.D. and the mean cup I.D. are used in the formulae. The physical properties such as Young's modulus of elasticity, Poisson's ratio and density for shaft, bearing, and housing material are assumed identical and the same as those of steel. In addition, it is assumed that all deformations take place within the proportional limit of the material.

4.1 Contact Pressure (Ref. 2)

Based on standard ring formulae the contact pressures due to interference fit are given below:

Contact pressure, cone/shaft,

$$P_i = \frac{E(D_1^2 - d_o^2)(D_2^2 - D_1^2)}{2D_1^3(D_2^2 - d_o^2)} \delta_i \quad (4.01)$$

Contact pressure, cup/housing,

$$P_o = \frac{E(D_4^2 - D_5^2)(D_o^2 - D_4^2)}{2D_4^3(D_o^2 - D_5^2)} \delta_o \quad (4.02)$$

Where; E = Young's modulus = 30×10^6 psi

4.2 Mean Cone O.D. Increase (Ref. 2)

When the cone is mounted on a shaft with an interference fit, the shaft and cone deform. The increase in cone O.D. can be calculated using the following formula:

$$\delta_1 = \frac{D_2 (D_1^2 - d_o^2)}{D_1 (D_2^2 - d_o^2)} \delta_i \quad (4.03)$$

4.3 Mean Cup I.D. Decrease (Ref. 2)

Similar to increase in cone O.D. due to interference fit, the decrease in cup I.D. is:

$$\delta_2 = \frac{D_5 (D_o^2 - D_4^2)}{D_4 (D_o^2 - D_5^2)} \delta_o \quad (4.04)$$

4.4 Inertia Stresses in Cone (Ref. 3)

At high speed, the cone is subjected to centrifugal force which induces radial and tangential (hoop) stress in the cone. The maximum radial stress in the average section of cone occurs at a radial distance = $.5 (D_1 D_2)^{0.5}$ and is:

$$\sigma_4 = 8.29 \times 10^{-7} S^2 (D_2 - D_1)^2 \quad (4.05)$$

$$\text{where; } 8.29 \times 10^{-7} = \frac{(3+\mu)\rho}{8g} \left(\frac{\pi}{60}\right)^2$$

$$\text{and } \mu = \text{Poisson's ratio} = .3$$

$$\rho = .283 \text{ lb/in.}^3$$

$$g = 386.088 \text{ in./sec}^2$$

Generally, the radial stress is much smaller compared to tangential stress due to rotation and may be neglected for approximate calculations.

The tangential tensile stress due to rotation at any point situated at a radial distance of r_x measured from the bearing centerline is given by the following formula:

$$\tau = 1.005 \times 10^{-6} s^2 \left[\frac{3+\mu}{4} (D_2^2 + D_1^2 + \frac{D_1^2 D_2^2}{4r_x^2}) - (1+3\mu)r_x^2 \right] \quad (4.06)$$

$$\text{where: } 1.005 \times 10^{-6} = \rho \left(\frac{\pi}{30} \right)^2 \frac{1}{8g}$$

The maximum tangential tensile stress in the average section of cone occurs at the perimeter of the cone bore and is given by:

$$\tau_i = 5.024 \times 10^{-7} s^2 \left[(3+\mu)D_2^2 + (1-\mu)D_1^2 \right] \quad (4.07)$$

$$\text{where; } 5.024 \times 10^{-7} = \frac{\rho}{16} \left(\frac{\pi}{30} \right)^2 \frac{1}{g}$$

4.5 Loss of Interference Fit Due to Inertia Stress (Ref. 4)

If the press fitted cone/shaft assembly is rotated at high speeds, both the cone bore and shaft O.D. increase due to inertia stresses. However, the increase in shaft O.D. is less than the increase in cone bore. Consequently, the fit is reduced and the loss of diametral interference fit can be estimated using the formula as given below:

$$\delta_{\text{loss}} = 5.526 \times 10^{-14} s^2 D_1 (D_2^2 - d_o^2) \quad (4.08)$$

$$\text{where; } 5.526 \times 10^{-14} = \left(\frac{\pi}{60} \right)^2 \frac{\rho(3+\mu)}{4gE}$$

4.6 Combined Effects of Interference Fit and Inertia Stresses

The following two formulae assume that the loss of fit (δ_{loss}) is less than the initial interference fit (δ_i) and the effect of thermal expansions is negligible.

effective contact pressure, cone/shaft = P_e

$$p_e = \frac{E}{2} \frac{(D_1^2 - d_o^2) (D_2^2 - D_1^2) (\delta_i - \delta_{loss})}{D_1^3 (D_2^2 - d_o^2)} \quad (4.09)$$

maximum tangential stress in the average section of cone which occurs at cone bore is:

$$\tau_1 = \tau_i + p_e \left(\frac{D_2^2 + D_1^2}{D_2^2 - D_1^2} \right) \quad (4.10)$$

where τ_i is defined in Section 4.4.

5. KINEMATICS AND DYNAMICS

5.1 Epicyclic Speeds

The derivations for RPM of the cage (N_c) and RPM of the roller about its own center (N_r) for the rotating cone and stationary cup condition assume rigid bodies, i.e. the bearing components will maintain exact geometrical shape under operation, and that pure rolling exists at roller-body/cone-race and roller-body/cup-race contacts. In addition, the bearing apex is assumed to be on the bearing centerline.

Under no slip condition, considering roller-body/cone-race contact, the linear tangential velocities for the mean cone O.D. and mean roller diameter can be equated as follows:

$$\pi S D_2 = \pi N_r d + \pi N_c D_2 \quad (5.01)$$

Similarly from roller-body/cup-race contact we can write

$$\pi N_r d = \pi N_c D_5 \quad (5.02)$$

Substitute for $D_2 = \frac{d \sin \beta}{\sin \nu}$; $D_5 = \frac{d \sin \alpha}{\sin \nu}$

(5.01) and (5.02) can be solved for N_c and N_r .

$$N_c = S \cdot \frac{\sin \beta}{\sin \alpha + \sin \beta} \quad (5.03)$$

$$N_r = S \cdot \frac{\sin \alpha \sin \beta}{\sin \nu (\sin \alpha + \sin \beta)} \quad (5.04)$$

5.2 Surface Velocities

Based on S , N_r and N_c various surface velocities can be written as follows:

Tangential velocity of roller-body mid-point with respect to roller centerline,

$$V_1 = \frac{\pi}{60} N_r d$$

Tangential velocity of the point on the roller at roller-end/rib contact center with respect to roller centerline,

$$V_2 = \frac{\pi}{30} N_r (0.5d_1 - h \cos v)$$

where, h is defined in Section 2.1.

Tangential velocity at mean cone O.D. with respect to bearing centerline,

$$V_3 = \frac{\pi}{60} S D_2$$

Rib velocity, i.e. tangential velocity of the point on the rib at roller-end/rib contact center,

$$V_{rib} = \frac{\pi}{60} S d_3$$

where, d_3 is defined in Section 2.1.

5.3 Sliding Velocity

At roller-end/rib contact center, the rib velocity (V_{rib}) is greater than the velocity (about bearing center) of the corresponding mating point on the roller-end and the difference between them is called sliding velocity.

$$V_s = V_{rib} - (V_2 + \frac{\pi}{60} N_c d_3)$$

this can be simplified to

$$V_s = \frac{\pi}{30} \text{ Sh } \left(\frac{\sin \alpha}{\sin 2\psi} \right) \quad (5.09)$$

5.4 Roller Centrifugal Force (Ref. 5)

Approximating the roller to a frustrum of right circular cone the roller weight can be estimated using:

$$w = \frac{\pi}{12} \rho L_1 \cos \psi (d_1^2 + d_1 d_2 + d_2^2) \quad (5.10)$$

Centrifugal force per roller which acts through the center of gravity can be computed as:

$$C_F = \frac{w}{g} \left(\frac{\pi}{30} N_c \right)^2 r_{cg} \quad (5.11)$$

where, r_{cg} is defined in Section 2.1 and represents the radial distance of roller c.g. from bearing centerline.

N_c is RPM of cage and given in Section 5.1.

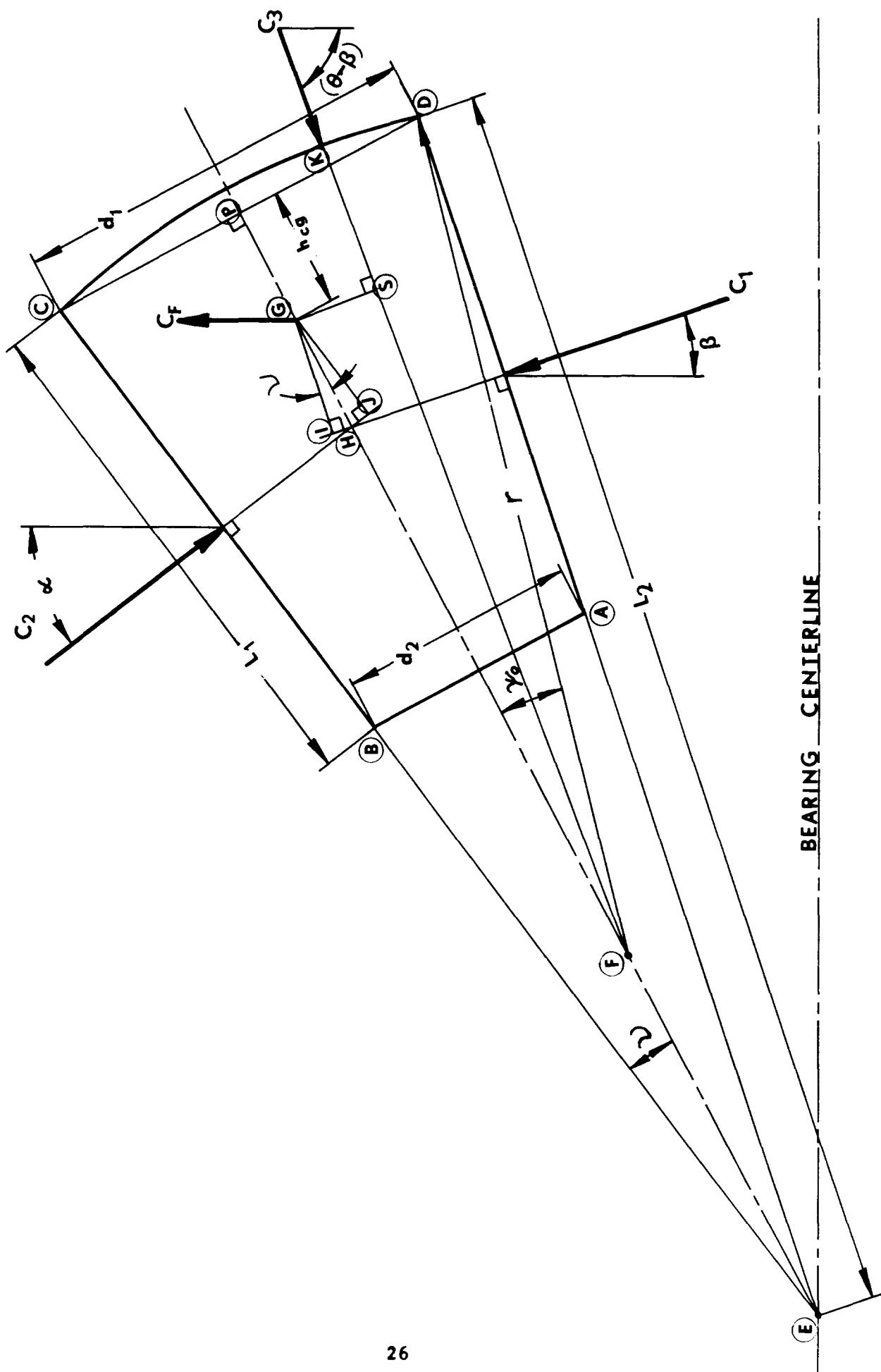
5.5 Normal Load Components Due to Roller Centrifugal Force

When a bearing is rotated at a constant high speed the roller centrifugal force becomes quite significant and as a consequence the cone and cup tend to separate from each other. However, if an external thrust equal to induced thrust due to roller centrifugal force (defined in Section 5.6) is applied to the bearing, the three normal load components acting on the roller can be estimated using three equations of equilibrium, namely $\Sigma F_x = 0$, $\Sigma F_y = 0$ and $\Sigma M = 0$.

Some of the assumptions are as follows:

1. All bearing components behave like a rigid body.
2. The normal loads, roller-body/cone-race and roller-body/cup-race, are uniformly distributed along the entire effective contact length.
3. The normal load, roller-end/rib passes through the center of spherical radius at the roller-end.
4. There is no bearing misalignment.

Figure 7 shows a schematic representation of three normal loads due to roller centrifugal force.



Based on the principals of plane geometry the following equations may be written:

$$\textcircled{E} \textcircled{P} = L_2 \cos v$$

$$\textcircled{E} \textcircled{H} = (L_2 - L/2) \cos v$$

$$\textcircled{H} \textcircled{I} = \textcircled{H} \textcircled{J}$$

$$\textcircled{G} \textcircled{J} = \textcircled{G} \textcircled{I} = \textcircled{H} \textcircled{I} / \tan v$$

$$\text{let } \textcircled{G} \textcircled{J} = A$$

$$\textcircled{F} \textcircled{G} = r \cos \psi_o - h_{cg}$$

$$\text{where } \psi_o = \sin^{-1} (d_1/2r)$$

By referring to Figure 8 it can be seen that

$$\begin{aligned} \angle \textcircled{G} \textcircled{F} \textcircled{S} &= v - (\pi/2 - \theta) \\ &= \theta + v - \pi/2 \end{aligned}$$

$$\text{Hence, } \textcircled{G} \textcircled{S} = \textcircled{F} \textcircled{G} \sin (\theta + v - \pi/2)$$

$$\text{let } \textcircled{G} \textcircled{S} = B$$

Now, considering the vertical components of all forces on the roller, we can write:

$$C_2 \cos \alpha + C_3 \cos (\theta - \beta) - C_1 \cos \beta = C_f \quad (5.12)$$

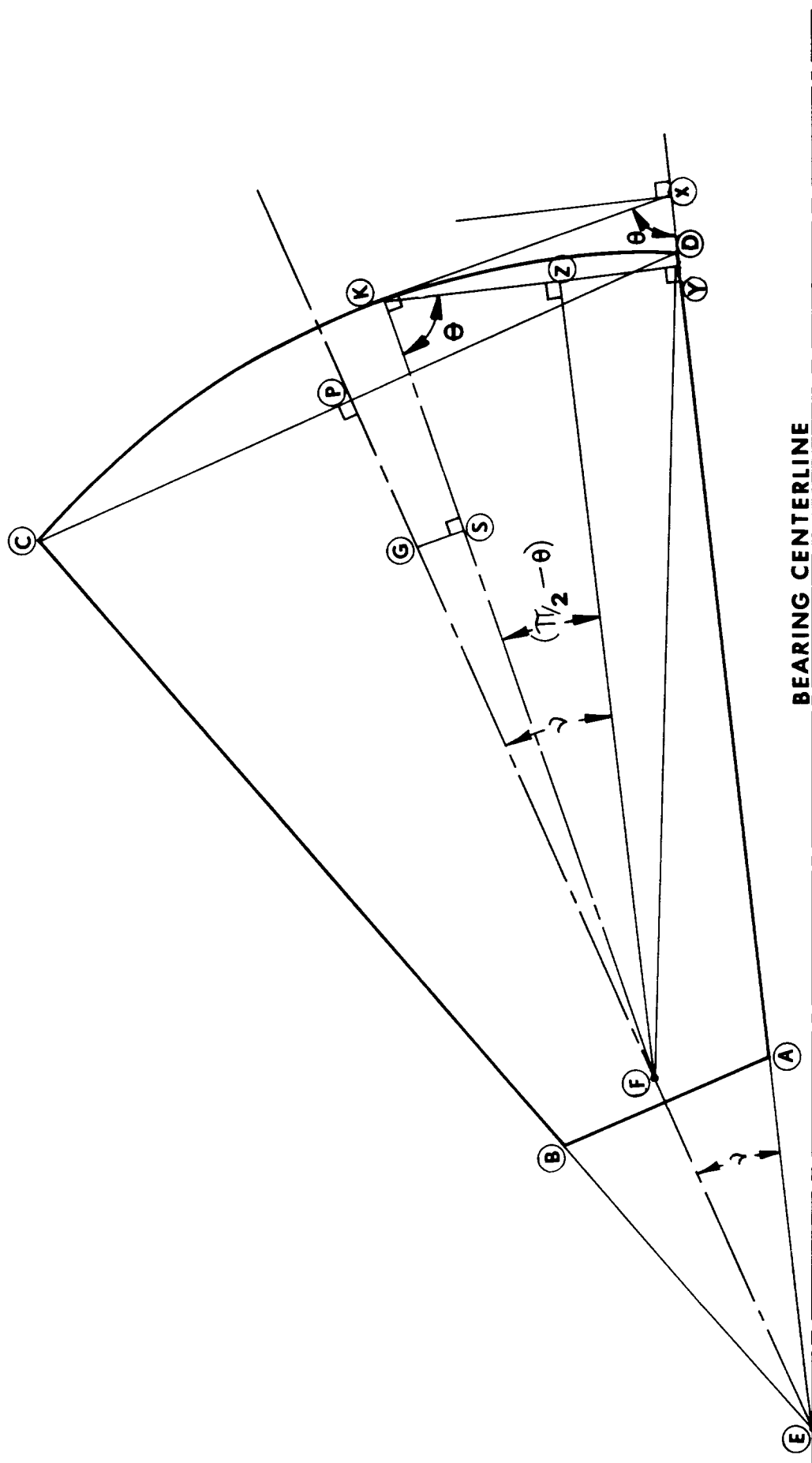


Figure 8 - Enlarged Roller Schematic

Similarly, summation of all horizontal components gives:

$$C_2 \sin \alpha - C_3 \sin (\theta - \beta) - C_1 \sin \beta = 0 \quad (5.13)$$

Finally, taking moment about c.g. of the roller we get

$$C_2 \textcircled{G} \textcircled{J} - C_3 \textcircled{G} \textcircled{S} - C_1 \textcircled{G} \textcircled{I} = 0$$

i.e. $C_2 - C_3 (B/A) - C_1 = 0 \quad (5.14)$

Equations (5.12), (5.13) and (5.14) can be solved simultaneously for C_1 , C_2 and C_3 as follows:

$$\begin{aligned} \text{let } D &= \begin{vmatrix} \cos \alpha & \cos (\theta - \beta) & -\cos \beta \\ \sin \alpha & -\sin (\theta - \beta) & -\sin \beta \\ 1 & -B/A & -1 \end{vmatrix} \\ &= \cos \alpha (\sin (\theta - \beta) - (B/A) \sin \beta) - \sin \alpha (-\cos (\theta - \beta) - (B/A) \cos \beta) \\ &\quad + (-\sin \beta \cos (\theta - \beta) - \cos \beta \sin (\theta - \beta)) \\ &= \cos \alpha (\sin (\theta - \beta) - (B/A) \sin \beta) + \sin \alpha (\cos (\theta - \beta) + (B/A) \cos \beta) \\ &\quad - \sin \theta \\ &= \sin (\alpha + \theta - \beta) + (B/A) \sin (\alpha - \beta) - \sin \theta \\ &\quad (\alpha - \beta = 2v) \\ &= \sin (\theta + 2v) + (B/A) \sin (2v) - \sin \theta \end{aligned} \quad (5.15)$$

$$\begin{aligned} \text{let } D_{11} &= \begin{vmatrix} \cos \alpha & \cos (\theta - \beta) & C_F \\ \sin \alpha & -\sin (\theta - \beta) & 0 \\ 1 & -B/A & 0 \end{vmatrix} \\ &= C_F [\sin (\theta - \beta) - (B/A) \sin \alpha] \end{aligned} \quad (5.16)$$

$$\begin{aligned}
D_{12} &= \begin{bmatrix} C_F & \cos (\theta-\beta) & -\cos \beta \\ 0 & -\sin (\theta-\beta) & -\sin \beta \\ 0 & -B/A & -1 \end{bmatrix} \\
&= C_F \begin{bmatrix} \sin (\theta-\beta) - (B/A) \sin \beta \end{bmatrix}
\end{aligned} \tag{5.17}$$

$$D_{13} = C_F (\sin \alpha - \sin \beta) \tag{5.18}$$

If $D = 0$, we can say

$$C_1 = D_{11}/D \tag{5.19}$$

$$C_2 = D_{12}/D \tag{5.20}$$

$$C_3 = D_{13}/D \tag{5.21}$$

Evaluation of the above equations results in a negative normal load (C_1) at the roller-body/cone-race contact. This cannot physically exist and equations (5.12) and (5.13) may be rewritten by dropping the terms containing C_1 .

Therefore,

$$C_2 \cos \alpha + C_3 \cos (\theta-\beta) = C_F \tag{5.22}$$

$$C_2 \sin \alpha - C_3 \sin (\theta-\beta) = 0 \tag{5.23}$$

$$\begin{aligned}
\text{i.e. } C_2 \left[\frac{\cos \alpha}{\cos (\theta-\beta)} + \frac{\sin \alpha}{\sin (\theta-\beta)} \right] &= \frac{C_F}{\cos (\theta-\beta)} \\
C_2 \left[\frac{\sin (\theta-\beta) \cos \alpha + \cos (\theta-\beta) \sin \alpha}{\sin (\theta-\beta) \cos (\theta-\beta)} \right] &= \frac{C_F}{\cos (\theta-\beta)}
\end{aligned}$$

$$C_2 \left[\frac{\sin (\theta-\beta+\alpha)}{\sin (\theta-\beta)} \right] = C_F$$

$$C_2 = C_F \left[\sin (\theta-\beta) / \sin (\theta+2v) \right] \quad (5.24)$$

$$C_3 = C_F \left[\sin \alpha / \sin (\theta+2v) \right] \quad (5.25)$$

5.6 Induced Thrust Due to Roller Centrifugal Force

The summation of axial component of normal load, roller-body/cup-race, for all rollers may be called induced thrust due to roller centrifugal force. Using the equation (5.20) or (5.24) for C_2 the induced thrust is given by the following formula:

$$T_i = z C_2 \sin \alpha \quad (5.26)$$

where: z = number of rollers

5.7 Moments of Inertia of Roller (Ref. 5 and 6), (Fig. 9)

Based on the standard formulae for moments of inertia for a solid right circular cone and using the parallel-axis theorem, we can write the moments of inertia for a tapered roller about axes through the center of gravity as follows:

$$I_x = \frac{3w}{40} \frac{(d_1^5 - d_2^5)}{d_1^3 - d_2^3} \quad (5.27)$$

$$I_x = \frac{I_x}{2} + \frac{w}{10} (L_1 \cos v)^2 \left[\frac{d_2^2 + 3d_1 d_2 + 6d_1^2}{d_1^2 + d_1 d_2 + d_2^2} - \frac{5}{8} \left\{ \frac{d_2^2 + 2d_1 d_2 + 3d_1^2}{d_1^2 + d_1 d_2 + d_2^2} \right\}^2 \right] \quad (5.28)$$

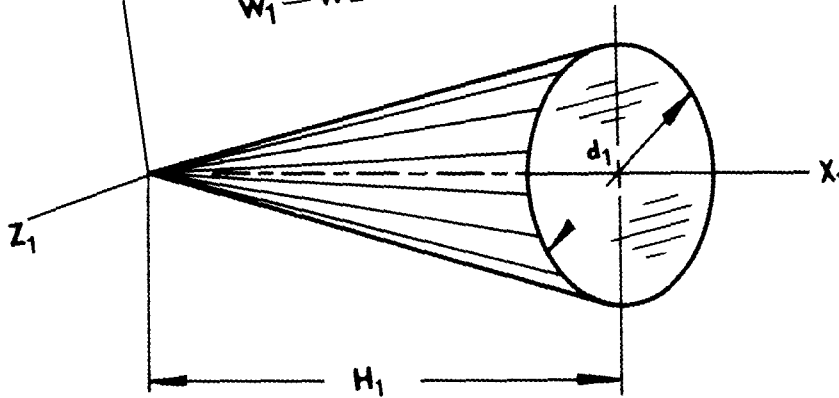
5.8 Gyroscopic Couple (Ref. 7)

The geometrical configuration of the tapered roller bearing gives rise to an inertia couple called gyroscopic couple which influences the distribution of the normal load at the roller-body/race contact. The direction of this couple is such that it tends to make the large end of the roller dig into the

$$I_{x_1} = \frac{3}{40} w_1 d_1^2$$

$$I_{y_1} = \frac{I_{x_1}}{2} + \frac{3W_1 H_1^2}{5}$$

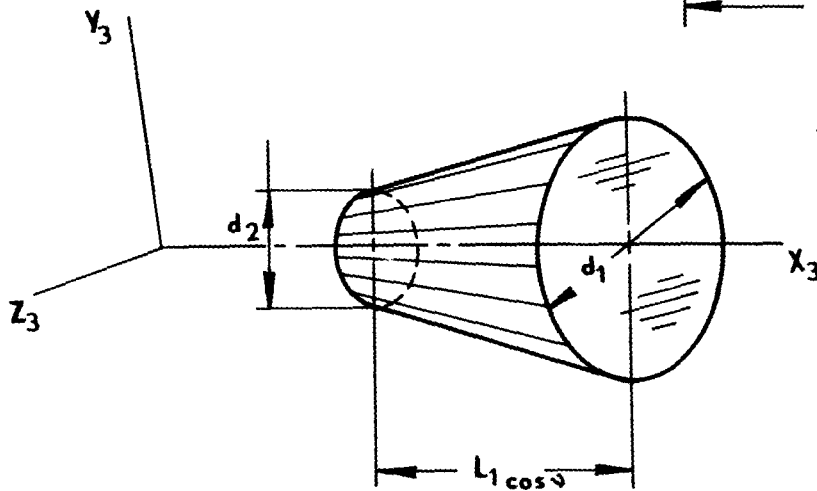
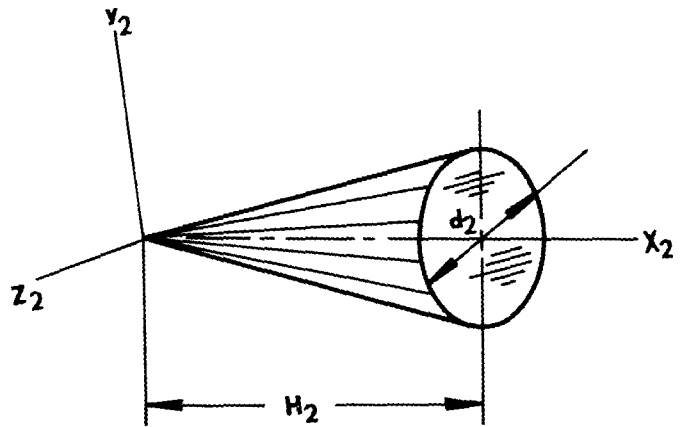
$W_1 = \text{WEIGHT OF CONE}$



$$I_{x_2} = \frac{3}{40} w_2 d_2^2$$

$$I_{y_2} = \frac{I_{x_2}}{2} + \frac{3W_2 H_2^2}{5}$$

$W_2 = \text{WEIGHT OF CONE}$



$$L_1 \cos v = H_1 - H_2$$

$$I_{x_3} = I_{x_1} - I_{x_2}$$

$$I_{y_3} = I_{y_1} - I_{y_2}$$

$$I_x = \text{EQUATION (5.27)}$$

$$I_y = \text{EQUATION (5.28)}$$

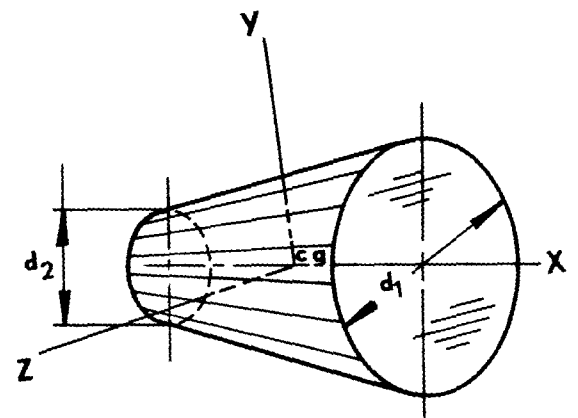


Figure 9 - Mass Moments of Inertia

cup-race and the small end into the cone-race. The magnitude of the couple is:

$$M_g = 2.84 \times 10^{-5} \left[\frac{(I_y - I_x)}{2} N_c^2 \sin 2\gamma + I_x N_r N_c \sin \gamma \right] \quad (5.29)$$

$$\text{where, } 2.84 \times 10^{-5} = \left(\frac{\pi}{30}\right)^2 \cdot \frac{1}{g}$$

5.9 Combined Effect of Roller Centrifugal Force and Gyroscopic Couple

In Section 5.5 we stated that for most of standard tapered roller bearing designs the cone-race would not support roller centrifugal force and equations (5.24) and (5.25) for normal loads, roller-body/cup-race (C_2) and roller-end/rib (C_3), were derived using $\Sigma F_y = \Sigma F_x = 0$. Now, based on this assumption the effects of gyroscopic couple may be superimposed on C_2 and load intensities q_1 and q_2 may be determined as follows:

Referring to Figures 7, 10 and 11 and taking moments about roller c.g. we get

$$C_2 (\textcircled{G} \textcircled{J} + \Delta X) + M_g = C_3 \textcircled{G} \textcircled{S}$$

Rearranging the terms,

$$\Delta X = (C_3 \textcircled{G} \textcircled{S} - M_g) / C_2 - \textcircled{G} \textcircled{J} \quad (5.30)$$

let $\textcircled{G} \textcircled{S} = B$ and $\textcircled{G} \textcircled{J} = A$ as defined in section 5.5

$$\Delta X = \frac{(C_3 B - M_g)}{C_2} - A \quad (5.31)$$

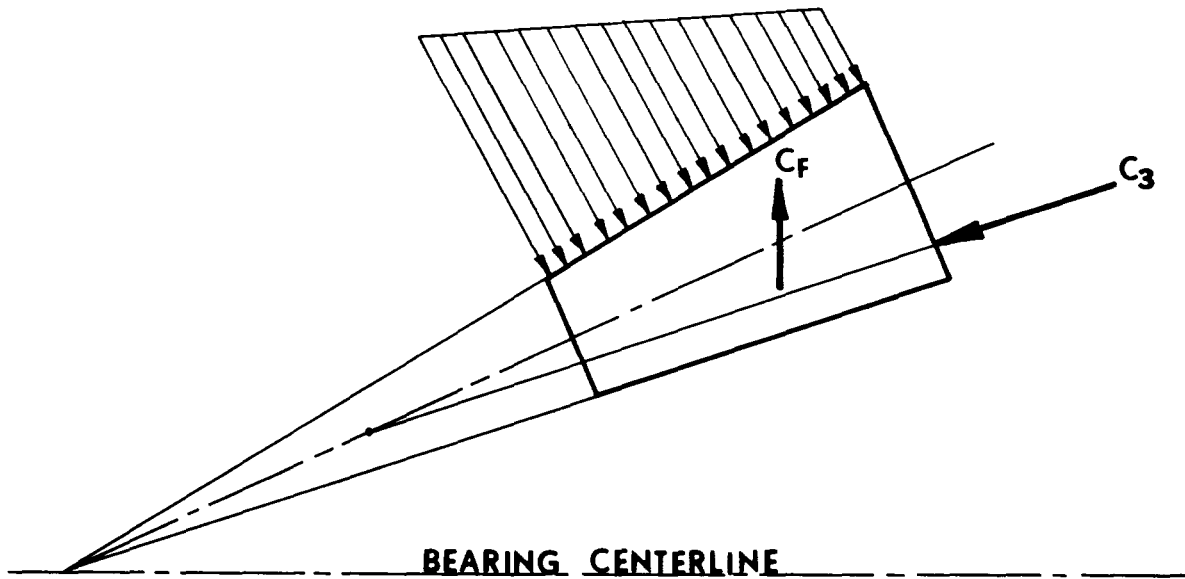


Figure 10 - Roller-Body/Cup-Race Load Due to Centrifugal Force

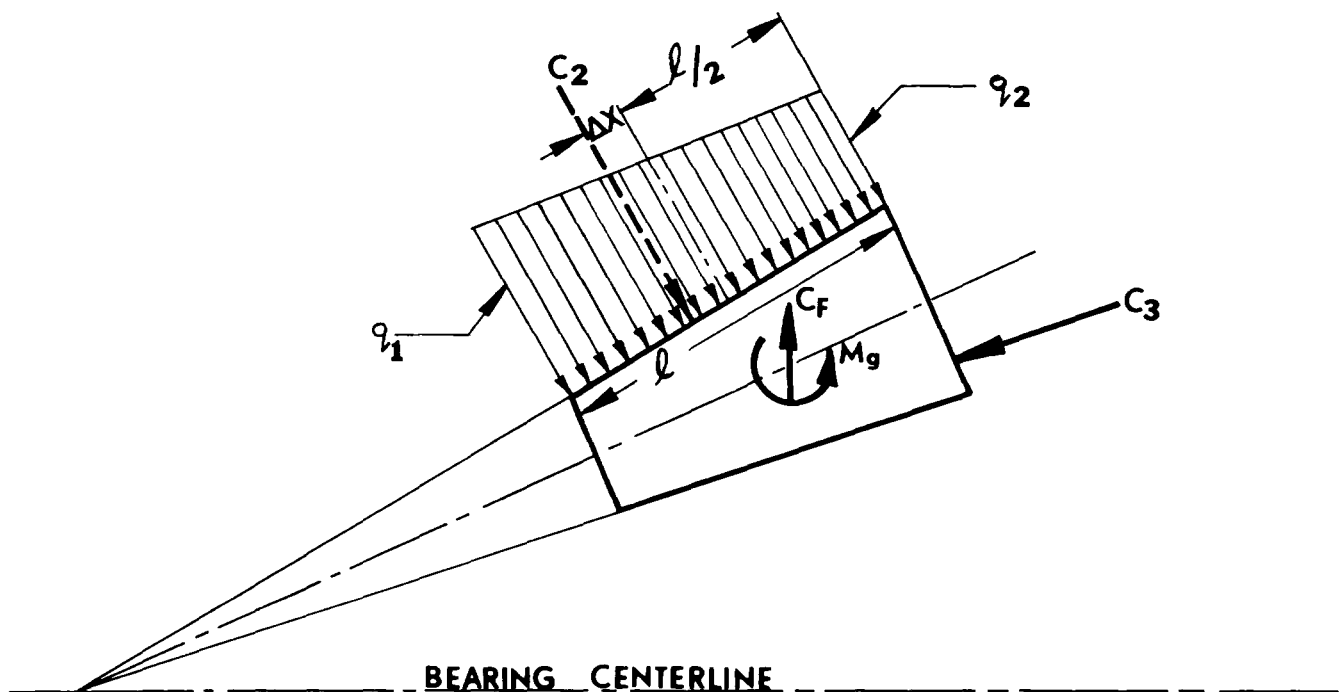


Figure 11 - Roller Loads Due to Both Centrifugal Force and Gyroscopic Couple

Assuming that normal load C_2 varies along the effective contact length (ℓ) linearly and using the formula for center of gravity of a plane trapezoid would yield the following two relationships

$$\Delta X = \frac{\ell}{2} - \frac{\ell(q_1 + 2q_2)}{3(q_1 + q_2)} = \frac{\ell}{2} \left[\frac{q_1 - q_2}{3(q_1 + q_2)} \right] \quad (5.32)$$

$$\text{and } (q_1 + q_2) \ell = 2C_2 \quad (5.33)$$

Substituting for ΔX from equation (5.32) in equation (5.31) we obtain,

$$\frac{\ell}{2} \left[\frac{q_1 - q_2}{3(q_1 + q_2)} \right] = \frac{(C_3 B - M_g)}{C_2} - A \quad (5.34)$$

Now, equations (5.33) and (5.34) can be solved simultaneously for q_1 and q_2 .

From equation (5.33)

$$q_1 = \frac{2C_2}{\ell} - q_2 \quad (5.35)$$

Substituting this in equation (5.34) we get

$$\begin{aligned} \frac{\ell}{2} \left[\frac{(C_2/\ell - q_2)}{3C_2/\ell} \right] &= \frac{C_3 B - M_g}{C_2} - A \\ \text{i.e. } \frac{\ell}{6} - \frac{q_2 \ell^2}{6C_2} &= \frac{C_3 B - M_g}{C_2} - A \\ \therefore q_2 &= \frac{6C_2}{\ell^2} \left[\frac{\ell}{6} - \frac{C_3 B - M_g}{C_2} + A \right] \\ \text{i.e. } q_2 &= \frac{C_2}{\ell} \left[1 - \frac{6}{\ell} \frac{C_3 B - C_2 A}{C_2} \right] + \frac{6 M_g}{\ell^2} \end{aligned} \quad (5.36)$$

Substituting for q_2 in equation (5.35) gives

$$q_1 = \frac{2C_2}{\ell} - \frac{C_2}{\ell} \left[1 - \frac{6}{\ell} \left(\frac{C_3^B - C_2^A}{C_2} \right) \right] - \frac{6 M_g}{\ell^2}$$

$$\text{i.e. } q_1 = \frac{C_2}{\ell} \left[1 + \frac{6}{\ell} \left(\frac{C_3^B - C_2^A}{C_2} \right) \right] - \frac{6 M_g}{\ell^2} \quad (5.37)$$

6. LOAD DISTRIBUTION UNDER EXTERNAL LOAD

6.1 Thrust Load

If the bearing is subjected to a thrust load only, all rollers are equally loaded under ideal conditions of operation. From conditions of equilibrium and considering the roller centrifugal force, the three normal load components can be calculated as follows:

$$\text{Normal Load, roller-body/cone-race} = P_1 = C_1 + \frac{T - T_i}{z \sin \alpha} \cos 2\psi \quad (6.01)$$

$$\text{Normal Load, roller-body/cup-race} = P_2 = \frac{T}{z \sin \alpha} \quad (6.02)$$

$$\text{Normal Load, roller-end/rib} = P_3 = C_3 + \frac{(T - T_i)}{z \sin \alpha} \sin 2\psi \quad (6.03)$$

where T = external bearing thrust

C_1, C_3, T_i are defined in Sections 5.5 and 5.6.

Above equations are based on the assumption that rib-race angle is, $\theta = 90^\circ$.

6.2 Combined Radial and Thrust Load (Ref. 8)

When a bearing is subjected to a radial and a centric thrust load, the cone and cup will remain parallel and will be relatively displaced in both axial and radial directions.

Under such conditions, the bearing is essentially of statically indeterminate design and the load distribution within the bearing may be estimated using Sjovall's integrals and load zone parameter ϵ . The step-wise procedure is as follows:

1. For a given speed, calculate the normal loads (C_1, C_2, C_3) and induced thrust (T_i) due to roller centrifugal force using the formulae given in Sections 5.5 and 5.6.
2. Corresponding to the given radial load and reduced thrust ($T - T_i$), calculate $\frac{R \tan \alpha}{T - T_i}$ and using the following Table III determine J_R and ϵ .
3. Approximating the roller-body/race contacts to a line contact for any roller situated in an angle of ψ_n (measured from the maximum loaded roller) the three normal loads may be estimated using the following formulae:

Normal load roller-body/cone-race,

$$P_1 = C_1 + P_{\max} \cos 2\psi \left[1 - \frac{1}{2\epsilon} (1 - \cos \psi_n) \right]^{1.1} \quad (6.04)$$

Normal load roller-body/cup-race,

$$P_2 = C_2 + P_{\max} \left[1 - \frac{1}{2\epsilon} (1 - \cos \psi_n) \right]^{1.1} \quad (6.05)$$

Normal load roller-end/rib,

$$P_3 = C_3 + P_{\max} \sin 2\psi \left[1 - \frac{1}{2\epsilon} (1 - \cos \psi_n) \right]^{1.1} \quad (6.06)$$

$$\text{In the above equations } P_{\max} = \frac{R}{zJ_R \cos \alpha} \quad (6.07)$$

TABLE III

J_R, J_T, ϵ vs. $\frac{R \tan \alpha}{T-T_i}$ for Line Contact

$\frac{R \tan \alpha}{T-T_i}$	J_R	J_T	ϵ
1	1/z	1/z	0
0.9215	0.1737	0.1885	0.2
0.8805	0.2055	0.2334	0.3
0.8380	0.2286	0.2728	0.4
0.7939	0.2453	0.3090	0.5
0.7480	0.2568	0.3433	0.6
0.6999	0.2636	0.3766	0.7
0.6486	0.2658	0.4098	0.8
0.5920	0.2628	0.4439	0.9
0.5238	0.2523	0.4817	1.0
0.3598	0.2078	0.5775	1.25
0.2340	0.1583	0.6790	1.67
0.1372	0.1075	0.7837	2.5
0.0611	0.0544	0.8909	5
0	0	1	

7. CONTACT STRESSES

The contact stresses caused by the normal loads at all three conjunctions in the bearing can be calculated using Hertz theory. Some of the basic assumptions are that the material is homogeneous, isotropic, and elastic in accordance with Hooke's law. The formulae for contact stresses for roller-body/cone-race and roller-body/cup-race given in the following sections are based on infinitely long cylinders, hence, the effects of end-stress are not considered. The formulae (7.01) and (7.02) are essentially the same as given in Ref. 3 and the derivations for equivalent radii are included in Section 9.2. In all three following sections dry contact between the bodies was assumed, i.e., effects of lubricant film at contacts were neglected.

7.1 Roller-body/Cone-Race

Contact stress at center of roller-body/cone-race contact.

$$\sigma_1 = .591 \left[\frac{30 P_1 \sin \gamma}{l d \sin \beta} \right]^{0.5} \quad (7.01)$$

Assumptions: Modulus of Elasticity = 30×10^6 psi

Poisson's Ratio = .3

7.2 Roller-Body/Cup-Race

Contact stress at center of roller-body/cup-race contact

$$\sigma_2 = .591 \left[\frac{30 P_2 \sin \gamma}{l d \sin \alpha} \right]^{0.5} \quad (7.02)$$

7.3 Roller-End/Cone Rib (Ref. 9)

The roller-end/rib contact can be represented by two general solid bodies in point contact and the Hertz equations can be used to estimate maximum contact stress at the center of ellipse. An important assumption is made that the ellipse is not truncated and without going into minute details, the procedure can be presented as follows:

Maximum contact stress at the center of roller-end/rib contact

$$\sigma_3 = \frac{1.5 \times 10^{-3} P_3}{\pi b a} \quad (7.03)$$

where,

a = semi-major axis of ellipse = $\mu_h G_h$

b = semi-minor axis of ellipse = $\nu_h G_h$

$$\text{where, } G_h = \left[\frac{3(1-\mu^2)P_3}{E(2/r+1/r')} \right]^{1/3} \quad (7.04)$$

$$E = 30 \times 10^6 \text{ psi}$$

$$\mu = 0.3$$

r' = radius of curvature of rib defined
by equation (9.15)

μ_h and ν_h are Hertzian parameters related as follows:

$$\mu_h = \frac{\nu_h}{\cos \xi} \quad (7.05)$$

$$\nu_h = \left[\frac{2}{\pi} E(\xi) \cos \xi \right]^{1/3} \quad (7.06)$$

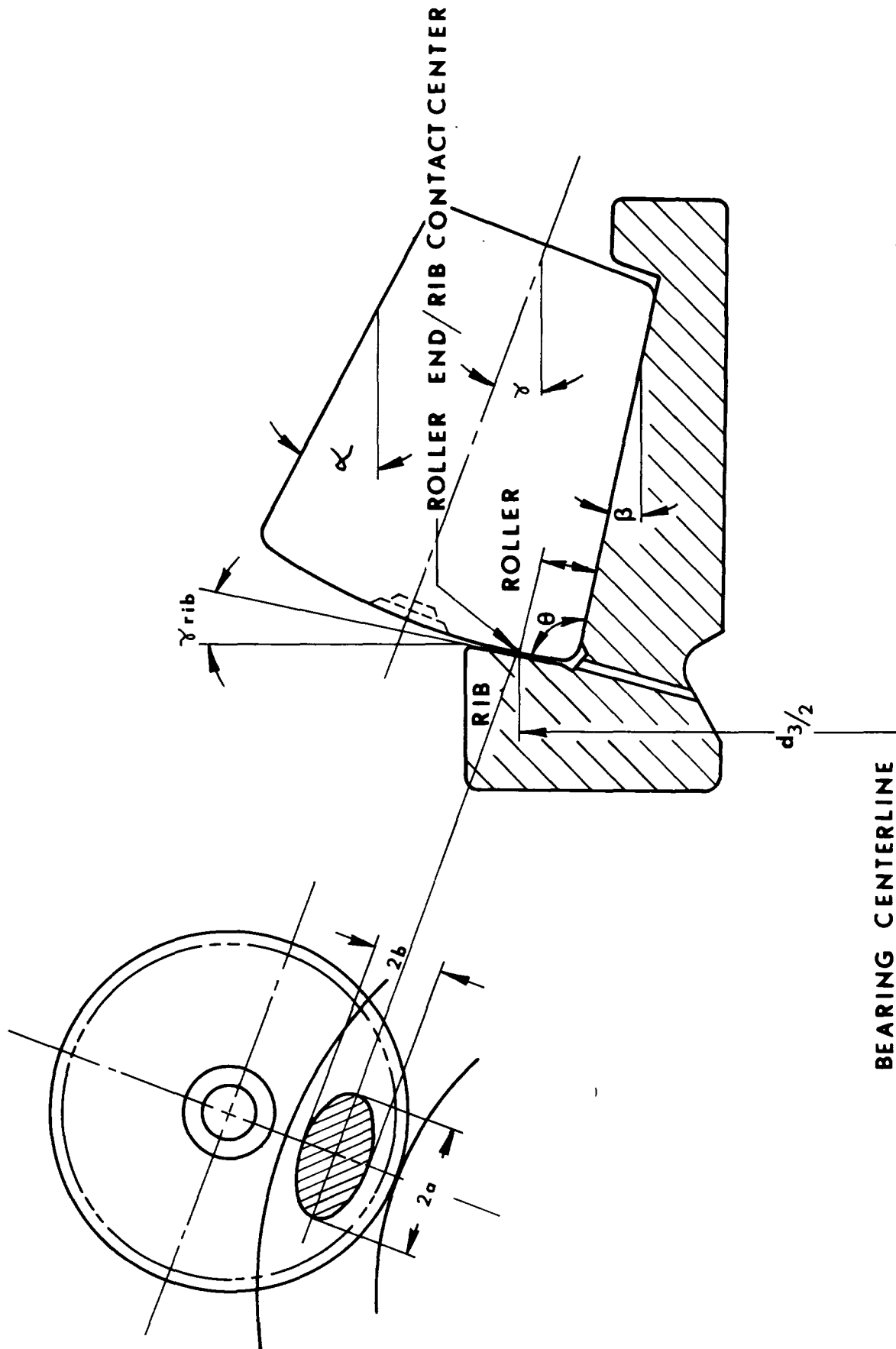


Figure 12 - Roller-End/Rib Contact

The value of ' ξ ' should be such that it satisfies the following equation:

$$\frac{\cos(\tau)-1}{2} + \frac{K(\xi)-E(\xi)}{E(\xi)} \times \cot^2 \xi = 0 \quad (7.07)$$

$$\text{where, } \cos(\tau) = \frac{\frac{1}{r'}}{2/r - 1/r'} \quad (7.08)$$

$K(\xi)$ = complete elliptic integral of the first kind

$$= \int_0^{\pi/2} \left[1 - \sin^2(\xi) \sin^2 x \right]^{-1/2} dx \quad (7.09)$$

$E(\xi)$ = complete elliptic integral of the second kind

$$= \int_0^{\pi/2} \left[1 - \sin^2(\xi) \sin^2 x \right]^{1/2} dx \quad (7.10)$$

The two integrals defined above may be approximated by the following polynomials as given in Ref. 10.

$$\begin{aligned} K(\xi) = & \xi^4 \left[Y(5) + Y(10) \ln(1/\xi) \right] + \xi^3 \left[Y(4) + Y(9) \ln(1/\xi) \right] \\ & + \xi^2 \left[Y(3) + Y(18) \ln(1/\xi) \right] \\ & + \xi \left[Y(2) + Y(7) \ln(1/\xi) \right] + Y(1) + Y(6) \ln(1/\xi) \end{aligned} \quad (7.11)$$

$$\begin{aligned} E(\xi) = & \xi^4 \left[Y(14) + Y(18) \ln(1/\xi) \right] + \xi^3 \left[Y(13) + Y(17) \ln(1/\xi) \right] \\ & + \xi^2 \left[Y(12) + Y(16) \ln(1/\xi) \right] \\ & + \xi \left[Y(11) + Y(15) \ln(1/\xi) \right] + 1 \end{aligned} \quad (7.12)$$

where, $Y(1), Y(2) \dots Y(18)$ are numerical constants as given below:

$Y(1) = 1.38629436$	$Y(10) = 0.0441787012$
$Y(2) = 0.0966634426$	$Y(11) = 0.443251415$
$Y(3) = 0.0359009238$	$Y(12) = 0.0626060122$
$Y(4) = 0.0374256371$	$Y(13) = 0.0475738355$
$Y(5) = 0.0145119621$	$Y(14) = 0.0173650645$
$Y(6) = 0.5$	$Y(15) = 0.249983683$
$Y(7) = 0.124985936$	$Y(16) = 0.0920018004$
$Y(8) = 0.0688024858$	$Y(17) = 0.0406969753$
$Y(9) = 0.032835535$	$Y(18) = 0.00526449639$

After substituting for $\cos(\tau)$, $K(\xi)$ and $E(\xi)$ from equations (7.08), (7.11) and (7.12) respectively in equation (7.07), it can be solved for ξ by Newton's iteration method.

8. LUBRICANT (MIL-L-7808G) PROPERTIES

In various EHD and related thermal computations, data are required on the variations of the rheological and thermal properties of the lubricants with temperature, pressure, rate of shear, etc. The following formulae used to describe the controlling properties of MIL-L-7808G are the recommendations of Southwest Research Institute based on the experimental data available on this type of fluid. The formulae are only representative of 7808G fluids. Different 7808G fluids may have slightly different formulae.

Density at atmospheric pressure

$$\rho_o = .9531 - 0.000394 (^\circ\text{F} - 60) \quad (8.01)$$

Kinematic viscosity at atmospheric pressure (ν_o) is

$$\text{given by, } \log \log (\nu_o + 0.6) = 11.75543 - 4.24477 \log (^\circ\text{F} + 460) \quad (8.02)$$

Absolute viscosity

$$\text{Centi-poise} = \rho_o \nu_o \quad (8.03)$$

$$\text{Reyn, } \mu_o = 1.45 \times 10^{-7} \rho_o \nu_o \quad (8.04)$$

Pressure-viscosity coefficient

$$\alpha_o = 12.717 \times 10^{-4} (^\circ\text{F})^{-0.566} \quad (8.05)$$

Temperature-viscosity coefficient

$$\beta_o = 0.0045 + 1.25 \times 10^{-7} p \quad (8.06)$$

$$\beta'_o = \frac{3400}{(^{\circ}F + 460)} \ln \left(\frac{\mu_o/100}{\mu_o/210} \right) \quad (8.07)$$

Specific Heat

$$c_p = 0.16 (^{\circ}F)^{.215} \quad (8.08)$$

Thermal Conductivity

$$k = 0.082 - 1.355 \times 10^{-5} \times ^{\circ}F \quad (8.09)$$

The following table was generated using the equations (8.01) through (8.05).

TABLE IV

Density, Viscosity and Pressure-Viscosity Coefficientfor MIL-L-7808G as a Function of Temperature

Temperature °F	Density gm/cc	-----Viscosity-----			Press-Vis Coefficient in ² lb x 10 ⁴
		Centi- Stokes	Centi- Poise	Reyn x 10 ⁶	
100	.937	16.393	15.3662	2.2281	.9384
110	.933	13.243	12.3612	1.7924	.8891
120	.929	10.882	10.1144	1.4666	.8464
130	.926	9.079	8.4027	1.2184	.8089
140	.922	7.678	7.0762	1.0261	.7757
150	.918	6.574	6.0323	.8747	.7460
160	.914	5.690	5.1993	.7539	.7192
170	.910	4.975	4.5259	.6563	.6949
180	.906	4.389	3.9753	.5764	.6728
190	.902	3.903	3.5202	.5104	.6525
200	.898	3.497	3.1405	.4554	.6339
210	.894	3.155	2.8208	.4090	.6166
220	.890	2.864	2.5494	.3697	.6006
230	.886	2.615	2.3172	.3360	.5857
240	.882	2.400	2.1173	.3070	.5717
250	.878	2.214	1.9440	.2819	.5587
260	.874	2.051	1.7929	.2600	.5464
270	.870	1.908	1.6604	.2408	.5349
280	.866	1.782	1.5437	.2238	.5240
290	.862	1.670	1.4402	.2088	.5137
300	.859	1.570	1.3483	.1955	.5039
310	.855	1.481	1.2661	.1836	.4946
320	.851	1.402	1.1924	.1729	.4858
330	.847	1.330	1.1261	.1633	.4774
340	.843	1.265	1.0662	.1546	.4694
350	.839	1.206	1.0119	.1467	.4618
360	.835	1.153	.9626	.1396	.4545
370	.831	1.104	.9176	.1331	.4475
380	.827	1.060	.8765	.1271	.4408
390	.823	1.019	.8388	.1216	.4344
400	.819	.982	.8042	.1166	.4282
410	.815	.947	.7723	.1120	.4222
420	.811	.916	.7429	.1077	.4165
430	.807	.887	.7157	.1038	.4110
440	.803	.859	.6905	.1001	.4057
450	.799	.834	.6770	.0967	.4006
460	.795	.811	.6453	.0936	.3956
470	.792	.789	.6249	.0906	.3908
480	.788	.769	.6060	.0879	.3862
490	.784	.751	.5882	.0853	.3817
500	.780	.733	.5716	.0829	.3774

TABLE V

Specific Heat and Thermal Conductivity
for MIL-L-7808G as a Function of Temperature

<u>Temperature</u> <u>°F</u>	<u>Specific Heat</u> <u>BTU/lb.°F</u>	<u>Thermal Conductivity</u> <u>BTU/hr.ft.°F</u>
100	.431	.0806
110	.440	.0805
120	.448	.0804
130	.456	.0802
140	.463	.0801
150	.470	.0800
160	.476	.0798
170	.483	.0797
180	.489	.0796
190	.494	.0794
200	.500	.0793
210	.505	.0792
220	.510	.0790
230	.515	.0789
240	.520	.0787
250	.524	.0786
260	.529	.0785
270	.533	.0783
280	.537	.0782
290	.541	.0781
300	.545	.0779
310	.549	.0778
320	.553	.0777
330	.557	.0775
340	.560	.0774
350	.564	.0773
360	.567	.0771
370	.571	.0770
380	.574	.0769
390	.580	.0766
410	.583	.0764
420	.586	.0763
430	.589	.0762
440	.592	.0760
450	.595	.0759
460	.598	.0758
470	.601	.0756
480	.603	.0755
490	.606	.0754
500	.609	.0752

9. EHD FILM THICKNESS (Ref. 11)

The classical theory of elasto-hydrodynamic lubrication is rather well known and its application to study the performance of lubricated concentrated contacts has been in existence for some time. Without going into details of the basic fundamentals and assumptions, the following sections briefly describe how we can estimate the operating film thickness at three major conjunctions using some empirical formulae.

9.1 Sum Velocities

The sum velocity for two bodies in contact is defined as a sum of the peripheral velocities of the surfaces relative to the conjunction. Based on the assumption of pure rolling at the race contacts the formulae are:

$$\left[\begin{array}{l} \text{The sum velocity at} \\ \text{roller-body/cone-race} \\ \text{contact } (U_1) \end{array} \right] = \left[\begin{array}{l} \text{The sum velocity at} \\ \text{roller-body/cup-race} \\ \text{contact } (U_2) \end{array} \right]$$
$$U_1 = U_2 = 2V_1 = \frac{\pi}{30} N_r d \quad (9.01)$$

where, V_1 is defined by equation (5.05)

The sum velocity at roller-end/rib contact

$$U_3 = 2V_2 + V_s \quad (9.02)$$

where, V_2 and V_s are given by equations (5.06) and (5.09) respectively.

9.2 Equivalent Radii

Two bodies forming a highly stressed contact can be represented mathematically by an equivalent cylinder near a plane for a rectangular conjunction, or by an equivalent sphere near a plane for an elliptical conjunction. Then, by definition the radius of the cylinder or the sphere is called equivalent radius. Neglecting the crown radius on roller-body for roller-body/race contacts and by referring to Figure 13 the equivalent radii at the center of contact can be derived as follows:

- a. Equivalent radius for roller-body/cone-race contact (Fig. 13).

$$R_1 = \frac{1}{1/(\textcircled{A} \textcircled{D}) + 1/(\textcircled{A} \textcircled{K})} \quad (9.03)$$

$$\begin{aligned} \text{where } \textcircled{A} \textcircled{D} &= \textcircled{A} \textcircled{C} / \cos v \\ &= \frac{d}{2 \cos v} \end{aligned} \quad (9.04)$$

$$\begin{aligned} \textcircled{A} \textcircled{K} &= \textcircled{A} \textcircled{I} / \cos \beta \\ &= \frac{D_2}{2 \cos \beta} \end{aligned} \quad (9.05)$$

Substituting for $\textcircled{A} \textcircled{D}$ and $\textcircled{A} \textcircled{K}$ in equation (9.03) we obtain,

$$R_1 = \frac{0.5}{\frac{\cos v}{d} + \frac{\cos \beta}{D_2}} \quad (9.06)$$

and we know, $D_2 = \text{mean cone O.D.} = \frac{d \sin \beta}{\sin v}$

substituting this in (9.06) we get

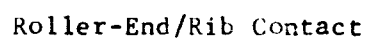
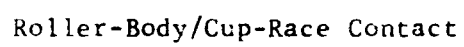


Figure 13 - Equivalent Radii

$$R_1 = \frac{0.5}{\frac{\cos v}{d} + \frac{\sin v \cos \beta}{d \sin \beta}}$$

rearranging terms and using the trigonometric identity

$$\sin \beta \cos \beta + \cos \beta \sin v = \sin (\beta + v)$$

and by definition $\beta + v = \gamma$

$$R_1 = \frac{0.5d \sin \beta}{\sin \gamma} \quad (9.07)$$

b. Equivalent radius for roller-body/cup-race contact

(Fig. 13)

$$R_2 = \frac{1}{1/(\textcircled{B}) (\textcircled{L}) - 1/(\textcircled{B}) (\textcircled{E})} \quad (9.08)$$

$$\text{where } (\textcircled{B}) (\textcircled{L}) = d/2 \cos v \quad (9.09)$$

$$(\textcircled{B}) (\textcircled{E}) = \frac{D_5}{2 \cos \alpha} \quad (9.10)$$

$$D_5 = \frac{d \sin \alpha}{\sin v} \quad (9.11)$$

Using equations (9.09), (9.10) and (9.11) and similar procedure as above equation (9.08) can be reduced to,

$$R_2 = \frac{0.5d \sin \alpha}{\sin \gamma} \quad (9.12)$$

c. Equivalent radius for roller-end/rib contact (Fig. 13)

$$R_3 = \frac{1}{1/r - 1/(\textcircled{F}) (\textcircled{H})} \quad (9.13)$$

$$\text{where, } (\textcircled{F}) (\textcircled{H}) = (\textcircled{F}) (\textcircled{G}) / \cos \gamma_{\text{rib}} = r' \quad (9.14)$$

$$\text{and } (\textcircled{F}) (\textcircled{G}) = d_3/2 \text{ (defined in section 2.1)}$$

therefore,

$$R_3 = \frac{rd_3}{1 - 2 \cos \gamma_{\text{rib}}} \quad (9.15)$$

9.3 Roller-Body/Race Contacts: (Ref. 11)

The general expression for minimum EHD - film thickness for a rectangular conjunction as given by Dowson in Ref. 11 is:

$$H_{\min}^* = \frac{2.65 G^{*0.54} U^{*0.7}}{W^{*0.13}} \quad (9.16)$$

where, H_{\min}^* , G^* , U^* , W^* are dimensionless parameters.

a. Roller-Body/Cone-race contact

The dimensionless parameters in equation (9.16) are as follows:

$$H_{\min}^* = \frac{h_1}{R_1} \quad \begin{array}{l} h_1 = \text{minimum film thickness at} \\ \text{center of contact} \end{array} \quad (9.17)$$

$$R_1 = \text{equivalent radius, equation (9.03)}$$

$$G^* = E' \alpha_o \quad (9.18)$$

E' = reduced modulus of elasticity

$$= \frac{E}{1-\mu^2} = 33 \times 10^6 \text{ psi}$$

α_o = lubricant pressure viscosity coefficient

$$U^* = \frac{\mu_o U_1}{E' R_1} \quad \begin{array}{l} U_1 = \text{sum velocity, equation (9.01)} \end{array} \quad (9.19)$$

$$W^* = \frac{P_1}{2E' R_1} \quad (9.20)$$

After substituting for dimensionless parameters in equation (9.16) it can be reduced to the following form:

$$h_1 = .68816 R_1^{0.43} (\alpha_o \times 10^4)^{0.54} (\mu_o \times 10^6 \cdot U_1)^{0.7} (\ell/P_1)^{0.13} \quad (9.21)$$

b. Roller-Body/Cup-Race contact.

$$h_2 = .68816 R_2^{0.43} (\alpha_o \times 10^4)^{0.54} (\mu_o \times 10^6 \times U_2)^{0.7} (\ell/P_2)^{0.13} \quad (9.22)$$

9.4 Roller-End/Rib Contact

The roller-end/rib contact is a critical area in high speed tapered roller bearings. In view of the spherical roller-end and a flat conical shaped rib the contact area is a point under no load and an ellipse under load. Several empirical formulae are available to calculate the minimum EHD film thickness for an elliptical contact. More recently Thorp and Gohar (Ref. 12) have presented some experimental data in terms of a dimensionless conforming groove with a .555 inch radius. The similarity in their test conditions and the roller-end/rib contact is that the major axis of the contact ellipse is parallel to the direction of lubricant flow. From Figure 14 of Reference 12, the relation between $\ln (H^*/W^*G^*)$ and $\ln (U^*/W^{*1.5}G^{*.5})$ is relatively linear and an expression that fits the data reasonably well is,

$$\frac{H^*}{W^*G^*} = 0.811 \left[\frac{U^*}{W^{*1.5}G^{*.5}} \right]^{.769} \quad (9.23)$$

or

$$H^* = 0.811 \frac{G^{*0.616} U^{*0.769}}{W^{*0.152}} \quad (9.24)$$

The above equation can be reduced to the following form in terms of dimensional variables:

$$h_3 = .066634 R_3^{0.535} (\alpha_o \times 10^4)^{0.616} (\mu_o \times 10^6 \times U_3)^{0.769} (P_3)^{-0.152} \quad (9.25)$$

9.5 Thermal Reduction Factor

The EHD film thickness equations given in the preceding sections all assume an isothermal flow process. This assumption implies that: (a) the motion is pure rolling so that the temperature distribution across the lubricant film can be taken as essentially uniform, (b) the rolling velocity and/or lubricant viscosity are low enough so that the temperature rise due to shearing of the lubricant film in the inlet region can be neglected, and (c) the lubricant film thickness in the conjunction is determined essentially by what happens in the inlet region so that lubricant shear within the conjunction has a negligible effect on the film thickness. These conditions are not satisfied in this analysis. Estimates of the effects are accounted for in the Thermal Reduction Factor. Cheng (Ref. 13) originated the numerical technique which was later modified by McGrew, et al (Ref. 14). The later version used in this analysis consists of first determining the viscous heating parameter, Q_m

$$Q_m = \frac{\mu_o (U_{sum})^2}{2k T_o} \quad (9.26)$$

(In the above equation U_{sum} represent sum velocities for a given conjunction, defining sum velocities at either the cone, cup or rib.)

Two lubricant parameters are computed

$$\alpha^* = \alpha_o \frac{\pi}{2} \times 10^5 \quad (9.27)$$

$$\beta'_o = \frac{3400 \ln \left[\frac{\mu_{o/100}}{\mu_{o/210}} \right]}{T_o + 460} \quad (9.28)$$

With these three parameters and Tables XIII and XIV of Reference 14, the coefficients f_1 and f_3 are determined.

For values different from those shown on the Tables, linear interpolation is used within the range and linear extrapolation outside the range. Thermal reduction factor is then computed by the following equation:

$$\phi_T = f_1 (1 - 0.1s) (1 + f_3 \left(\frac{\sigma}{E^*} \right)) \quad (9.29)$$

The slip ratio is 's'. Multiplying the isothermal film thickness by the factor ϕ_T gives the nonisothermal film thickness

10. CAGE FRICTIONAL FORCES

10.1 Roller Body/Cage Pocket Friction

The friction developed between the roller-body and the cage pocket is due to shearing of the lubricant or rubbing of the surfaces. In general, the roller does not operate concentrically to the cage pocket due to weight, unbalance, whirl and dimensional variations. However, if the cage is relatively light weight and well balanced, weight and unbalance effects can be minimized. Accurate manufacturing and quality control reduces dimensional effects. Also, previous experience indicates that any region of metal to metal contact will wear only at initial run-in. No further wear occurs with subsequent operation.

The final condition assumed is that the cavity between the roller-body and cage pocket is completely filled with oil. This conjunction for both cage designs (roller and race guided) is shown on Figure 14.

With the above assumptions the friction is calculated as in a journal bearing operating at no-load using the experimental data of Smith and Fuller (Ref. 15). Their friction data are for a full 360° journal bearing operating in the laminar, transition and fully turbulent regimes. Figure 15 is a plot of their friction coefficient versus Reynolds number. The Reynolds Number for the roller-body/cage pocket conjunction is

$$Re_p = \frac{V_l C_p}{\mu_o} \quad (10.01)$$

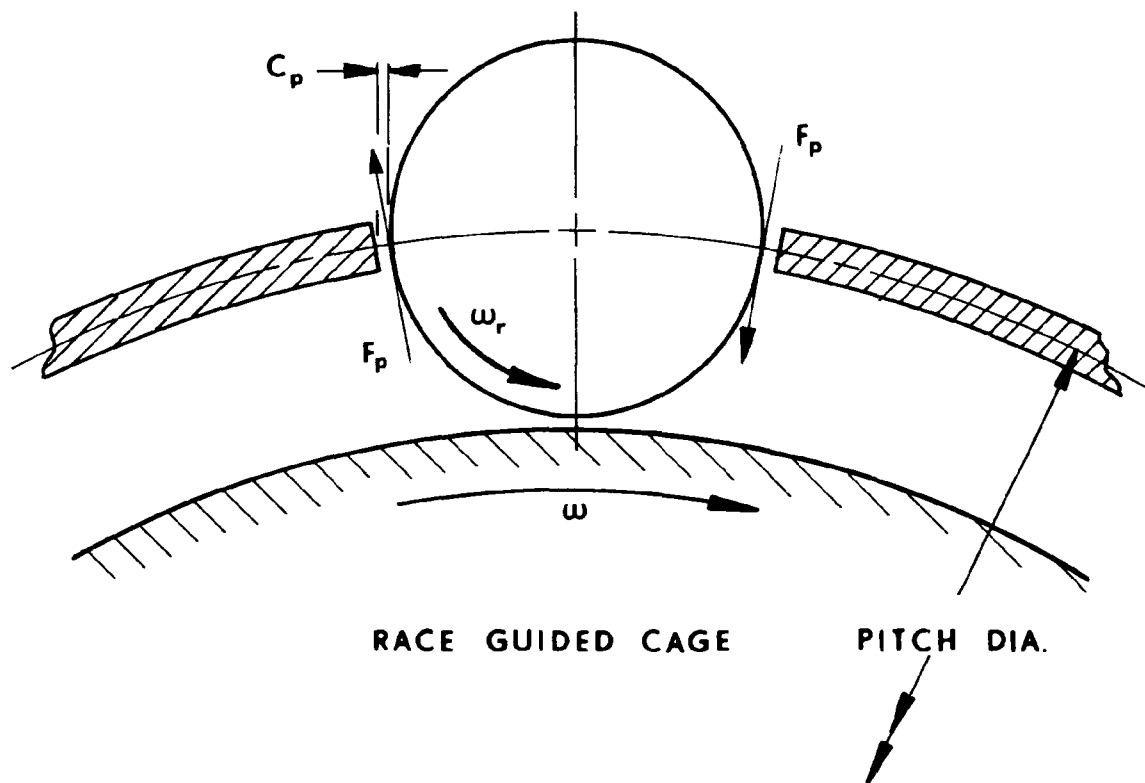
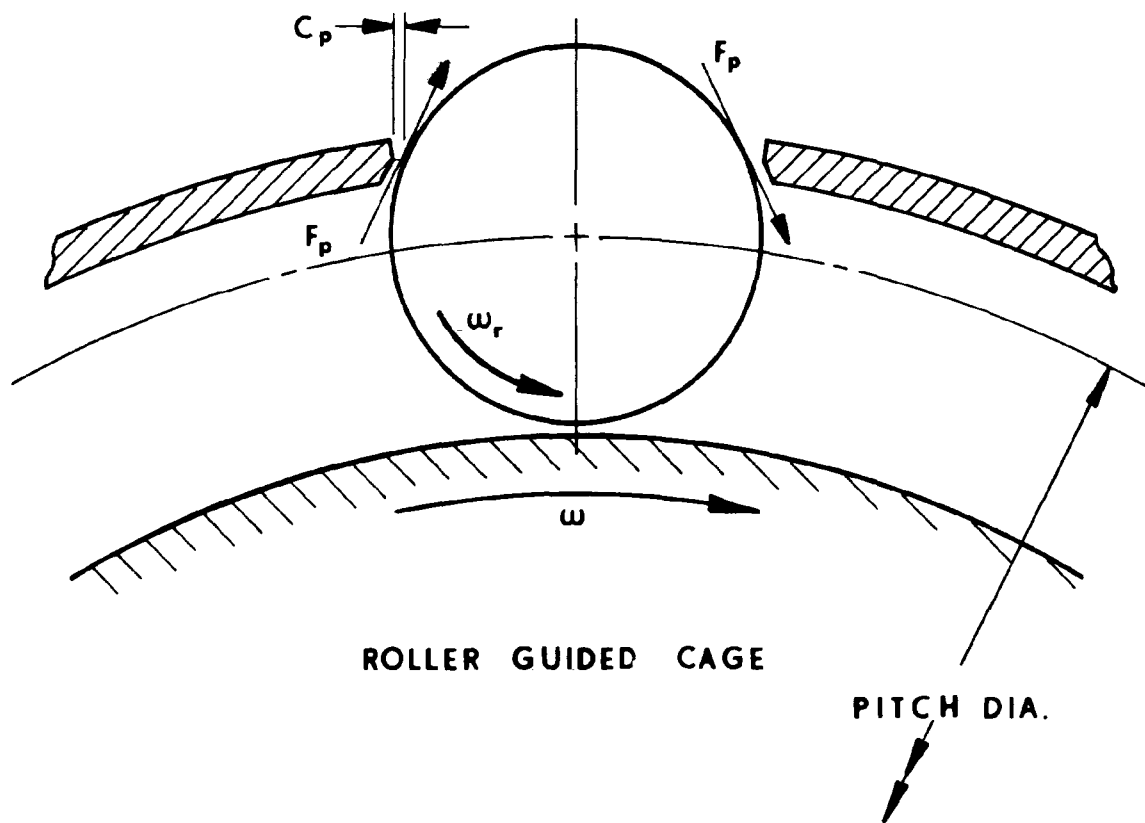


Figure 14 - Section Views Through Roller Mean Diameter for Roller and Race Guided Cages

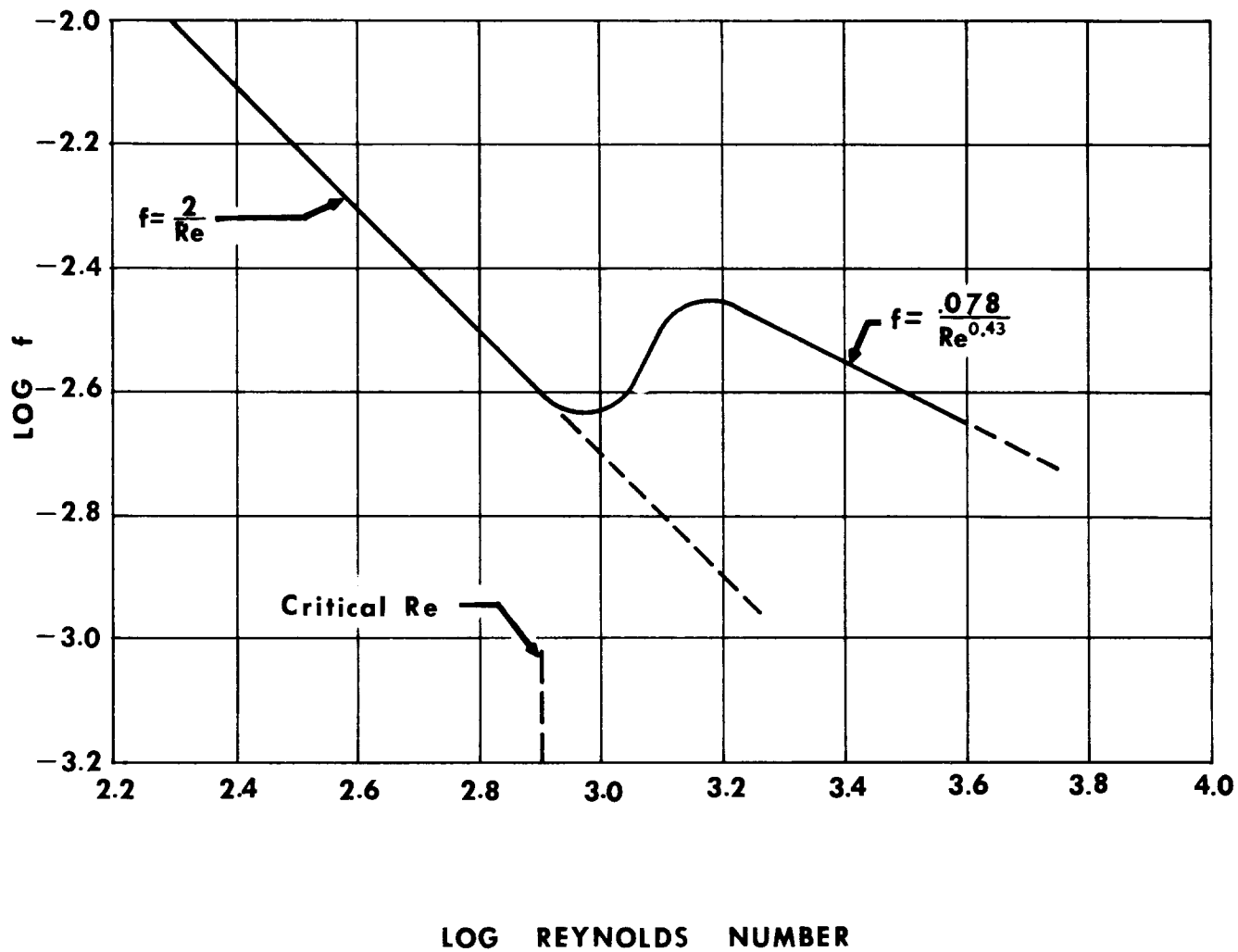


Figure 15 - Friction As a Function of Reynolds Number
for Unloaded Journal Bearing

Empirical formulas for the friction coefficient in the three (3) regimes are tabulated below.

TABLE VI
Empirical Formulas for Friction Coefficient

<u>Regime</u>	<u>Reynolds Number</u>	<u>Formulas</u>
Laminar	$\text{Log } (Re_p) \leq 2.87$	$f_p = \frac{2}{Re_p}$
Transition	$2.87 < \text{Log}(Re_p) \leq 3.04$	$f_p = .00251$
	$3.04 < \text{Log}(Re_p) \leq 3.16$	$f_p = \frac{5.19 Re_p^{1.212}}{10^7}$
Turbulent	$\text{Log } (Re_p) > 3.16$	$f_p = \frac{0.078}{Re_p^{.43}}$

Shear stress for the journal bearing is defined as

$$T_o = \frac{f_{p_o'} v_1^2}{2g} \quad (10.02)$$

To apply the friction data to the roller-body/cage pocket "bearing", the assumption is that the shear stress, in the two partial-arc "bearings" is the same as it would be in a full journal bearing with a journal diameter equal to the roller diameter and with the same radial clearance as exists between the roller body and cage pocket. The friction force in each fluid film is calculated by:

$$F_p = T_o L_{arc} \ell_p \quad (10.03)$$

The total friction force then would be twice this amount, since there are two partial-arc "bearings" formed by each roller and cage pocket.

This same technique has been recently used by Astridge and Smith (Ref. 16) to estimate the heat generation in high speed cylindrical roller bearings.

10.2 Cage-Pilot/Race-Guide Friction

In the race-guided cage design, there is an addition to the friction developed at the roller body/cage pocket, a frictional force between the cage pilot and race guide. Depending on which surface the cage is piloted, this friction force may either drive or impose a drag on the cage. See Figure 16. A pilot relative to the higher speed cone or shaft drives the cage. A pilot relative to the stationary cup or housing apply a resistance to rotation.

To apply the friction data given in Reference 15, the assumptions are as follows:

1. Cage Weight, unbalance and whirl effects are neglected.
2. The cavity between the cage pilot and race guide is filled with oil.

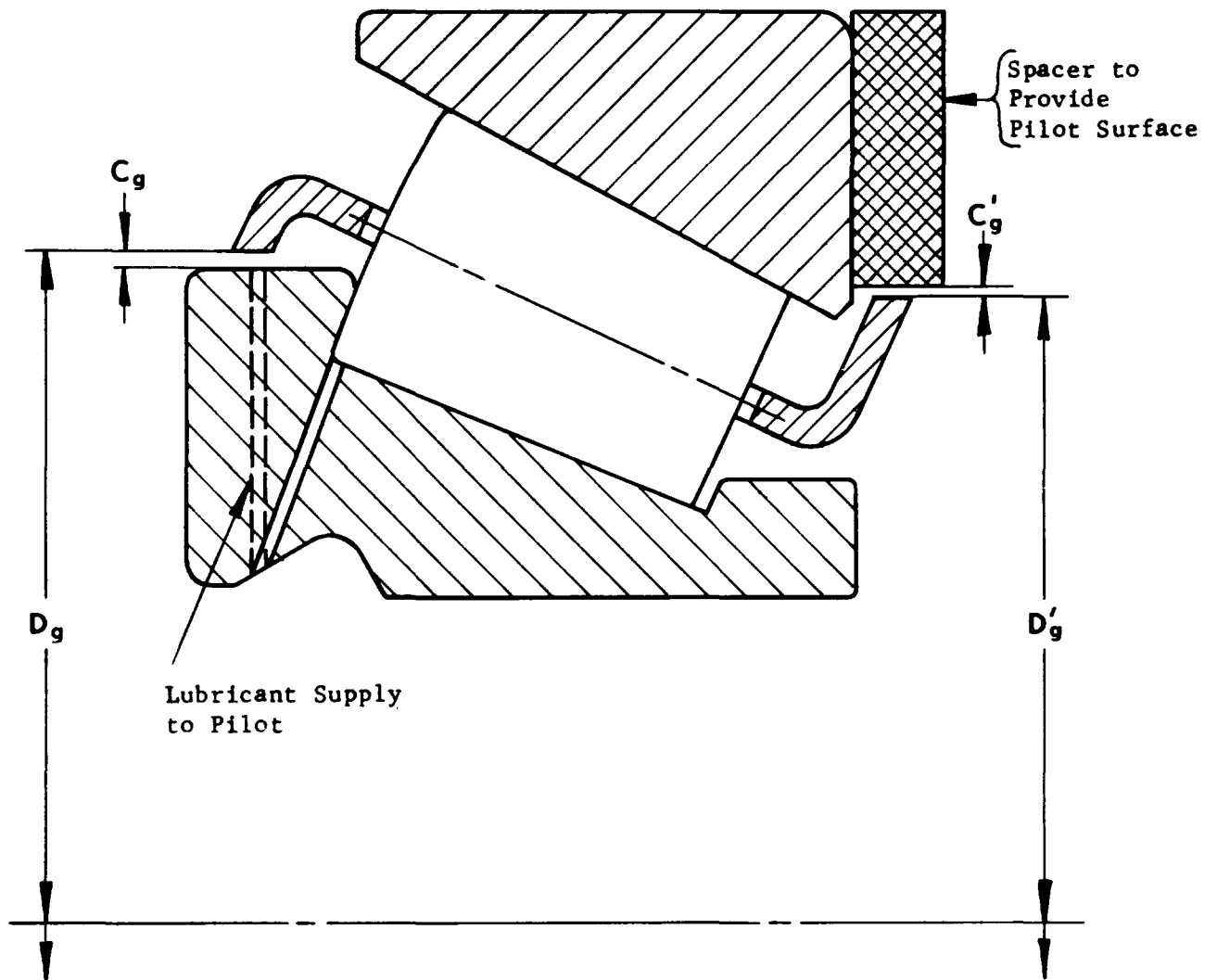


Figure 16 - Method of Piloting
Race Guided Cage

3. The shear stress in the narrow journal bearing formed by the cage pilot and race guide is the same as it would be in an infinitely long journal bearing operating with the same journal diameter, clearance and speed.

As done in the previous section, the friction coefficient is calculated by empirical formulas of the Reynolds Number fit to the data of Smith and Fuller. These formulas have been tabulated in the previous section. Reynolds Number for the cage pilot/race guide is

$$Re_g = \frac{V_4 C_g}{\mu_o} \quad (10.04)$$

The shear stress in the fluid film is

$$\tau_o = \frac{f_g \rho'_o V_4^2}{2g} \quad (10.05)$$

The total force required to shear the fluid film is

$$F_g = \tau_o \pi D_g L_g \quad (10.06)$$

Since this is a resistance to rotation acting over the full circumference, it can better be defined as a couple

$$M_c = \frac{F_g D_g}{2} \quad (10.07)$$

11. EHD FRICTION AND PRESSURE FORCES

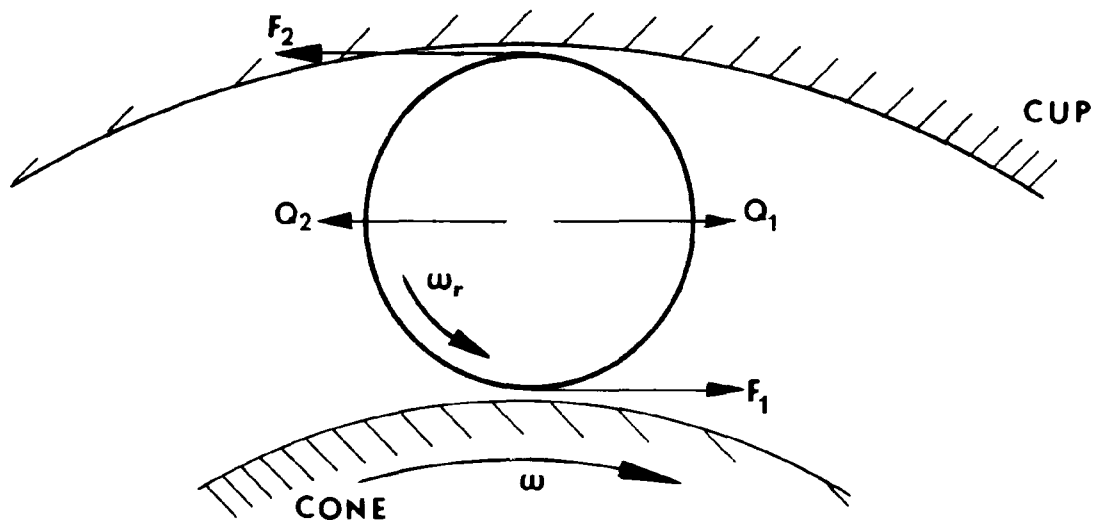
The objective of this program is to operate a bearing at 3.5 million DN. Assuming epicyclic motion, this results in a roller-body/race conjunction sum velocity in excess of 8000 inches per second. Further, the bearing is likely to be operating in a starved boundary lubrication condition. Considering this, there is currently no analytical techniques available to compute friction.

In order to estimate friction and pressure forces several assumptions are needed.

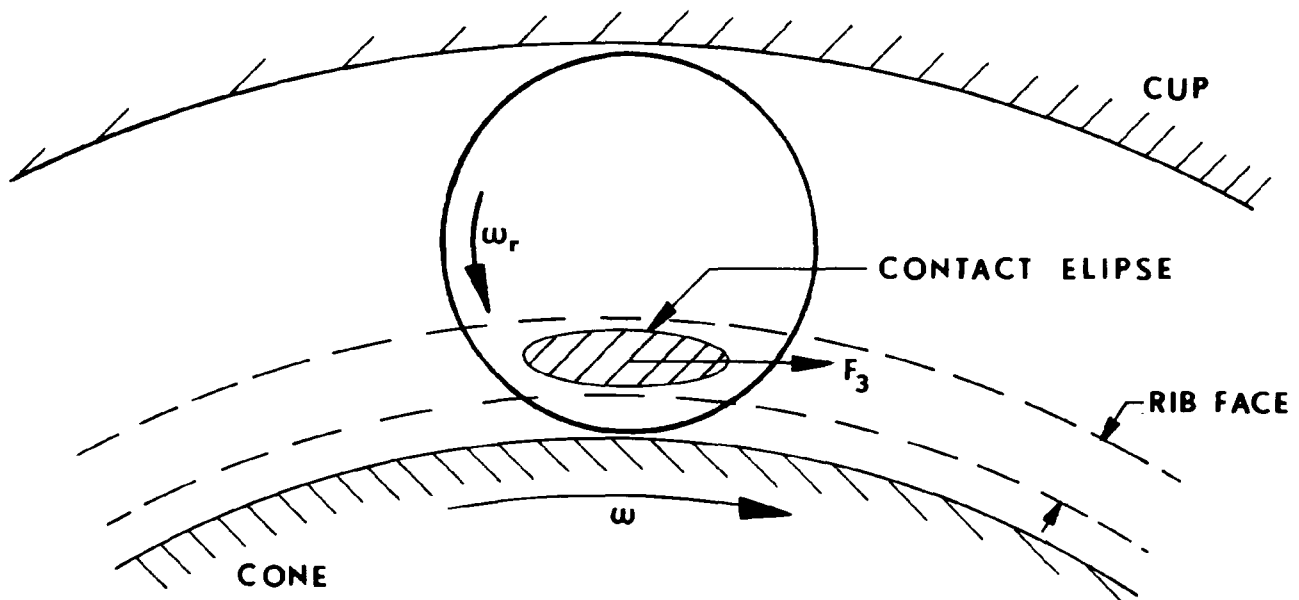
First, assume the bearing is operating under full EHD conditions, where a continuous and intact lubricant film separates the surfaces. Second, assume there is sufficient supply of lubricant at each of the race and rib conjunctions so that the effects of starvation can be neglected. And finally, assume the bearing is operating at or near the epicyclic mode for the rolling element contacts.

This latter assumption has been verified at speeds to 1.8 million DN. Up to this speed, there was no measurable cage slip.

Location and orientation of the EHD friction and pressure forces are shown on Figure 17.



SECTION THROUGH
MEAN ROLLER DIAMETER



SECTION THROUGH
LARGE END ROLLER DIAMETER

Figure 17 - EHD Friction and
Pressure Forces

11.1 Roller-Body/Race Friction and Pressure Forces

Based largely on the success of the predictive schemes employed by Harris (Ref. 17) and Poplawski (Ref. 18) the estimating procedure for nearly pure rolling is to use the following equations first developed by Dowson and Higginson (Ref. 19) and later modified by Harris. In dimensionless terms and for the present, neglecting sliding

$$F_1^* = -9.2G^{-0.3}U_1^{*0.7} \quad (11.01)$$

$$F_2^* = -9.2G^{-0.3}U_2^{*0.7} \quad (11.02)$$

$$\text{where, } U_1^* = \frac{\mu_o U_1}{E'R_1} \quad \text{and} \quad U_2^* = \frac{\mu_o U_2}{E'R_2}$$

The forces shown on the preceding Figure 17, Q_1 and Q_2 are components of the hydrodynamic pressure forces which result from the pressure buildup in the inlet region of the conjunctions. See Ref. 18 and 19. In dimensionless terms these are

$$Q_1^* = 18.4 \left[1 - \left(\frac{2d}{D_2 + D_5} \right) \right] G^{-0.3} U_1^{*0.7} \quad (11.03)$$

$$Q_2^* = 18.4 \left[1 + \left(\frac{2d}{D_2 + D_5} \right) \right] G^{-0.3} U_2^{*0.7} \quad (11.04)$$

The force components (Q_1 and Q_2) act through the center of the roller and are colinear with the direction of roller motion. These forces are considered in the translation of the roller but do not enter into a summation of moments about the roller center.

To convert the dimensionless equations (11.01) through (11.04) to a dimensional form in pounds, divide by ($\ell E' R_x$) where R_x is the "equivalent radius" for the conjunction (cone or cup).

11.2 Roller-End/Rib Friction

Roller end/rib friction, where sliding is predominant, is determined empirically based on experimental data of Johnson and Cameron (Ref. 20). The method was first developed by McGrew, et al (Ref. 14). It involves first calculating three dimensionless parameters G_1 , G_2 and G_3 at 86° F, which are

$$G_1 = \frac{\mu_o V_s}{\sigma_3 h_3} \quad (11.05)$$

$$G_2 = \frac{\beta_o \mu_o V_s^2}{8k} \quad (11.06)$$

$$G_3 = \alpha_o \sigma_3 \quad (11.07)$$

The parameters measure the effect of shear rate, thermal heating and pressure-viscosity, respectively.

Reference 14 has a family of curves for the friction coefficient as a function of the three parameters G_1 , G_2 and G_3 . The curves are all based on a lubricant inlet temperature of 86° F. A method for adjusting for lubricant inlet temperatures other than 80° F is given.

The procedure used in this analysis differs from McGrew's in that the dimensionless parameters are computed using the actual lubricant supply temperature, then interpolating or extrapolating from the curves directly. Symbolically, the friction coefficient for the roller end/rib conjunction, f_{rib} , is

$$f_{rib} = f(G_1, G_2, G_3, T_o) \quad (11.08)$$

where T_o is actual lubricant supply temperature. For further discussion regarding modifications to procedures of Reference 14, refer to Appendix A.

12. CONE RIB LUBRICATION SYSTEM

12.1 System Pumping

The prime function of the cone rib lubrication system is to maintain a sufficient supply of lubricant to the roller-end/rib conjunction. Centrifugal force pumps the lubricant from the shaft I.D. to the rib. In order to estimate the relative effectiveness of a design it is necessary to know the trajectory of the lubricant as it travels from the cone and wets the rib face.

Schematic section views of the system are shown on Figures 18 and 18a. Figure 18 defines the various pertinent radial distances from the bearing centerline. Figure 18a shows the path of flow internally through the system.

The first assumption is that flow through the shaft, manifold and cone is much less than the capacity of any single component and there is no accumulation of lubricant at either the shaft I.D. or manifold.

It will be shown later that this assumption is reasonable for the flow rates encountered in these bearings. The effects of gravity and Coriolis acceleration are neglected.

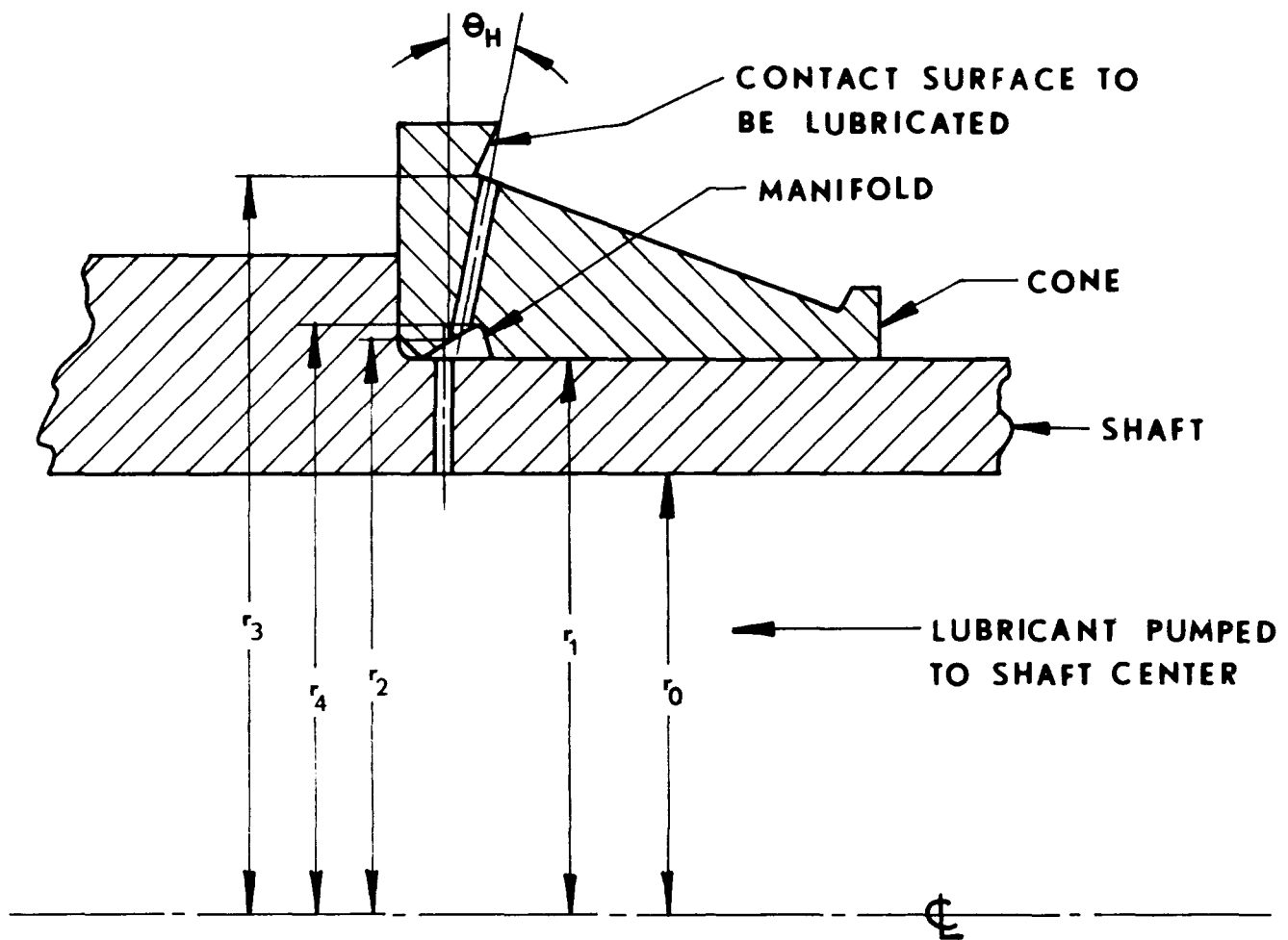


Figure 18 - Cone Large Rib Lubrication System
(Section View Parallel to Shaft)

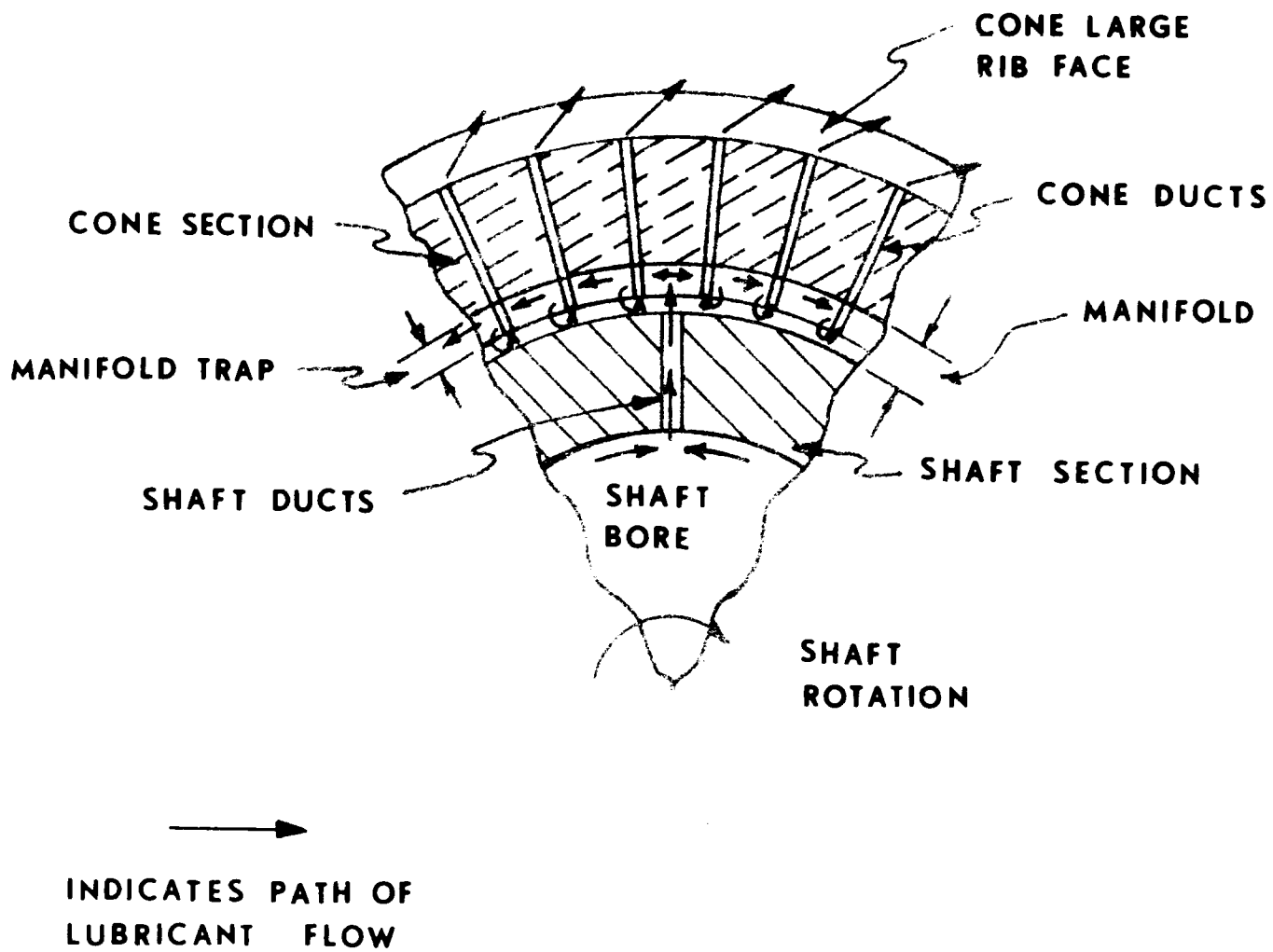


Figure 18a - Cone Large Rib Lubrication System
(Section View Perpendicular to Shaft)

Shaft Duct

First, consider a fluid element in the rotating shaft duct. Refer to Figure 19. The origin of the coordinate system is at the bearing centerline which coincides with the z-axis. This fluid element with cross-sectional area, A_s , accelerates from a velocity approximately equal to zero at r_0 ($v_0 \approx 0$) to v_1 at the outlet r_1 . The mass of the fluid element is d_m and the radial component of acceleration is a_r . For the force balance assume the flow is frictionless. Later, frictional losses will be introduced. The force balance yields

$$p A_s - (p + dp) A_s = a_r d_m \quad (12.01)$$

From kinematics the radial components of acceleration of the rotating duct is

$$a_r = \frac{d^2 r}{dt^2} - r \omega^2 \quad (12.02)$$

and the mass of the fluid element is

$$d_m = \frac{\rho'_0}{g} A_s dr \quad (12.03)$$

Substituting equations (12.02) and (12.03) into (12.01) and rearranging terms

$$dp + \frac{\rho'_0}{g} \frac{d^2 r}{dt^2} dr - \frac{\rho'_0}{g} \omega^2 r dr = 0 \quad (12.04)$$

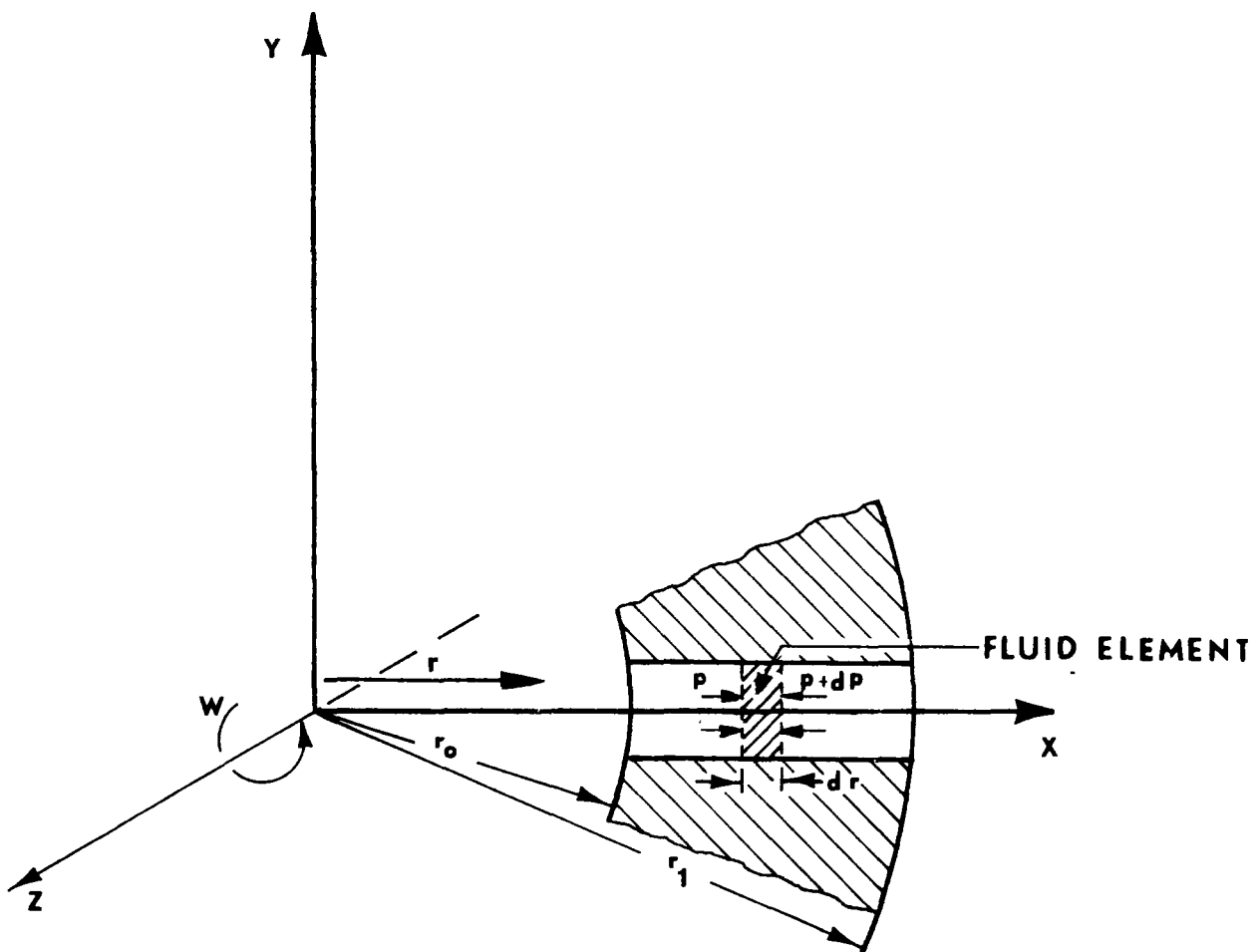


Figure 19 - Segment of Rotating
Shaft Duct

but since $v_r = \frac{dr}{dt}$

$$dp + \frac{\rho'_0}{g} \frac{dv_r}{dt} dr - \frac{\rho'_0}{g} \omega^2 r dr = 0 \quad (12.05)$$

now

$$\frac{dv_r}{dt} = \frac{dv_r}{dr} \frac{dr}{dt} = \frac{dv_r}{dr} v_r$$

equation 12.05 can be written

$$dp + \frac{\rho'_0}{g} v_r \frac{dv_r}{dr} - \frac{\rho'_0}{g} \omega^2 r dr = 0 \quad (12.06)$$

Integrating equation 12.06 and dividing by the mass density term $\frac{\rho'_0}{g}$

$$\frac{p}{\rho'_0/g} + \frac{v_r^2}{2} - \frac{\omega^2 r^2}{2} = \text{Constant} \quad (12.07)$$

Incorporating a head loss to account for friction between the inlet and outlet denoted by subscripts 0 and 1, respectively, yields

$$\frac{p_0}{\rho'_0/g} + \frac{v_0^2}{2} - \frac{\omega^2 r_0^2}{2} = \frac{p_1}{\rho'_0/g} + \frac{v_1^2}{2} - \frac{\omega^2 r_1^2}{2} + H \quad (12.08)$$

To further simplify this equation assume the flow is steady, incompressible and the pressures adjacent the inlet and outlet are equal to atmospheric ($P_o \approx P_1 \approx P_{atm}$)

$$v_o^2 - \omega r_o^2 = v_1^2 - \omega^2 r_1^2 + 2H \quad (12.09)$$

Now, from the previous assumption, v_o is approximately equal to zero. The lubricant exit velocity can be determined by

$$v_1 = \left[\omega^2 (r_1^2 - r_o^2) - 2H \right]^{1/2} \quad (12.10)$$

Some of the previous assumptions are not compatible with the continuity equation and the lubricant is probably pumped as an air-oil mixture. Regardless, equation 12.10 should reasonably estimate the exit velocity.

To calculate the flow losses due to friction in the ducts, the headloss from Reference 21 is:

$$H = \frac{\bar{v}_s}{2} \frac{L_{sd}}{D_{sd}} f \quad (12.11)$$

where \bar{v}_s is the mean velocity of the lubricant flowing through the shaft duct and f is the flow friction factor.

Figure 20 taken from Reference 21 is "Nikuradse Data for Artificially Roughened Pipe Flows". This series of curves gives the friction factor as a function of Reynolds number and roughness to diameter ratio. The three (3) flow regimes are laminar, frictional transition and turbulent. The empirical equations of Blasius, van Karman, Prandtl, et al are used to compute f and are listed in Table VII.

$$\frac{\epsilon}{D_{cd}}$$

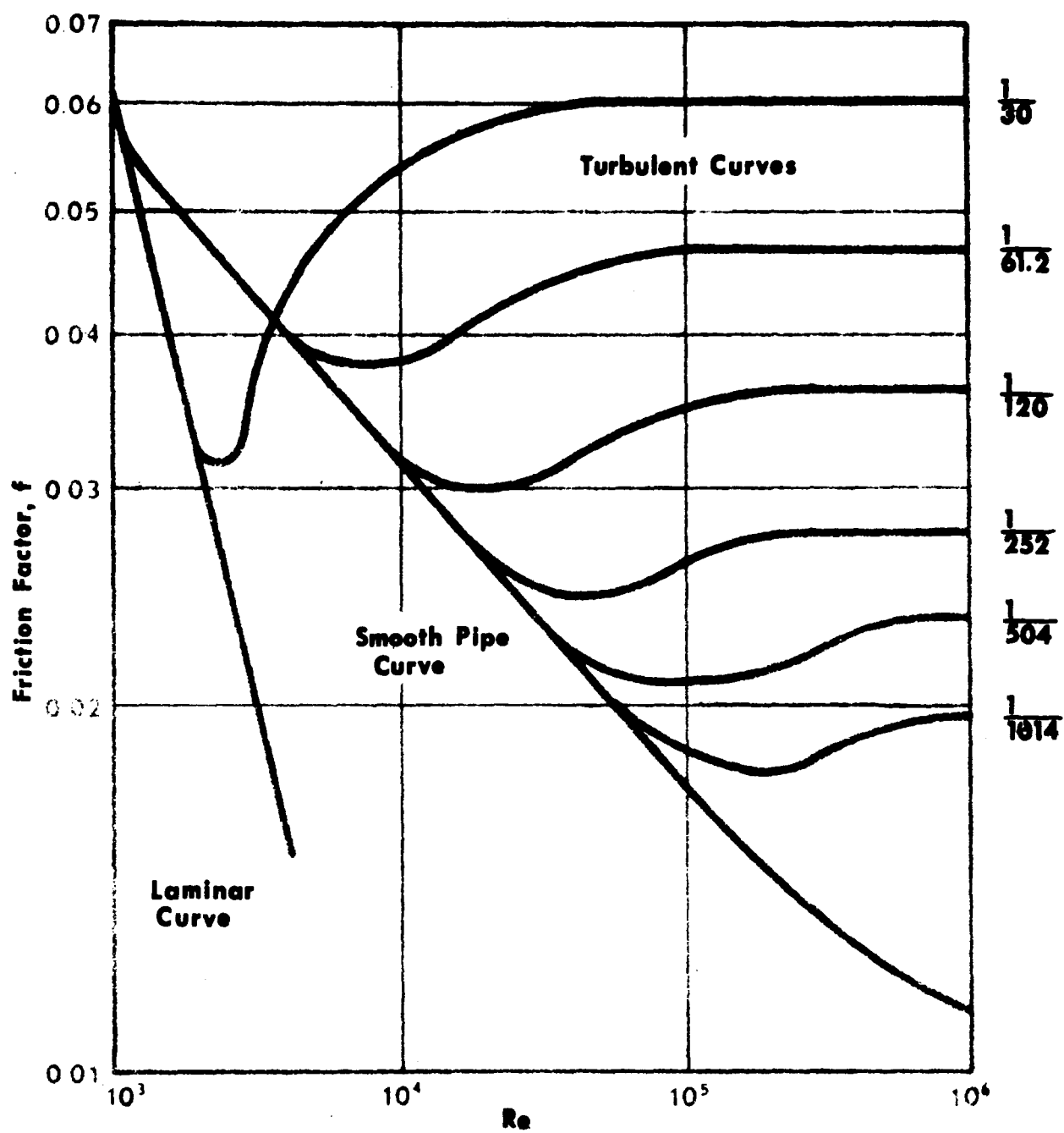


Figure 20 - Nikuradse's Data From Artificially Roughened Pipe Flows

TABLE VII

Empirical Formulas for Friction Factor

<u>Regime</u>	<u>Reynolds Number</u>	<u>Friction Factor</u>
Laminar	$R_e \leq 2300$	$f = 64/R_e$
Frictional Transition (Smooth Pipe Curve)	$2300 < R_e \leq \left(\frac{.316}{f'}\right)^4$	$f = \frac{.316}{R_e^{.25}}$
where $f' = \frac{1}{\left(2 \log \left(\frac{D_{sd}}{2e_f}\right) + 1.74\right)^2}$		
Turbulent	$R_e > \left(\frac{.316}{f'}\right)^4$	$f = f'$

Equation (12.10) is an implicit function of bearing angular velocity, duct geometry and frictional flow losses. To solve for v_1 an iterative technique is used. First v_1 is calculated with $H = 0$, then a mean time velocity, next a friction factor and finally, a headloss. With this headloss a new v_1 is computed. This procedure is repeated until a satisfactory degree of convergence is obtained in v_1 .

Having computed the shaft duct exit velocity, the volumetric flow rate is

$$Q_{sd} = A_s \times v_1 \quad (12.12)$$

Cone Ducts

The assumptions and boundary conditions used in the analysis of the shaft ducts can be applied to the cone ducts. As these two segments of the system are analogous then the equations defining lubricant velocity and volumetric flow rates are similar.

Substituting the corresponding variables into equations 12.10, 12.11 and 12.12

$$v_3 = \left[\omega^2 (r_3^2 - r_2^2) - 2H \right]^{1/2} \quad (12.13)$$

$$H = \frac{\bar{v}_{cd}^2}{2} \frac{L_{cd}}{D_{cd}} f \quad (12.14)$$

$$Q_{cd} = A_{cd} \times v_3 \quad (12.15)$$

Friction factor f is determined using Table VII.

12.2 Manifold Flow

The analyses of lubricant flow through the manifold presents a complex problem. Efforts will be limited to developing some estimates of manifold cross-sectional area and flow capacity. A segment of the manifold is shown on Figure 21. The control volume shown will be used later in the analysis.

The singular function of the manifold is to collect lubricant pumped through the shaft ducts and distribute it equally to each of the cone ducts. The lubricant flowing through one shaft duct is assumed to be divided equally at the manifold. Therefore, manifold capacity is not only dependent on cross-sectional area and velocity, but also, the number of shaft ducts. Let the m subscript denote manifold conditions, then this relationship can be written

$$Q_m = n_{sd} A_m v_m \quad (12.16)$$

A segment of the manifold adjacent to a shaft duct is shown on Figure 22. The mass of the element of lubricant is dm with an area dA . From kinematics, acceleration in the radial direction is

$$a_r = -r \omega^2 + \frac{d^2 r}{dt^2} \quad (12.17)$$

At this segment of the manifold neglect flow in the radial direction so that $\frac{d^2 r}{dt^2} = 0$

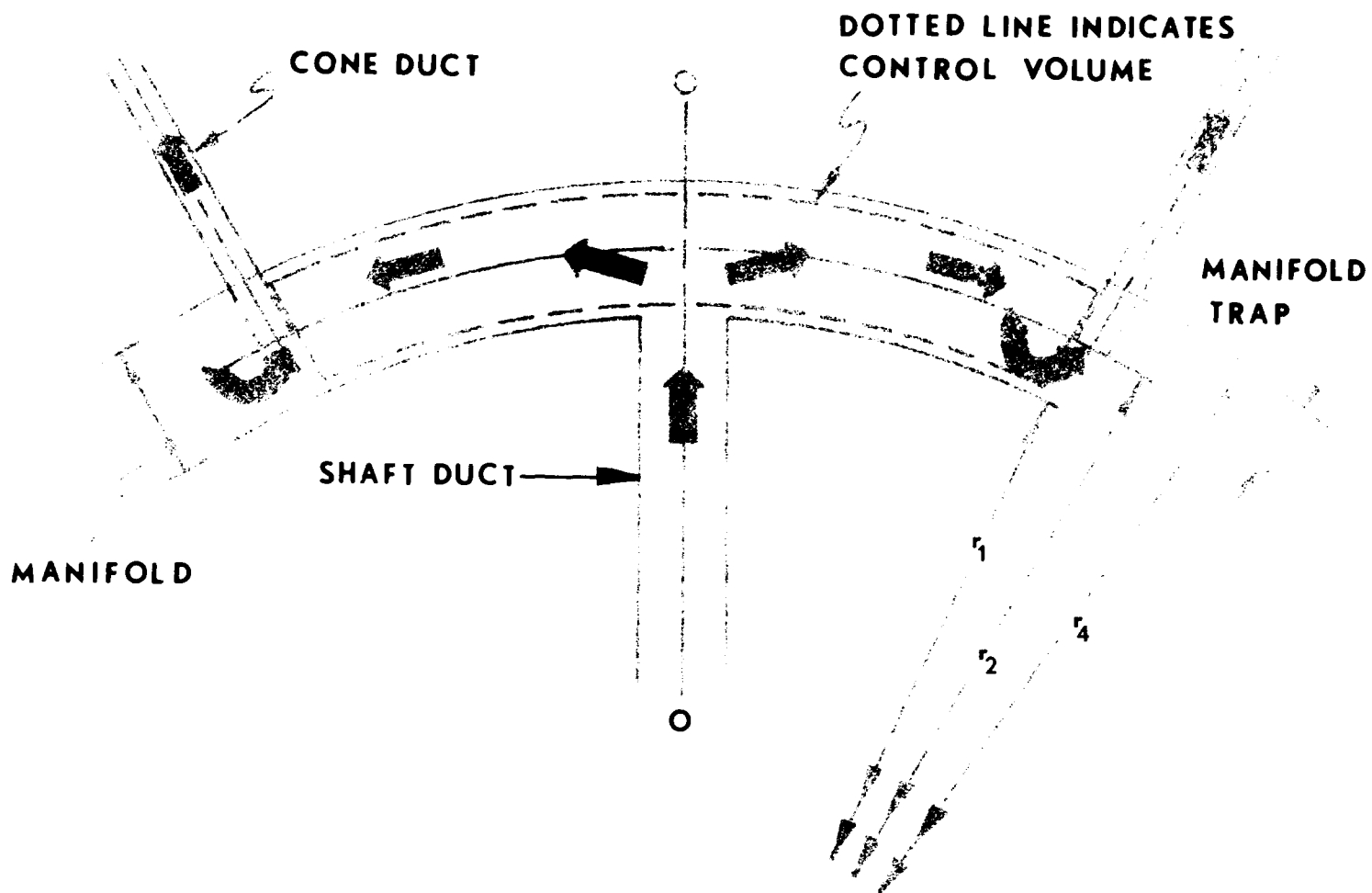


Figure 21 - Control Volume For Analysis of Manifold

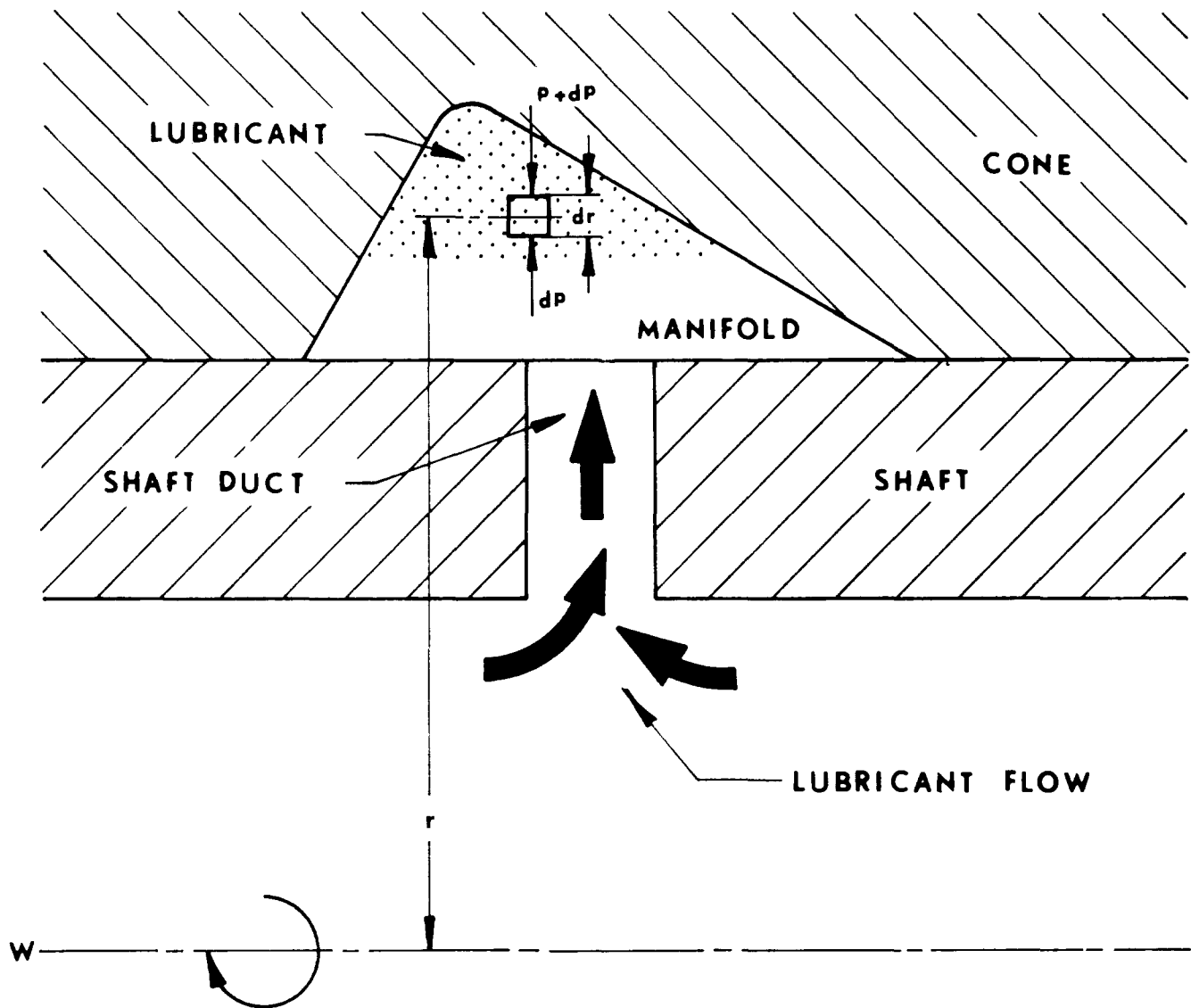


Figure 22 - Manifold Section Adjacent
Shaft Duct

A force balance yields

$$p dA - (p + dp) dA = a_r dm \quad (12.18)$$

For the element of lubricant

$$dm = \frac{\rho'_o}{g} dA dr \quad (12.19)$$

Substituting equations 12.17 and 12.19 into 12.18 and rearranging terms

$$dp = \frac{\rho'_o}{g} \omega^2 r dr \quad (12.20)$$

This can be integrated directly to determine the pressure differences between any two radial distances.

Referring back to Figure 21, let the m subscript denote manifold conditions just prior to a cone duct and the subscript o to represent manifold conditions adjacent the shaft duct. As lubricant accumulates at the shaft duct, it forces oil circumferentially around the manifold. Further simplifying this, assume that the cross-sectional area of the manifold being used at the junction of the shaft duct is considerably larger than the area adjacent the cone duct. A_o is bounded by r_1 and r_4 and A_m is bounded by r_2 and r_4 . Applying the "Bernoulli Equation" to this control volume and letting v_o equal zero and neglecting effects of gravity and friction

$$\frac{v_m^2}{2} = \frac{p_o g}{\rho'_o} - \frac{p_m g}{\rho'_o} = \frac{g}{\rho'_o} (\Delta P) \quad (12.21)$$

Pressure difference across the manifold control volume
from equation 12.20

$$\Delta P = \frac{\rho' \omega^2}{2g} (r_2^2 - r_1^2) \quad (12.22)$$

and $V_m = \omega (r_2^2 - r_1^2)^{1/2}$

Then the manifold flow rate can be estimated by

$$Q_m = 2n_{sd} \times A_m \times \omega (r_2^2 - r_1^2)^{1/2} \quad (12.23)$$

12.3 Effectiveness of System

The analysis of the previous two sections developed equations to predict lubricant velocities and flow rates. This section will determine the trajectory of the lubricant as it leaves the cone ducts and quantitatively define the effectiveness of distribution around the circumference of the rib.

In this section, effectiveness is defined as the percentage of rib circumference covered by the stream of lubricant. The effects of roller-end/rib starvation and surface wetting are beyond the scope of this analysis. Furthermore, the lubricant stream is considered useful only between the diameters of the cone direct outlet ($2r_3$) and the center of the roller-end/rib contact ($2r_5$). Once the lubricant leaves the cone duct, its motion is independent of the cone and atmospheric drag is neglected.

This coordinate system is shown on Figure 23. The components of velocity in the X and Y direction are \dot{X} and \dot{Y} .

The angle γ for a single cone duct is formed with the bearing center and is opposite the segment of the rib transversed by a particle of lubricant as it leaves the cone duct and intersects the center of the roller-end/rib conjunction.

System effectiveness is defined as

$$E_s = 100 \frac{n_{cd} \lambda}{2\pi} \quad (12.24)$$

To determine λ , first the Cartesian coordinates of the point where the path of the lubricant particle intersects the roller-end/rib radius r_5 is determined. Using the equation of a circle with the origin at zero.

$$x^2 + y^2 = r_5^2 \quad (12.25)$$

X and Y as a function of time are

$$X = \omega r_3 T \quad (12.26)$$

$$Y = r_3 + v_3 \cos(\theta_H) T \quad (12.27)$$

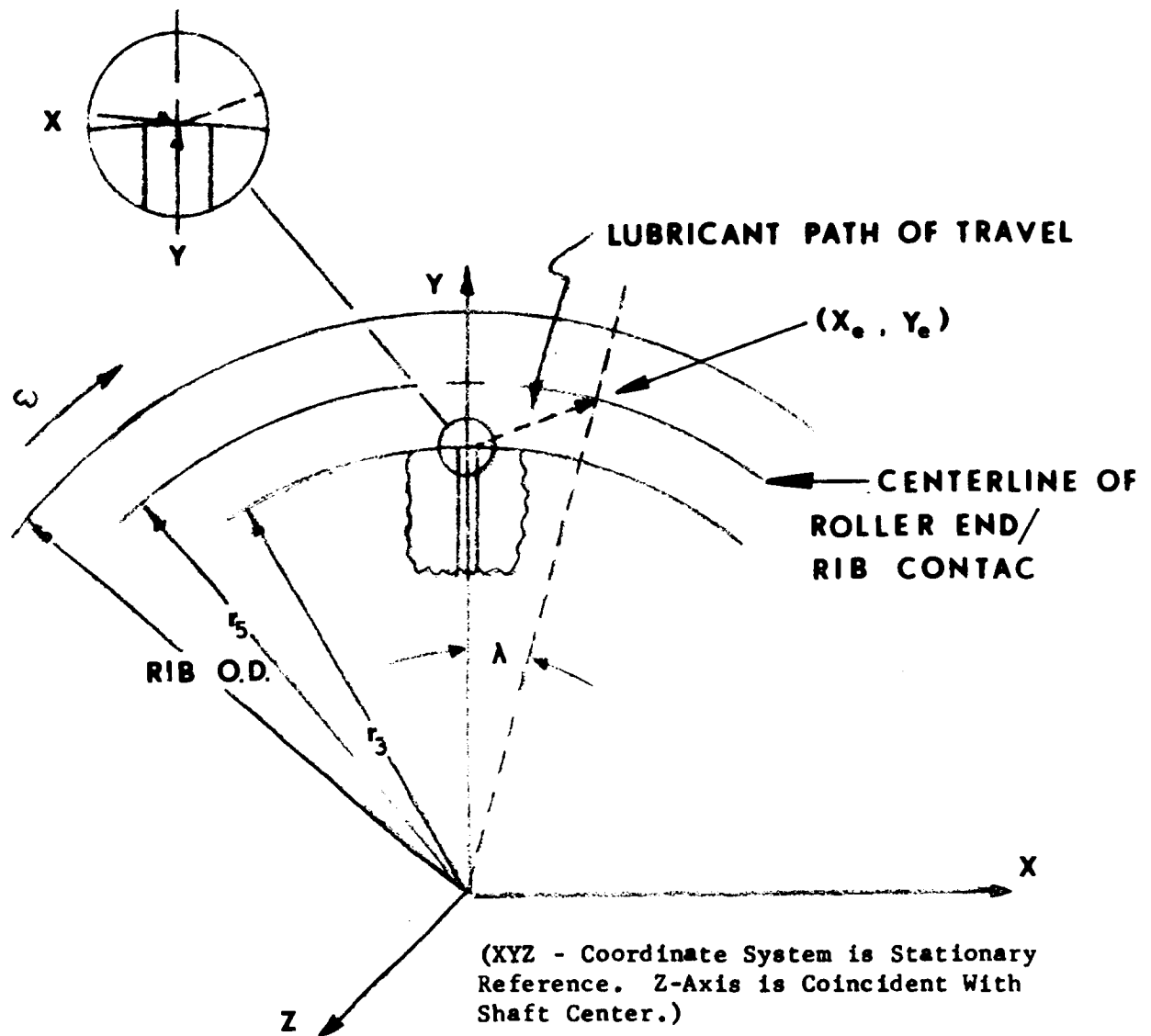


Figure 23 - Coordinate System to Calculate Effectiveness of Lubrication System

Substituting equations 12.26 and 12.27 into 12.25 and
solving for the elapsed time t_e

$$t_e = \frac{\left[(r_3^2 v_3^2 \cos^2 \theta_H) - (\omega^2 r_3^2 + v_3^2 \cos^2 \theta_H) (r_3^2 - r_5^2) \right]^{1/2} - r_3 v_3 \cos \theta_H}{(2 r_3^2 + v_3^2 \cos^2 \theta_H)} \quad (12.28)$$

Now knowing t_e , x_e and y_e can be calculated and

$$\lambda = \tan^{-1} \left(\frac{x_e}{y_e} \right) \quad (12.29)$$

13. DISCUSSION AND RECOMMENDATIONS

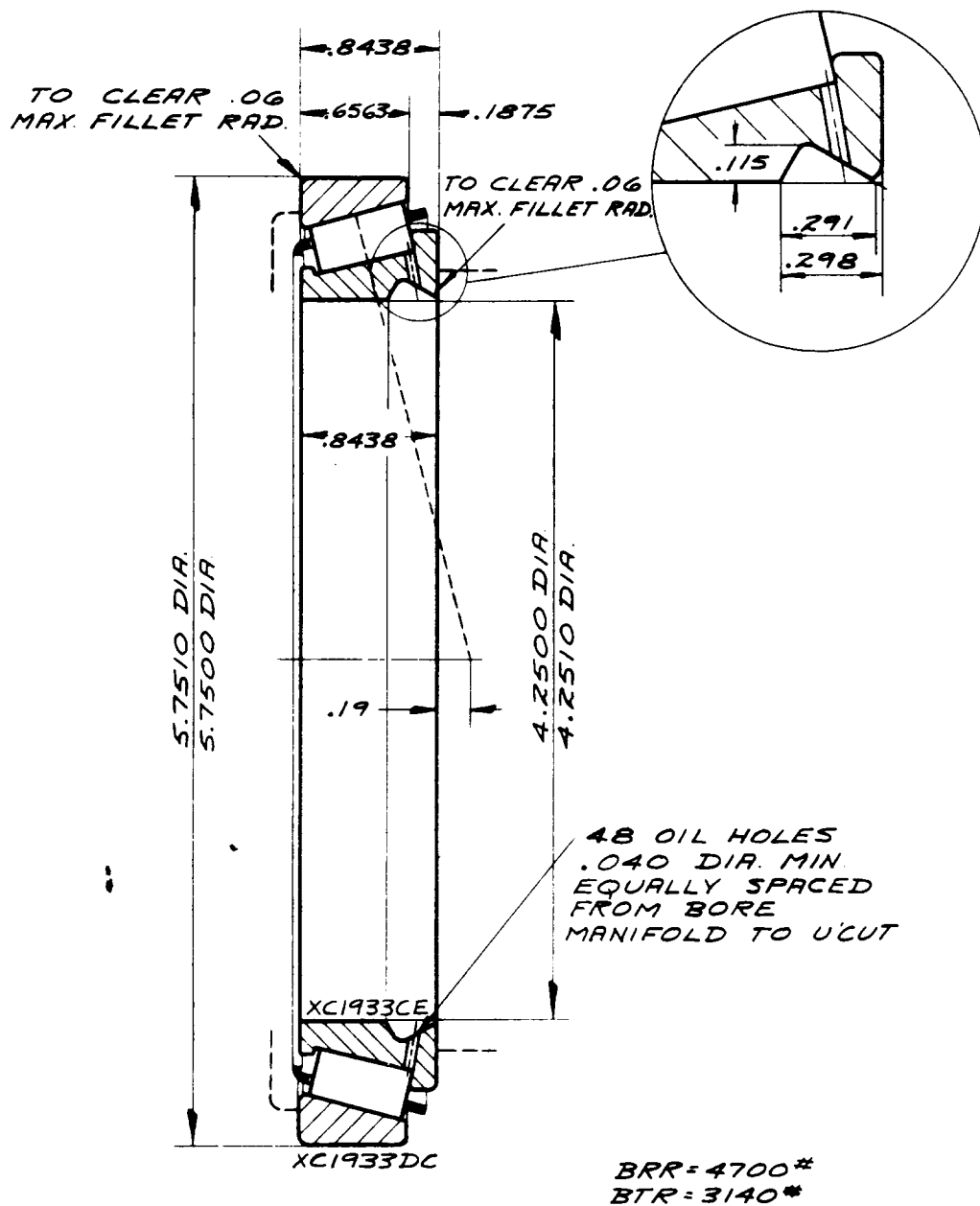
A Timken developed, Fortran language computer program has been written which includes all of the foregoing analyses. Appendix B is the printout of this program entitled, "High Speed Tapered Roller Bearing Analysis". The data shown is for the candidate test bearing XC1933CE-XC1933CD operating at 3.5×10^6 DN, maximum program thrust load of 5000 pounds, lubricant supply (MIL-L-7808G) temperature of 300°F and with an assumed conjunction inlet temperature of 350°F.

Under pure thrust loading each roller is assumed to be similarly loaded. If radial load was considered, all the parameters such as load, stress, film thickness, friction, etc. would be computed throughout the load zone.

A parametric study was conducted to determine whether this candidate bearing would be suitable for high speed development testing. Assembly drawings of the XC1933 series bearing assembly with the standard roller guided cage and alternate race guided cage are shown on Figures 24 and 25 respectively.

The two study bearings were chosen with the following design considerations:

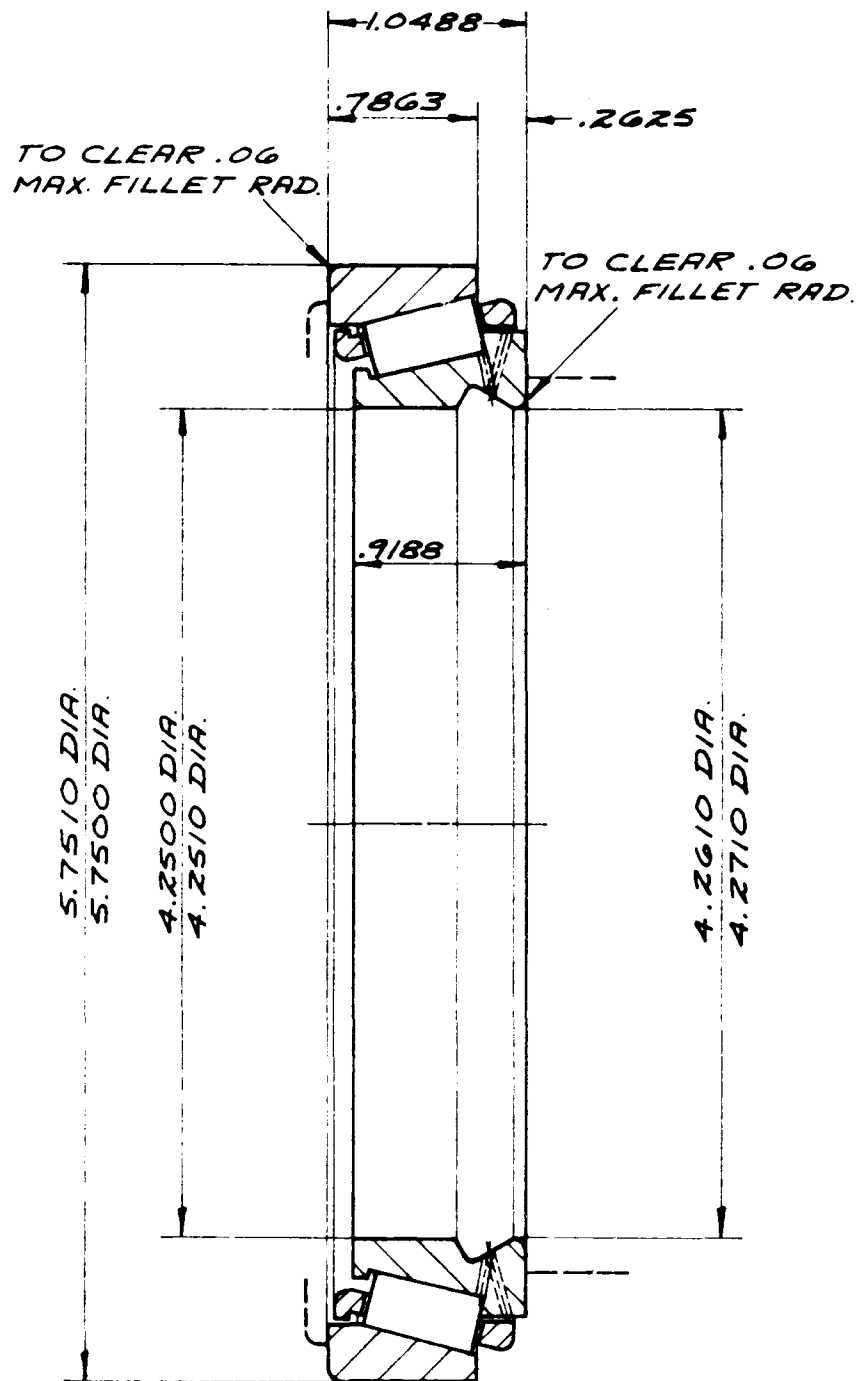
- a. Keeping the inside and outside diameters constant with slight variation in overall bearing width.



THE CONE, CUP, AND ROLLERS
ARE TO BE MADE FROM CBS1000M STEEL.

Figure 24 - Proposed Test Bearing With
Roller Guided Cage

		XC1933CE - XC1933DC SPEC. TS BEARING ASSEMBLY	
		THE TIMKEN COMPANY CANTON, OHIO, U. S. A.	
89	DRAWN JUN GLL 5-73	CHECKED BRJ 5-73	APPROVED DATE DLS JUN. 5-73
	A-39898		



L521900 SERIES
37 ROLLERS
GLL JUL-20-73

Figure 25 - Proposed Test Bearing With
Race Guided Cage

- b. Reduced roller diameters to minimize effects of centrifugal force.
- c. Steeper and shallower contact angles to determine geometry effects.

A summary of the pertinent results are shown on Table VIII. Overall, these studies indicated that changing the existing geometry (new tooling requirements and increased costs) would not be warranted based on these computed parameters.

In both study bearings the roller diameter was reduced by 8.33%. With the reduced roller size and a slightly increased pitch diameter an additional five rollers could be added to the bearing. For the steeper angle study No. 1, the race stresses were reduced by approximately 5% with a negligible change in rib stress and a slight reduction of lubricant film thickness. The shallower angle study No. 2 developed increased race stresses (3.4% at cone), reduced rib loading with 5% thicker film at the rib conjunction.

The initial studies were conducted using a roller spherical end radius equal to 77% of the apex length. Past development tests have shown this to be the optimum radius for high speed operation. Figure 26 is a plot of the calculated lubricant film thickness (central region) at the roller-end/cone rib conjunction as a function of roller spherical end radius.

TABLE VIII

Effects of Bearing Geometry on Operating Parameters

*Note: Dimensions in inches, force and weight in pounds and stresses in KSI.

Study conditions: R = 0; T = 5000#; S = 32422 RPM;
T₁, T₂, T₃ = 350°F

	<u>XC1933CE/ XC1933DC</u>	<u>Study No. 1</u>	<u>Study No. 2</u>
<u>*Geometry</u>			
Included Cone Angle (2 β)	26° 8'	27° 54'	24° 54'
Included Cup Angle (2 α)	29° 20'	31° 0'	27° 40'
Roller Diameter (d ₁)	.300	.2755	.2747
Roller End Radius (r)	8.2723	7.8418	8.7610
Mean Cone O.D. (D ₂)	4.7218	4.7659	4.7764
Cone Base Diameter (D ₃)	4.8578	4.9103	4.9059
Mean Cup I.D. (D ₅)	5.2880	5.2832	5.2973
Number of Rollers	39	44	44
<u>*Computed Parameters</u>			
Weight/Roller	.0114	.0095	.0096
Centrifugal Force/Roller	189	161	162
Roller RPM (No Slip)	277347	303804	304484
Cage RPM (No Slip)	15294	15377	15373
Net Bearing Induced Thrust			
Due to C _f	1812	1832	1658
Normal Loads/Stresses			
At Conjunctions: Cone	322/149.7	269/142.6	318/154.8
Cup	506/177.4	425/170.1	475/179.8
Rib	56.9/23.0	50.2/22.9	46.3/20.7
EHD Minimum Film Thickness Without Thermal Reduction (Microinches)			
Roller-Body/Cone	7.6	7.5	7.4
Roller-Body/Cup	7.5	7.4	7.3
Roller-End/Rib	14.2	13.9	14.9

Note: Central Film Thickness at Rib/
 Roller End Conjunction Computed
 Using: Archard and Cowking Formula,
 References 22 & 23
 Proposed Test Bearing - XC1933
 Lubricant - MIL-L-7808G
 At Inlet Temperature 350°F

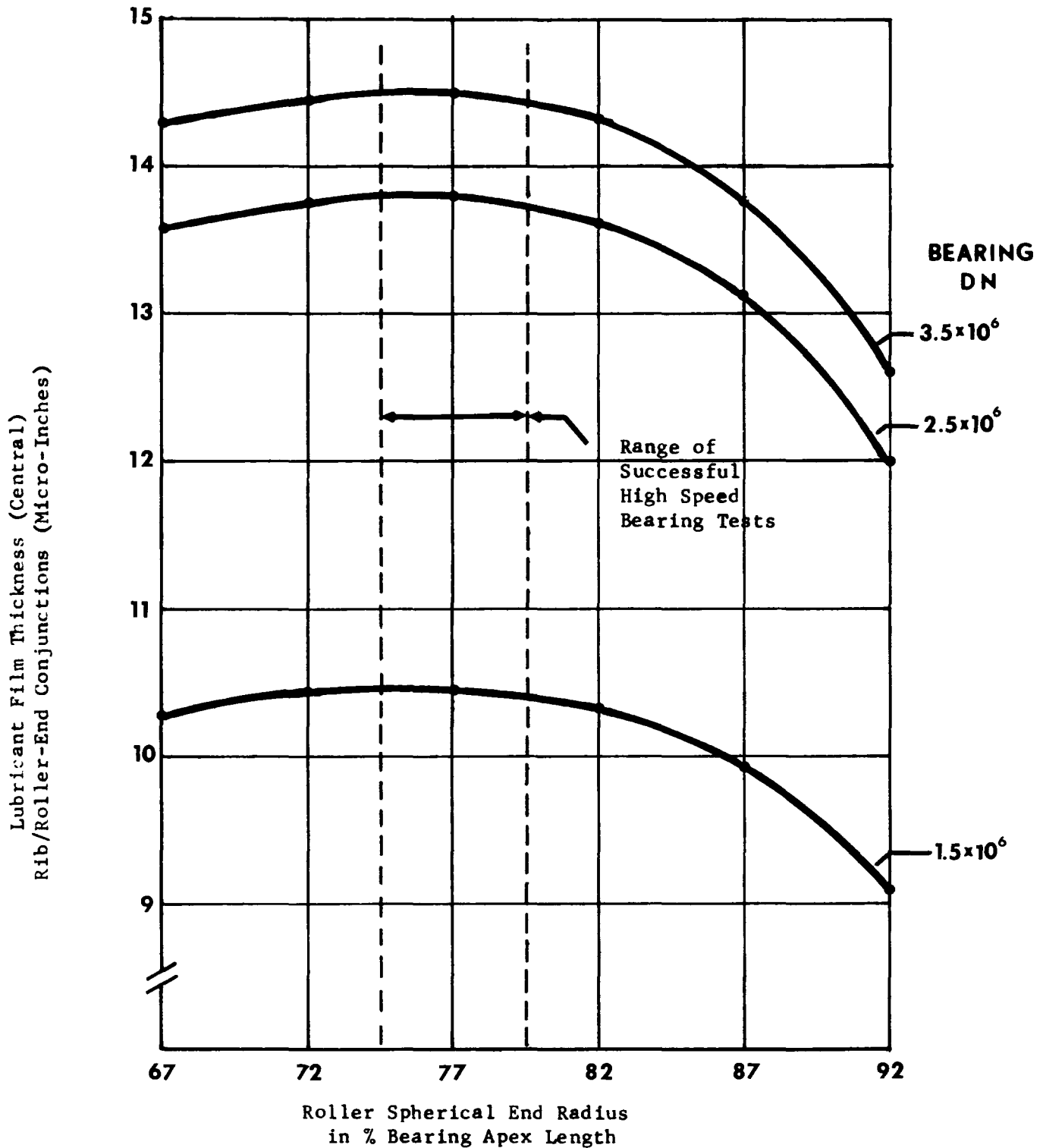
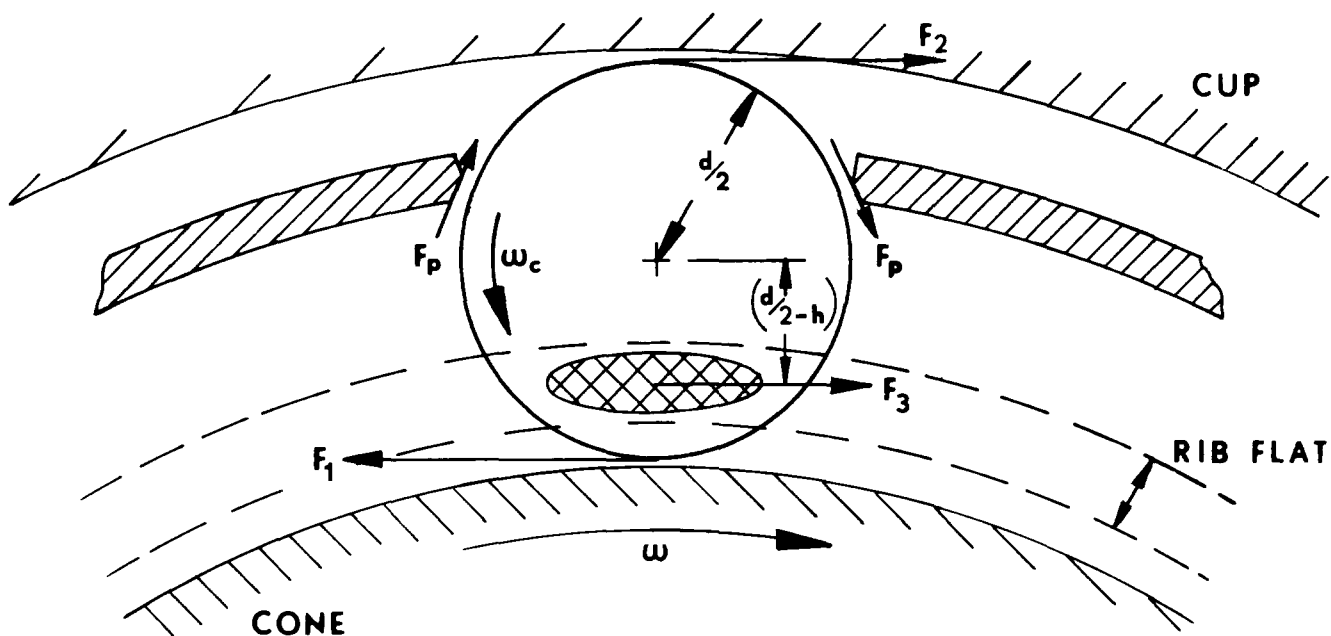


Figure 26 - Film Thickness Versus % Apex
 Roller Spherical End Radius

The maximum film thickness of the central region is developed with a roller spherical end radius of 75% to 80% of the apex length. Previous development testing have verified these results.

At the present time, it is not anticipated that roller slip will be a problem. The tapered roller bearing (unlike ball or cylindrical roller bearings) has a rib which tends to drive the roller at a speed greater than the epicyclic speed. (Refer to Figure 27.) This sketch illustrates the forces that drive the roller. A summation of roller moment loading Table IX indicates that there is a positive driving moment over the full range of speed. In addition to this positive moment, it is reasonable to assume that there is asperity contact between mating surfaces which would also tend to keep the roller rotating at its epicyclic speed.

The selection of 48 ducts for the cone rib lubrication system is based on empirical data of previous tests. The two parameters used for estimating the number of cone ducts are peripheral rib speed and the percent of the rib circumference covered by a stream of oil. Refer to Figure 28 to compare these test conditions with previous work.



$E_m =$ SUMMATION OF MOMENTS ABOUT ROLLER CENTER
(CCW - POSITIVE)

$$E_m = (d/2 - h) \times F_3 - d \times F_p - (d/2) \times F_1 - (d/2) \times F_2$$

Figure 27 - Forces Effecting Roller Moment
Loading (Roller-End/Rib Conjunction
Shown Out of Plane)

TABLE IX

Summation of Moments About Roller Center

Calculations based on the following conditions:

Bearing: XC1933CE-XC1933DC
 Lubricant: MIL-L-7808G
 Temperature: Supply - 300°F
 Conjunction Inlet - 350°F
 Loading: Thrust - 5000 Pounds
 Radial - 0
 Roller-Body/Cage
 Pocket Clearance: .0001"

Speed		Friction Forces (Pounds)				Summation Of Moments About Roller Center Inch-Pounds
<u>DN</u>	<u>RPM</u>	<u>Cone F₁</u>	<u>Cup F₂</u>	<u>Rib F₃</u>	<u>Cage F_p</u>	
1.5x10 ⁶	13895	.1796	.1858	.8929	.0713	+.0009
2.5x10 ⁶	23159	.2569	.2657	1.3262	.1188	+.0006
3.5x10 ⁶	32422	.3251	.3363	1.9048	.1663	+.0151

*Plus Sign indicates positive moment in direction of rolling.

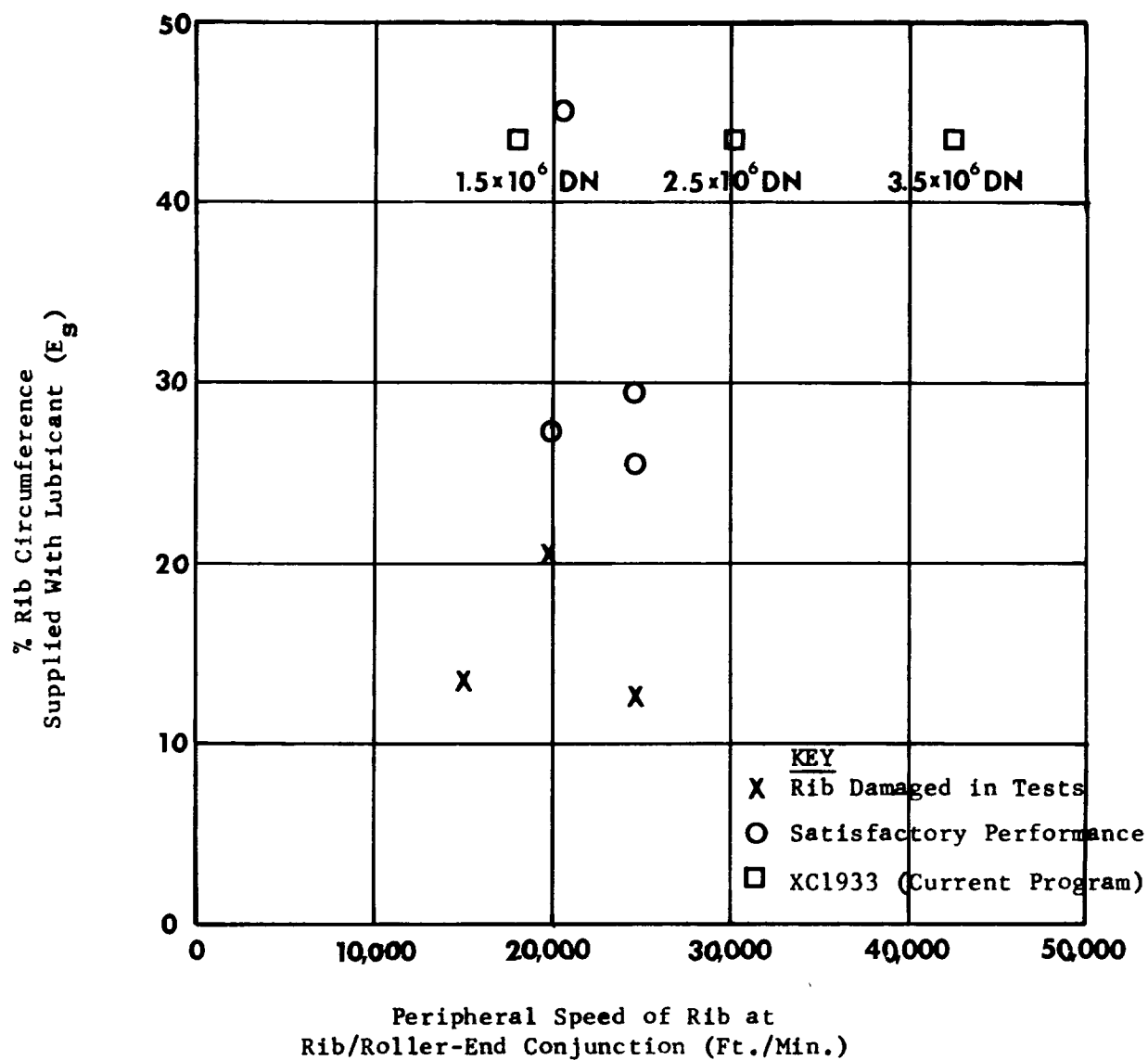


Figure 28 - % Lubricant Coverage Versus Rib Speed

RECOMMENDATIONS

It is recommended that the XC1933 series bearing assembly incorporating the following design be tested to 3.5 million DN:

- a. Roller spherical and radius equal to 77% of apex length.
- b. Standard stamped roller guided cage.
- c. A cone rib lubrication system with 48 - .040" diameter ducts.

APPENDIX A

Friction Analysis for High Sliding Combined With Rolling (Roller End/Rib)

For selected friction data (supplied by Southwest Research Institute) in studies with disks in rolling/sliding contact, the three parameters G_1 , G_2 and G_3 were calculated and friction coefficient was plotted against G_1 , for various values of G_2 and G_3 . These friction data are for the full EHD regime. Oil and test conditions are as follows:

Oil: SwRI Oil B, a straight mineral oil

	<u>$T_O = 140^\circ\text{F}$</u>	<u>$T_O = 190^\circ\text{F}$</u>
μ_O (cp)	29.73	11.55
α_O (psi^{-1})	1.38×10^{-4}	1.20×10^{-4}
k (BTU/hr./ft./ $^\circ\text{F}$)	.0075	.0075
$\beta = .0272 \text{ } ^\circ\text{R}^{-1} \text{ @ } 150,000 \text{ psi}$		
$v_S = 210 \text{ and } 350 \text{ in./sec.}$		
sum velocity = 1050 in./sec.		
$\sigma_m = 140,000 \text{ to } 300,000 \text{ psi}$		

These conditions give three values of G_2 : 38.6×10^{-3} , 42.8×10^{-3} and 107×10^{-3} , and values of G_3 between 16 and 32. These values of G_2 more closely approximate the conditions at the roller end/rib conjunction than those plotted in Reference 14. Figure 29 shows the data for the two lower values of G_2 , which are approximately the same and can be averaged to give a nominal $G_2 = 41 \times 10^{-3}$, this represents the lowest G_2 for which SwRI data are available for full EHD regime. Figure 30 presents SwRI data for an even larger $G_2 = 107 \times 10^{-3}$. Figure 31 is a plot of the "ceiling" friction coefficient versus G_2 . The data points shown in Figure 31 are from Reference 14, and the curve shown has been linearly extrapolated to higher values of G_2 . From this extrapolated curve, the ceiling friction coefficients at $G_2 = 41 \times 10^{-3}$ and 107×10^{-3} were determined and each is shown as the dashed line in Figures 29 and 30. As can be seen in those figures, the "ceiling" friction coefficients look reasonable in comparison with SwRI experimental data.

In comparing Figures 92 through 98 in Reference 14, it will be seen that as G_2 increases, the family of curves of constant G_3 shift to the right. Also, in the Reference and SwRI data, the "ceiling" friction coefficient decreases

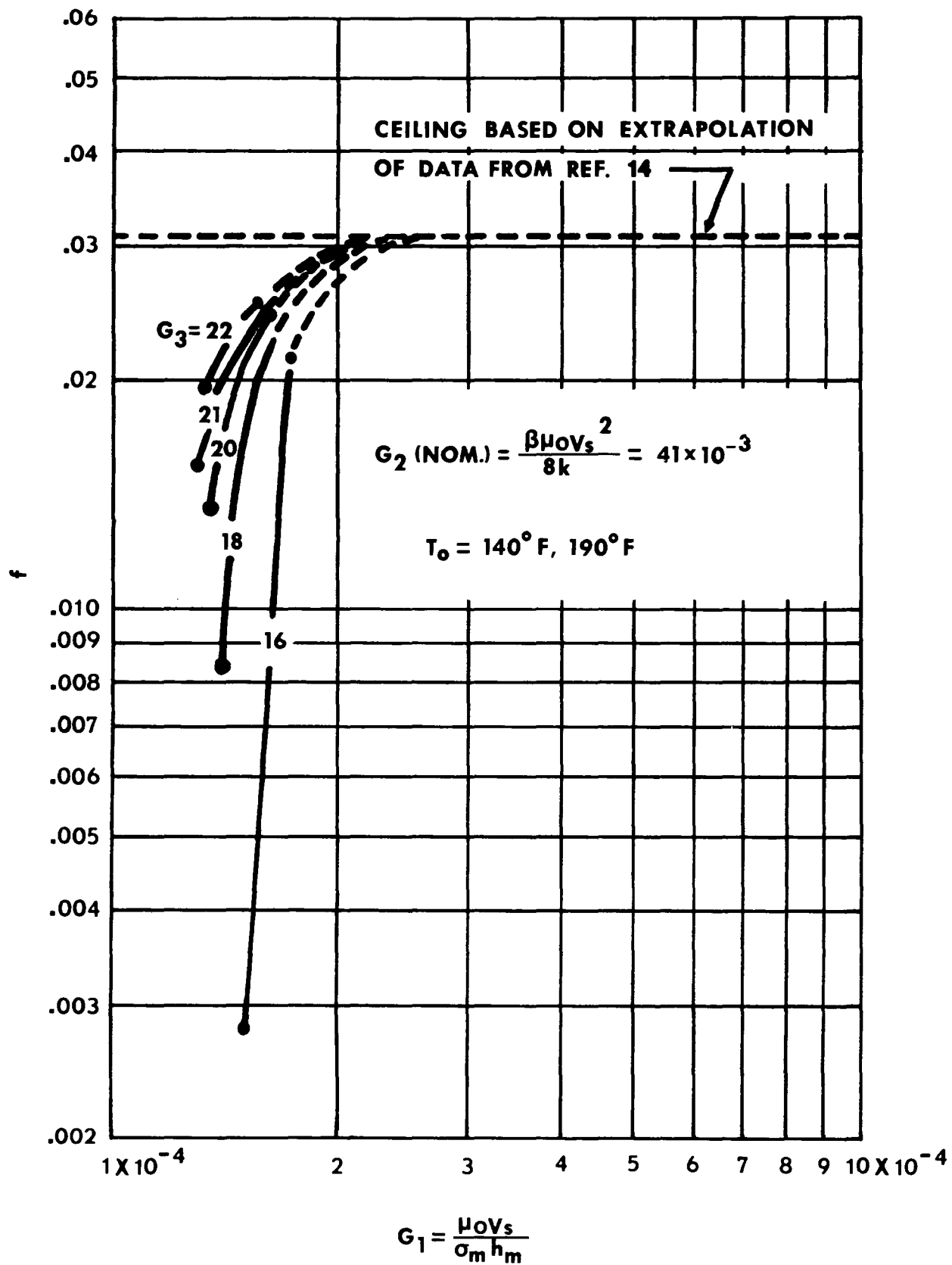


Figure 29 - Friction Coefficient Behavior
For $G_2 = 41 \times 10^{-3}$

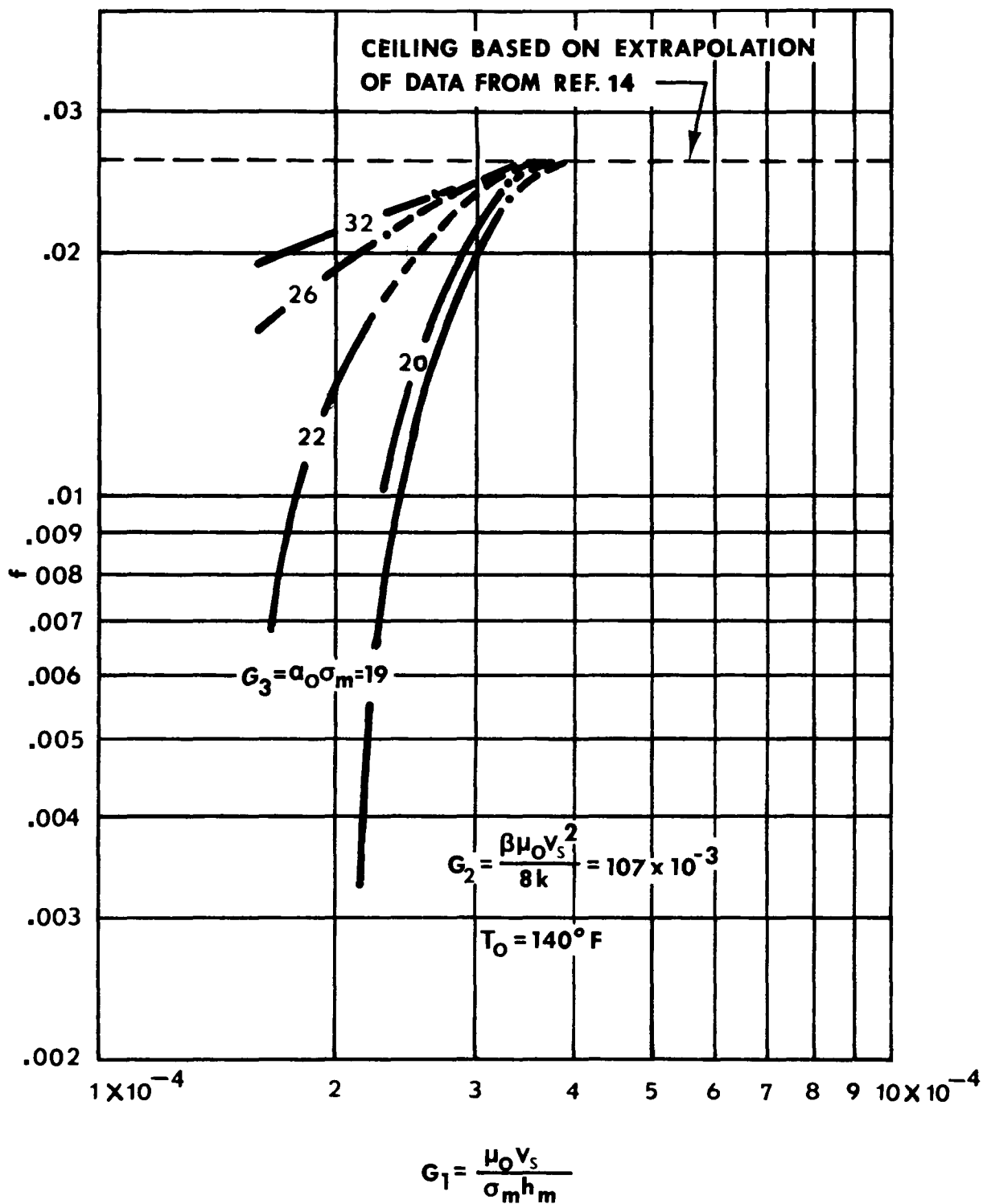


Figure 30 - Friction Coefficient Behavior
For $G_2 = 107 \times 10^{-3}$

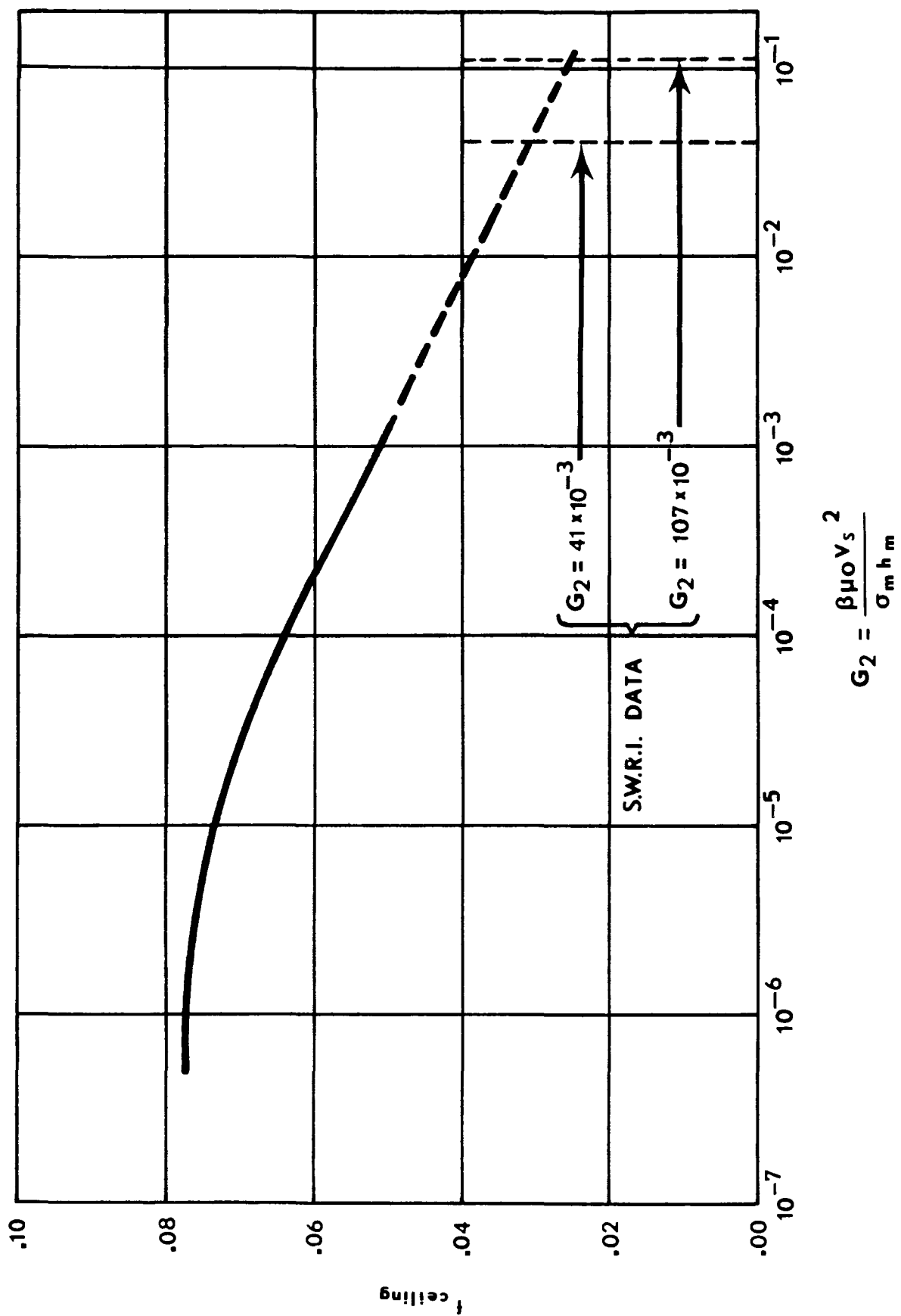


Figure 31 - Behavior Of Ceiling Friction Coefficient With G_2

as G_2 increases. For a given G_2 , as G_3 decreases the curves of constant G_3 shift to the right, and enter the "ceiling" asymptote more sharply. SWRI data in Figures 29 and 30 also exhibit all these characteristics, and are in line quantitatively with the data in Reference 14.

The procedure recommended in Reference 14 consisted of calculating G_1 , G_2 and G_3 at the reference supply temperature of 86°F, then compensating for the supply temperature difference.

The reason given for this extrapolation technique is that Plint (Ref. 24) and Johnson and Cameron (Ref. 20) found the friction coefficient varies with supply temperature. The application of this extrapolation technique as a generalized procedure is subject to question, since it is doubtful that the relationship between supply temperature and friction coefficient would be the same for all test rigs and mechanisms such as bearings and gears. Moreover, if G_1 , G_2 and G_3 do represent the parameters necessary to describe the friction coefficient, then they should apply for any oil supply temperature T_o as long as operation is in full EHD regime.

The effect of the variation of temperature would be taken into account in the μ_o , k , h_3 and α_o variables. This appears to be the case, since the data furnished by SwRI in Figure 31 are for two supply temperatures, and the viscosity at the lower temperature is nearly three times that at the higher temperature. The sliding velocity is different for the two

supply temperatures with the results that G_2 is approximately the same for both sets of data. Refer to Figures 29 and 30. When plotted on the same graph, the friction coefficient data (SwRI) behaves in the same way as they do for all the data in Reference 14, which are for a single temperature.

Friction coefficient is estimated by first calculating the G parameters at the actual lubricant supply temperature. Then using the same numerical techniques as in Reference 14 to extrapolate for G values outside the range of data.

APPENDIX B

Sample Computer Printouts

CONE NO. XC1933CE

CUP NO. XC1933DC

RUN 500

** ALL DIMENSIONS IN INCHES - ANGLES IN DEG-MIN-SEC - UNLESS NOTED **

APPENDIX BRoller_Guided_Cage_

CONE DATA

INCLUDED ANGLE 26- 8- 0	RIB-RACE ANGLE 89-49-30	BORE 4.2500
MEAN RACE C.D. 4.7218	BASE DIA. 4.8578	WIDTH 0.8438
LARGE RIB C.D. 5.0500	SMALL RIB O.D. 4.6900	RIB FACE FLAT .0620

CUP DATA

INCLUDED ANGLE 29-20- 0	MEAN I. D. 5.2880	O. D. 5.7500
----------------------------	----------------------	-----------------

ROLLER DATA

NO. OF ROLLERS 39	L. E. DIA. 0.3000	S. E. DIA. 0.2832
SLANT LENGTH 0.6016	EFF. LENGTH 0.5475	APEX LENGTH 10.7433
WEIGHT (LBS.) 0.0114	CONTACT HT. 0.0598	SPHERICAL END RADIUS 8.2724 (77.0%)
MASS-MOMENT OF INERTIA (LB.INCH-SQ.)	I(X) = 0.00012 I(Y) = 0.00040	

CAGE DATA

TYPE OF GUIDE ROLLER	STOCK THICKNESS 0.0620	POCKET CLEARANCE 0.0001
WING ANGLE 14-48- 0	WING LENGTH 0.0352	CAGE C.D. TO ROLLER C-L 0.0845
L.E. LAND DEPTH 0.0310	S.E. LAND DEPTH 0.0250	% ROLLER PROJECTION 21.02

CONE NO. XC1933CE

CUP NO. XC1933DC

RUN 500

LARGE RIB LUBRICATION SYSTEM DATA

CONE HOLE
INLET DIA.
4.3800CONE HOLE
OUTLET DIA.
4.8580HOLE ANGLE
10- 0- 0NO. OF SHAFT HOLES
2INSIDE DIA.
0.1250SURFACE FINISH (MU)
140.0NO. OF CONE HOLES
48INSIDE DIA.
0.0400SURFACE FINISH (MU)
140.0MANIFOLD TRAP WIDTH
0.0930MANIFOLD DIA.
4.4800

MOUNTING DATA

SHAFT I. D.
3.6250

MATERIAL

HOUSING O. D.
9.0000

MATERIAL

CONE NO. XC1933CE

CUP NO. XC1933DC

RUN 500

OPERATION DATA

EXTERNAL RADIAL LOAD (LBS)
0EXTERNAL THRUST LOAD (LBS)
5000SHAFT SPEED (RPM)
32422BULK INLET TEMPERATURE (DEG.F)
300CONJUNCTION TEMPERATURE (DEG.F)
350

LUBRICANT - MIL-L-7808G

	AT BULK INLET -----	AT CONJUNCTION -----
KINEMATIC VISCOSITY (CENTISTOKES)	1.570	1.206
ABSOLUTE VISCOSITY (CENTIPOISES)	1.348	1.012
ABSOLUTE VISCOSITY (MICRO-REYNS)	0.195	0.147
DENSITY (GRAMS/CC)	0.8585	0.8386
PRESSURE-VISCOSITY COEF. (SQ. INCH/LB*10**4)	0.504	0.462
SPECIFIC HEAT (BTU / LB-DEG.F)	0.5384	0.5508
THERMAL CONDUCTIVITY (BTU / HR-FT-DEG.F)	0.0841	0.0825

COEFFICIENT OF THERMAL EXPANSION (CC / DEG.F) = 0.000394

TEMPERATURE-VISCOSITY COEFFICIENT (DEG.F ** (-1))

(.0045 + (1.25*10**(-7)) * (HERTZ STRESS))

CONE NO. XC1933CE

CUP NO. XC1933DC

RUN 500

RPM = 32422 R = 0 T = 5000 INLET/CONJ. TEMP = 300/350 F.

----- INTERFERENCE FITS -----

STATIC EFFECTS

DIAMETRICAL FIT	.001	.005	.009
CONTACT PRESS. CONE/SHAFT (PSI)	444	2223	4002
CONTACT PRESS. CUP/HSG (PSI)	363	1818	3273
INCREASE IN MEAN CONE O.D.	.000597	.002987	.005376
DECREASE IN MEAN CUP I.D.	.000831	.004156	.007481
HOOP STRESS CONE I.D. (PSI)	4239	21198	38157
HOOP STRESS CONE O.D. (PSI)	3795	18975	34155

THERMAL EFFECTS

REDUCTION OF DIAMETRICAL FIT PER 10 DEG.F (CONE/SHAFT) = 0.000255 (IN)

DYNAMIC EFFECTS

LOCATION	HOOP STRESS (PSI)
CONE I.D.	45531 (MAX)
CONE O.D.	39719

COMBINED EFFECTS STATIC & DYNAMIC (CONE / SHAFT)

STATIC DIAMETRICAL FIT	.001	.005	.009
CONTACT PRESS. (PSI)	0	1218	2997
HOOP STRESS CONE I.D. (PSI)	45531	57148	74107
HOOP STRESS CONE O.D. (PSI)	39719	50118	65298

LOSS OF DIAMETRICAL FIT DUE TO ROTATION = 0.002260

CONE NO. XC1933CE CUP NO. XC1933DC RUN 500

RPM =32422 R = 0 T = 5000 INLET/CONJ. TEMP = 300/350 F.

** BEARING KINEMATICS EPICYCLIC DN = 3.500 (10**6)

-- ALL VELOCITIES IN INCH / SECONO - UNLESS NOTED --

CONE

ANGULAR VELOCITY (RPM) = 32422 (RADIAN/SEC) = 3395

MEAN O.D. TANGENTIAL VELOCITY ABOUT OWN CENTER 8015

RIB / ROLLER CONTACT ABOUT CENTER (FT/MIN) 42221

ROLLER

ANGULAR VELOCITY ABOUT OWN CENTER (RPM) 277347

MEAN O.D. TANGENTIAL VELOCITY ABOUT OWN CENTER 4234

RIB / ROLLER CONJUNCTION ABOUT ROLLER CENTER 2620

RIB / ROLLER CONJUNCTION ABOUT CONE CENTER 6603

RIB / ROLLER RUBBING VELOCITY 1840

CAGE

ANGULAR VELOCITY (RPM) = 15294 (RADIAN/SEC) = 1601

SUM VELOCITIES OF CONJUNCTIONS (EHD)

CONE RACE / ROLLER BODY 8469

CUP RACE / ROLLER BODY 8469

CONE-RIB / ROLLER END 7081

CONE NO. XC1933CE CUP NO. XC1933DC RUN 500

RPM = 32422 R = 0 T = 5000 INLET/CONJ. TEMP = 300/350 F.

** BEARING DYNAMIC LOADING DUE TO ROTATION ONLY

-- ALL FORCES IN POUND - COUPLE IN POUND-INCH --

CENTRIFUGAL FORCE & GYROSCOPIC COUPLE

CENTRIFUGAL FORCE PER ROLLER 189.2

TOTAL BEARING INDUCED THRUST DUE TO CF 1819.

INTERFACE	COMPONENT		RESULTANT NORMAL
	RADIAL	AXIAL	
CONE RACE / ROLLER BODY	0.0	0.0	0.0
CUP RACE / ROLLER BODY	178.2	46.6	184.2
CONE-RIB / ROLLER END	11.0	46.6	47.9

DISPLACEMENT OF CUP RACE / ROLLER BODY RESULTANT FOR
 STATIC MOMENT EQUILIBRIUM = 0.0189

CUP LOAD PER UNIT LENGTH ADJACENT ROLLER (LB/IN)

L.E.D.	S.E.D.
266.8	406.1

GYROSCOPIC COUPLE PER ROLLER = 3.931

COMBINED EFFECTS OF CENTRIFUGAL FORCE & GYROSCOPIC COUPLE

CUP LOAD PER UNIT LENGTH ADJACENT ROLLER (LB/IN)

L.E.D.	S.E.D.
345.5	327.4

CONE NO. XC1933CE

CUP NO. XC1933DC

RUN 500

RPM =32422 R = 0 T = 5000 INLET/CONJ. TEMP = 300/350 F.

LOAD DISTRIBUTION FACTORS (LINE CONTACT)

<u>R*TAN(A)/T</u>	<u>SJOVALL'S RADIAL</u>	<u>INTEGRALS THRUST</u>	<u>PARAMETER EPSILON</u>	<u>LOAD ZONE DEGREES</u>
0.0	0.0	1.0000	INFINITY	360

STRESSES AT RACE CONTACTS FOR MAX LOADED ROLLER

	<u>CONE/ROLLER</u>	<u>CUP/ROLLER</u>
NORMAL LOAD (LBS)	322.0	506.3
CONTACT STRESS AT CENTER (KSI)	149.7	177.4
CONTACT WIDTH	0.0050	0.0066
CONTACT LENGTH	0.5475	0.5475
MAX SHEAR STRESS (KSI)	44.9	53.3
DEPTH OF MAX SHEAR STRESS	0.0020	0.0026
MAX SHEAR STRESS AT SURFACE (KSI)	29.9	35.5
MAX RANGE (+,-) OF ORTHOGONAL (KSI)	76.6	90.8
DEPTH OF MAX ORTHOGONAL SHEAR	0.00125	0.00166

ENGRG PHL022-01 HIGH SPEED TAPERED ROLLER DATE PAGE
 BEARING ANALYSIS 18 JULY 1973

CONE NO. XC1933CE CUP NO. XC1933DC RUN 500

RPM =32422 F = 0 T = 5000 INLET/CONJ. TEMP = 300/350 F.

***** LOAD ** STRESS ** LUBRICANT FILM *****

CONE RACE / ROLLER BODY

AZIMUTH (DEG)	RADIAL (LBS)	AXIAL (LBS)	NORMAL (LBS)	STRESS (KSI)	FACTOR	FILM (MU)
0.0	313.7	72.8	322.0	149.7	0.6841	5.2

*** ALL ROLLERS IDENTICALLY LOADED ***

CGNE NO. XC1933CE

CUP NO. XC1933DC

RUN 500

RPM = 32422 R = 0 T = 5000 INLET/CONJ. TEMP = 300/350 F.

***** LOAD ** STRESS ** LUBRICANT FILM *****

CUP RACE / ROLLER BODY

AZIMUTH (DEG)	RADIAL (LBS)	AXIAL (LBS)	NORMAL (LBS)	STRESS (KSI)	FACTOR	FILM (MU)
0.0	489.9	128.2	506.3	177.4	0.6856	7.8

*** ALL ROLLERS IDENTICALLY LOADED ***

CONE NO. XC1933CE

CUP NO. XC1933DC

RUN 500

RPM = 32422 R = 0 T = 5000 INLET/CONJ. TEMP = 300/350 F.

***** LOAD ** STRESS ** LUBRICANT FILM *****

CONE RIB / ROLLER END

B/A = 0.38742

AZIMUTH (DEG)	RADIAL (LBS)	AXIAL (LBS)	NORMAL (LBS)	STRESS (KSI)	FACTOR	FILM (MU)	2B CONTACT ELLIPSE
0.0	13.0	55.4	56.9	23.1	0.7410	10.7	0.0427

*** ALL ROLLERS IDENTICALLY LOADED ***

CONE NO. XC1933CE

CUP NO. XC1933DC

RUN 500

RPM = 32422 R = 0 T = 5000 INLET/CONJ. TEMP = 300/350 F.

CAGE ANALYSIS
-----ROLLER BODY / CASE POCKET CONJUNCTION
-----INCLUDED ANGLE (RADIAN)
0.2418ARC LENGTH
0.0353REYNOLDS NUMBER
173FRICTION FACTOR
0.01150SHEAR STRESS (PSI)
8.253DRAG FORCE (LBS)
0.1663

L
ENGRG PHL022-01
HIGH SPEED TAPERED ROLLER BEARING ANALYSIS
DATE 18 JULY 1973
PAGE

CONE NO. XC1933CE
CUP NO. XC1933DC
RUN 500

RPM =32422
R = 0
T = 5000
INLET/CONJ. TEMP = 300/350 F.

TRACTION

		TRACTIVE LOADING & FLUID PRESSURE FORCES				
AZIMUTH (DEG)	ROLLER ANGULAR VELOCITY (RAD/SEC)CUP.....	CONE.....		...RIB..
		ROLLING TRACTION	PRESS. FORCE	ROLLING TRACTION	PRESS. FORCE	SLIDING TRACTION
-----	-----	-----	-----	-----	-----	-----
0.0	29043	-0.33630	0.63342	-0.32507	0.61226	1.97916

CONE NO. XC1933CE

CUP NO. XC1933DC

RUN 425

** ALL DIMENSIONS IN INCHES - ANGLES IN DEG-MIN-SEC - UNLESS NOTED **

APPENDIX BRace Guided Gage

CONE DATA

INCLUDED ANGLE 26- 8- 0	RIB-RACE ANGLE 89-49-30	BORE 4.2500
MEAN RACE O.D. 4.7218	BASE DIA. 4.6578	WIDTH 0.8438
LARGE RIB O.D. 5.0500	SMALL RIB O.D. 4.6900	RIB FACE FLAT .0620

CUP DATA

INCLUDED ANGLE 29-20- 0	MEAN I. D. 5.2880	O. D. 5.7500
----------------------------	----------------------	-----------------

ROLLER DATA

NO. OF ROLLERS 39	L. E. DIA. 0.3000	S. E. DIA. 0.2832
SLANT LENGTH 0.6016	EFF. LENGTH 0.5475	APEX LENGTH 10.7433
WEIGHT (LBS.) 0.0114	CONTACT HT. 0.0598	SPHERICAL END RADIUS 8.2724 (77.0%)
MASS-MOMENT OF INERTIA (LB.INCH-SQ.)	I(X) = 0.00012 I(Y) = 0.00040	

CAGE DATA

TYPE OF GUIDE RACE	STOCK THICKNESS 0.0900	POCKET CLEARANCE 0.0020	
L.E. PILOT SURFACE SHAFT OR CONE	DIA. 5.1000	CLEARANCE 0.0030	RELIEF 0.0
S.E. PILOT SURFACE HOUSING OR CUP	DIA. 5.0950	CLEARANCE 0.0030	RELIEF 0.0

CCONE NO. XC1933CE

CUP NO. XC1933DC

RUN 425

RPM = 32422 R = 0 T = 5000 INLET/CONJ. TEMP = 300/350 F.

CAGE ANALYSISROLLER BODY / CAGE POCKET CONJUNCTIONINCLUDED ANGLE (RADIAN)
0.0275ARC LENGTH
0.0915REYNOLDS NUMBER
3479FRICTION FACTOR
0.00234SHEAR STRESS (PSI)
1.680DRAG FORCE (LBS)
0.0879CAGE / PILOT INTERFACELARGE END PILOTSMALL END PILOT

CAGE LOAD DIRECTION

DRIVE

DRAG

REYNOLDS NUMBER

5624

5028

FRICTION FACTOR

0.00190

0.00200

SHEAR STRESS (PSI)

1.5871

1.3312

MOMENT (LB-IN)

4.047

3.391

CONE NO. XC1933CE

CUP NO. XC1933DC

Appendix BCALCULATIONSCone Rib Lubrication

SHAFT SPEED (RPM)=32422.

RIB VELOCITY (FT/MIN)= 42318.

DN = 3499954.

LUBRICANT FLOW CONDITIONS

SHAFT DUCTS

CONE DUCTS

FRICTION FACTOR

0.0202

0.0273

HEADLOSS (IN/SEC)**2

88334.

253199.

REYNOLDS NUMBER

98719.

29505.

EXIT VELOCITY (IN/SEC)

3742.6743

3495.6187

MAXIMUM MANIFOLD PRESSURE (PSI)= 102.20

TANGENTIAL VELOCITY OF LUBRICANT @ OUTLET (IN/SEC)= 8247.00

ANGLE OF EXIT RELATIVE TO OUTLET (DEGREES)= 22.657

EFFECTIVE EXPOSURE TIME (SEC)= 0.000017

% COVERAGE OF RIB = 43.85

	FLOW (PT/MIN)
CONE	438.13
MANIFOLD	68.89
SHAFT	190.88

References

1. Cornish, R. F. and Benes, J. J., "Tapered Roller Bearing Take Off", Machine Design, July 22, 1971.
2. Clinedinst, W. O., "How Shrink Fits Affect Bearing Clearance", Machine Design, June, 1936.
3. Roark, R. J., "Formulas for Stress and Strain", Fourth Edition, McGraw-Hill Book Company, 1965.
4. Horger, O. J. and Nelson, C. W., "Design of Press and Shrink-Fitted Assemblies", Journal of Applied Mechanics, 1937.
5. Marks, L. S., "Mechanical Engineers' Handbook", Sixth Edition.
6. Beer, F. P. and Russell, Jr., E. R., "Mechanics for Engineers", McGraw-Hill Book Company, 1957.
7. Higginson, G. R. and Leaver, R. H., "Fluid Lubrication for Tapered Roller Bearings", I.Mech.E., May 1970.
8. Palmgren, A., "Ball and Roller Bearing Engineering", Third Edition, S. H. Burbank & Co., Inc., Philadelphia, 1959.
9. Seely, F. B. and Smith, J. O., "Advanced Mechanics of Materials", Second Edition, John Wiley and Sons, Inc., 1965.
10. Abramowitz, M. and Stegun, I. A., "Handbook of Mathematical Functions", Dover, 1965, Page 591-592.
11. NASA, "Interdisciplinary Approach to the Lubrication of Concentrated Contacts", NASA SP-237, July 1969.
12. Thorp, N. and Gohar, R., "Oil Film Thickness and Shape for a Ball Sliding in a Grooved Raceway", Journal of Lubrication Technology, Transactions of the ASME, July 1972.
13. Cheng, H. S., "Calculation of Elastohydrodynamic Film Thickness in High Speed Rolling and Sliding Contacts", MTI 67TR24, 1967.
14. McGrew, et al, "Elastohydrodynamic Lubrication", MTI, Technical Report AFAPL-TR-70-27, November 1970.
15. Smith, M. I. and Fuller, D. D., "Journal-Bearing Operation at Superlaminar Speeds", Trans. ASME, Vol. 78, 1956.
16. Astridge, D. G. and Smith, C. F., "Heat Generation in High-Speed Cylindrical Roller Bearings", Elastohydrodynamic Lubrication, 1972 Symposium, I.Mech.E., April 1972.

17. Harris, T. A., "An Analytical Method to Predict Skidding in High-Speed Roller Bearings", ASLE Trans., Vol. 9, 1966.
18. Poplawski, J. V., "Slip and Cage Forces in High Speed Roller Bearing", ASME Preprint 71-Lub-17.
19. Dowson, D. and Higginson, G. R., "Theory of Roller-Bearing Lubrication and Deformation", Proc. Inst. Mech. Eng. (London) 177, 58-69, 1963.
20. Johnson, K. L. and Cameron, R., "Shear Behavior of Elastohydrodynamic Oil Film at High Rolling Contact Pressures", Proc. of Inst. of Mech. Eng. 1967-1968, Vol. 182, P. 307.
21. Shames, I. H., "Mechanics of Fluids", McGraw-Hill Book Company, Inc., 1962.
22. Archard, J. F. and Cowking, E. W., "Elastohydrodynamic Lubrication at Point Contacts", Proc. of Inst. of Mech. Eng., 1965-66.
23. Moyer, C. A. and Wren, F. J., "Understanding Friction and EHL Films in Concentrated Contacts of a Tapered Roller Bearing", EHL Symposium, Leeds, England, 1972.
24. Plint, M. A., "Traction in Elastohydrodynamic Contacts", Proc. of Inst. of Mech. Eng. 1967-1968, Vol. 182, P. 307.